Regge Calculus as a Numerical Approach to General Relativity

by

Parandis Khavari

A thesis submitted in conformity with the requirements
for the degree of Doctor of Philosophy
Department of Astronomy and Astrophysics
University of Toronto

Abstract

Regge Calculus as a Numerical Approach to General Relativity

Parandis Khavari

Doctor of Philosophy

Department of Astronomy and Astrophysics

University of Toronto

2009

A (3+1)-evolutionary method in the framework of Regge Calculus, known as "Parallelisable Implicit Evolutionary Scheme", is analysed and revised so that it accounts for causality. Furthermore, the ambiguities associated with the notion of time in this evolutionary scheme are addressed and a solution to resolving such ambiguities is presented. The revised algorithm is then numerically tested and shown to produce the desirable results and indeed to resolve a problem previously faced upon implementing this scheme.

An important issue that has been overlooked in "Parallelisable Implicit Evolutionary Scheme" was the restrictions on the choice of edge lengths used to build the space-time lattice as it evolves in time. It is essential to know what inequalities must hold between the edges of a 4-dimensional simplex, used to construct a space-time, so that the geometry inside the simplex is Minkowskian. The only known inequality on the Minkowski plane is the "Reverse Triangle Inequality" which holds between the edges of a triangle constructed only from space-like edges. However, a triangle, on the Minkowski plane, can be built from a combination of time-like, space-like or null edges. Part of this thesis is concerned with deriving a number of inequalities that must hold between the edges of mixed triangles.

Finally, the Raychaudhuri equation is considered from the point of view of Regge Cal-

culus. The Raychaudhuri equation plays an important role in many areas of relativistic Physics and Astrophysics, most importantly in the proof of singularity theorems. An analogue to the Raychaudhuri equation in the framework of Regge Calculus is derived. Both (2+1)-dimensional and (3+1)-dimensional cases are considered and analogues for average expansion and shear scalar are found.

Dedication

To my beloved Husband and my Dear Parents

Acknowledgements

The acknowledgement section was the very last section that I had to complete to formally submit my thesis. At first, I intended to write a "standard acknowledgement" similar to what is seen in most Ph.D. theses. On a second thought however, I decided to write a document that reflects upon my characteristics as a person not as a Ph.D. candidate. Fifteen years ago, I could not decide whether I wanted to become an astrophysicist or a musician. Just the thought of achieving either of these two goals made me very happy. When I entered university to study engineering, I thought that my dream would never come true. If I have learned one thing during the past few years, it is that:

> *"Men can do all things if they will."*

After obtaining my B.Sc., I realised that the passion for Astrophysics in me is too strong to be killed. So I decided to start studying Astrophysics despite the fact that changing my field of study appeared to be quite challenging. All I had was the passion for Astrophysics and it turned out that it was all that I needed. Indeed, writing this document brings extreme joy to me as I now know that despite all hardships one of my dreams has indeed come true.

I shall confess that I have learned many things during the completion of this thesis that might appear utterly irrelevant to this work. Most importantly, I have come to a deep understanding of Sir Isaac Newton's statement that:

> *"To explain all nature is too difficult a task for any one man or even for any one age."*

Over the past four years, I have learned not to get disappointed with failure and not to be overjoyed with success. I have learned not to believe anyone's scientific statements unless I follow in their footsteps and come to the same conclusions. Finally, I have learned that

even those in whom I have much faith can make mistakes.

During these years, I was blessed with having a companion without whose support and encouragement entering the Ph.D. program in Astrophysics and completing it was not possible. My greatest gratitude goes to my beloved husband Mahdi to whom I dedicate this thesis. He always listened to me when I needed to and always encouraged me when I was most disappointed. He gently endured me when I was upset or stressed out and always tried his best to calm me.

The completion of this thesis was concurrent with the birth of my precious son, Yusuf whose arrival has brighten up my life. I wish that he will respect science and more importantly the quest for the truth in his future life. I would like to sincerely thank my parents for igniting the passion for learning in me. I am grateful to them for providing me with an outstanding education. I am also much indebted to them for taking excellent care of my son and thus providing me with the opportunity to finish my work.

I am much grateful to my supervisor, Professor Charles C. Dyer, for teaching me not only General Relativity but more importantly life lessons. He patiently taught me many things and supported me whenever I faced a barrier in my work. I will always be indebted to him. I am also thankful to my supervisory committee for supporting me through my Ph.D. program and providing me with constructive comments. My sincere appreciation goes to Professors Mochnacki, McCann, Abraham, and Hobill for reading my thesis and making excellent comments.

Finally, I would like to thank all my friends in the Department of Astronomy and Astrophysics. In particular, I would like to thank Ivana Damjanov, Marzieh Farhang, Preethi Nair, Maria Stankovic, Samaya Nissanke, Brian Lee, Duy Nguyen, Marc Goodman, and

Lee Robbins.

Contents

Chapter 1

Introduction

The beginning of the twentieth century witnessed the development of a revolutionary new theory called the Special Theory of Relativity. Although simple, this theory gave a radically different view of the physics that govern our universe. It did not take long, before Albert Einstein, to whom most of the credit for developing Special Relativity is given, noticed that gravity does not fit well in this new realm. This marked the beginning of a challenging era in Einstein's life. It took him ten years to develop the General Theory of Relativity. This geometrically beautiful theory describes gravity not as a force, as was perceived by Sir Isaac Newton, but as the curvature of the fabric of the space-time. Perhaps nobody has put the essence of Einstein's General Relativity into words better than John Archibald Wheeler:

"Matter tells space how to curve, and space tells matter how to move."

[Misner, Thorne & Wheeler (1972)]

Einstein's theory, although elegant, was mathematically very complicated. Einstein's struggle with the difficulty of the Mathematics involved in General Relativity can be clearly seen in his own words:

"Do not worry about your difficulties in Mathematics. I can assure you mine

1

are still greater!" [1]

Einstein himself doubted that there existed an analytical solution to the complicated set of equations that related the curvature of space-time to the distribution of energy-matter in his theory. He was much surprised when Karl Schwarzschild first presented a unique exact solution to his field equations for a spherically symmetric vacuum space-time. Today, this solution is known as the Schwarzschild solution and is well known to anyone who has some interest in Black Holes.

Einstein's equations consist of ten non-linear, coupled, hyperbolic partial differential equations. To date the number of exact solutions to these equations is not small but most of these analytical solutions rely heavily on the symmetries present in the cases they describe; consequently these solutions only depict the properties of a number of ideal phenomena. Today however, we are interested in understanding situations devoid of symmetry or with complicated topologies [Misner, Thorne & Wheeler (1972)]. To decode the hidden messages that General Relativity holds about these sophisticated problems, one is faced with the formidable task of solving the above-mentioned system of equations *numerically.*

The launch of projects such as LIGO (Laser Interferometer Gravitational-Wave Observatory) and LISA (Laser Interferometer Space Antenna) heralds a revolution in the world of Astronomy, opening up a new window from which a totally different view of the universe is observable [Abbott et al. 2004]. There certainly is a need to numerically solve Einstein's equations for many physical phenomena which could potentially give rise to gravitational waves so that the data from these gravitational wave observatories can be used as evidence for the existence of Black Holes and many other exotic phenomena as predicted by General Relativity. A typical event that can be detected by LIGO is for

---

[1]Letter to Barbara Lee Wilson, Einstein Archives 42-606, (1943).

instance the merger of two Black Holes with masses 10 times that of our Sun. We are still nowhere close to having a precise theoretical description of how such events in cosmos take place. The answer might just lie within the treasure box of Numerical Relativity.

1.1 Numerical Relativity

The goal of "Numerical Relativity" is to find descriptions of space-times, with little or no symmetries, by numerically solving Einstein's field equations. Numerical Relativity was born in the 1960's with the inaugural work of Hahn and Lindquist [Hahn & Lindquist 1964]. They tried to numerically solve Einstein's equation for two colliding black holes. They however did not succeeded as proper techniques for obtaining such numerical solutions did not exist at that time. The field of Numerical Relativity has come a long way since then. The technological advancements, in particular the development of supercomputers, during the past 50 years, have turned Numerical Relativity into a promising approach in the quest for finding explanations to complicated relativistic phenomena. Numerical Relativity has affected the work of both theorists and experimentalists significantly.

Numerical Relativity has two main approaches towards solving Einstein's Field Equations: Finite Difference Methods and Finite Element Methods. Finite differencing approaches a problem by replacing all derivatives by finite differences on a numerical grid. The solution is then advanced using a time marching method [Font 2000]. Finite difference methods have dominated the world of numerical relativity.

This thesis however is entirely centred on a promising finite element method called "Regge Calculus" [Regge 1961]. Instead of filling space-time with a grid of points, one approximates a space-time with a net of simplices [Sorkin 1975]. Regge Calculus, which

is named after its developer, Tullio Regge, will be described in detail in chapter (2). It has long been conjectured that Regge Calculus, would serve as an effecient tool in examining situations with non-trivial topology or devoid of symmetry, two areas that have remained rather unexplored in the context of General Relativity. The applications of Regge Calculus in Classical General Relativity however, have so far been mostly limited to re-generating known solutions to Einstein's equation [Wong 1971], [Collins & Williams 1973], [Lewis 1982] and [Brewin 1987]. To our knowledge, no one has ever attempted applying Regge Calculus to examine the evolution and properties of an arbitrary manifold. The realm of Regge Calculus has remained largely unexplored. This thesis is intended to bring Regge Calculus a few steps closer to being a viable tool in Numerical Relativity.

1.2   Objectives of this Thesis and its Contributions

Our initial intent, upon commencing this thesis, was to examine the role of non-triavial topology in the evolution of manifolds using Regge Calculus. The role of non-trivial topology in General Relativity is not well understood as this theory only provides one with geometry or local properties of a certain manifold and gives very little information about its global features or topology. A (3+1)-evolutionary method in the context of Regge Calculus is an ideal tool for this purpose. A closer review of the relevant literature showed that a couple of such methods have so far been proposed. However, most of them had a number of draw-backs (for example those used by [Collins & Williams 1973],[Brewin 1987] and [Lewis 1982]). The most promising (3+1)-evolutionary method based on Regge Calculus, so far presented, is known as "Parallelisable Implicit Evolution Scheme for Regge Calculus" [Barrett et al. 1997] or "Sorkin Triangulation" [Tuckey 1993]. This method however, had faced a few obstacles as will be described in chapter (3). Although the idea behind

the method and the algorithm to apply it to evolution of skeletonised (approximated by simplices) manifolds appeared to be reasonable and correct, Sorkin Triangulation did not produce the expected results when employed to re-produce known analytical solutions. We will describe this problem in detail in chapter (4).

A close inspection of the Parallelisable Implicit Evolution Scheme (PIES) convinced us that causality had not been included in this method properly. Causality was an aspect that was briefly mentioned in Barrett et al.'s seminal paper on PIES but the authors did not investigate its role deeply. In this thesis, we show how causality can be accounted for in PIES. The notion of time was another issue that required clarification in this method. In this thesis, we have discussed the ambiguities associated with the notion of proper time in skeletonised space-times in detail and have introduced ways to find a sense of lapse of time in PIES. By accounting for causality as well as obtaining an appropriate understanding of the notion of time in Sorkin Triangulation, we succeeded in resolving one of the biggest problems facing this method. We illustrate the success of the revised algorithm by a numerical example in chapter (4).

Another important question that had remained unanswered at the time this thesis started was related to the nature of the inequalities that have to be satisfied by the edges of a lattice used in Regge Calculus. In particular, in implementing methods of Regge Calculus, one has to ensure that the geometry inside the lattice blocks is Minkowskian (flat with our choice of $(-+++)$ signature). This indeed requires that certain inequalities hold between the edge lengths of a lattice. These inequalities are counter-parts of the familiar triangle inequality in Euclidean geometry. It turns out that the number of these inequalities is more than one. This is because one can build triangles with edges that are different in character (for example a triangle with two space-like edge and one time-like edge). In chapter (5), we add a number of such inequalities to the famous

"Reverse Triangle Inequality" satisfied by triangles built out of only space-like (time-like) edges. The results of chapter (5) are very useful in picking the correct choice of length for edges which are freely chosen in a (3+1)-evolutionary method, corresponding to the freedom in the choice of Lapse and Shift.

There are many aspects of Classical General Relativity that have not been explored in the context of Regge Calculus. Examining the parameters and equations of the continuum in the framework of Regge Calculus provides us with a better understanding of how this numerical method works. In addition, it allows us to interpret the numerical results obtained using Regge Calculus correctly. The behaviour of a congruence of geodesics in a skeletonised space-time is among these aspects. It is interesting to see what the Raychaudhuri equation, one of the most important equations in General Relativity, looks like in the context of Regge Calculus. We have investigated this problem in chapter (6). We find analogues to expansion and shear scalar for (2+1) and (3+1) dimensional lattice space-times. In addition, we write the skeletonised version of the Raychaudhuri equation in (2+1) and (3+1) dimensions. The piece of work presented in chapter (6) provides us with deeper insight about the notion of collapse and singular state in Regge Calculus.

Chapter 2

Regge Calculus

2.1 Introduction

Regge Calculus [Regge 1961] is a finite element method introduced by Tullio Regge in (1961). The idea behind Regge Calculus is to approximate a manifold with rigid simplices. A simplex is the convex hull of $(n+1)$ affinely independent points[1] in some n or higher dimensional Euclidean space. Thus a point is the zero dimensional simplex. By joining two points, a line segment or the 1-dimensional simplex is obtained. Joining the two vertices of a line segment to a point not on the line segment, i.e. a point residing in the second dimension, a triangle or a 2-d simplex is formed. H.S.M. Coxeter puts this simply as [Coxeter 1973]:

> "Any $(n+1)$ points that do not lie in an $(n-1)$-space are the vertices of an n-dimensional simplex."

Figure (2.1) shows simplices of different dimensions. Each n-simplex itself, consists of simplices of lower dimensions. In general, the number of k-simplices in an n-dimensional simplex $(k < n)$ is given by $N_k = \binom{n+1}{k+1}$. The advantage of a simplex, as a structure, is

---

[1]Let $S = \{p_0, p_1, p_2, ..., p_k\} \subseteq \mathcal{R}^d$. A linear combination is $x = \sum_{i=0}^{k} \lambda_i p_i$ for some $\lambda_i \in \mathcal{R}$. An affine combination is a linear combination such that $\sum_{i=0}^{k} \lambda_i = 1$. A convex combination is an affine combination such that $\lambda_i \geq 1$ for all i. The set of all convex combinations is the convex hull of S.
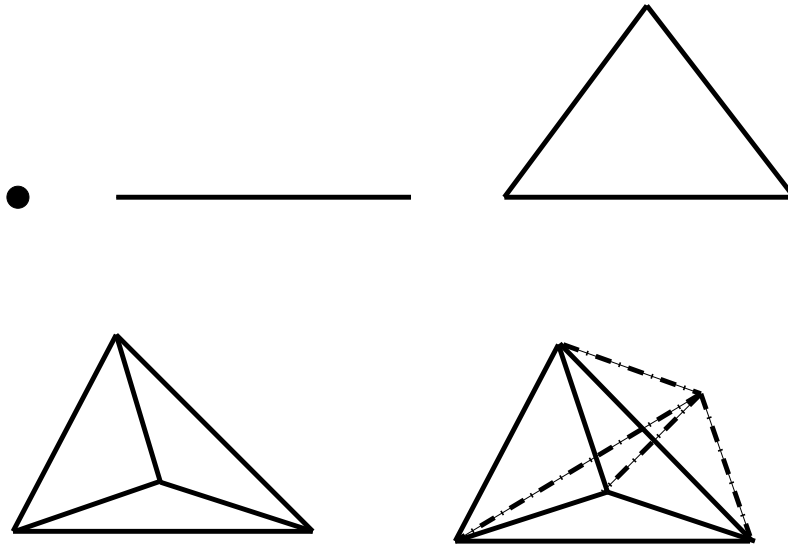
Figure 2.1: Simplices of different dimensions.

that it is rigid. In other words, all the information about it is given once its edge lengths are known.

An n-dimensional manifold can be approximated using a number of simplices of the same dimension. The outcome of such a procedure is the so-called "Connection Matrix" or "Incidence Matrix" which contains all the data on the edge lengths and instructions on how different points are to be connected [Regge 1961]. Consequently, the connection matrix contains all the information about geometry and topology of the skeletonised space under consideration. Indeed the connection matrix conveys discrete information similar to the continuum information conveyed by the metric. The larger the number of the simplices, the finer the tessellation and consequently the better the approximation. One of the best examples of this type of approximation is the so-called geodesic dome, an example of which is shown in figure (2.2), where a 2-sphere is approximated using triangles.
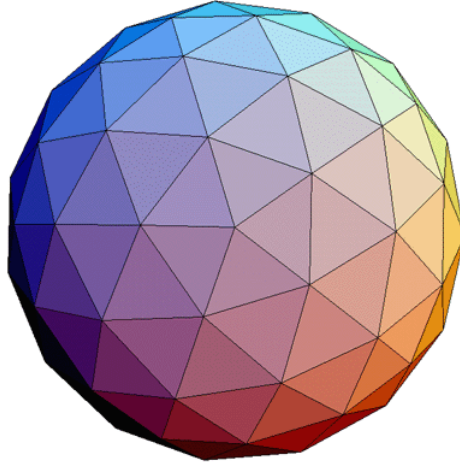
Figure 2.2: A 2-sphere is triangulated by triangles. The curvature is concentrated on vertices.

When a curved manifold is approximated by simplices, the goemetry is flat within each simplex; the curvature of the manifold is concentrated on sub-simplices of dimension $(n - 2)$ or equivalently co-dimension two. Regge calls these sub-simplices "hinges" or "bones" and we will continue using these expressions thoroughout this thesis interchangeably. The amount of curvature residing on a hinge is represented by the so-called "Deficit Angle".

Figure (2.3) depicts the notion of deficit angle, or deficiency for short, on skeletonised manifolds of dimensions two and three. Figure (2.4) visualises the deficiency residing on a triangular bone of a 4-dimensional skeletonsied space. A positive deficit angle represents positive curvature and a negative deficit angle stands for negative curvature.

In the continuum regime, the curvature of space-time manifests itself through the notion of parallel transportation and the fact that the change in the parallel transported vector depends on the amount of curvature enclosed by the loop around which it is parallel transported. A very similar notion applies in the case of skeletonised spacetimes. If one parallel transports a vector around a loop containing a hinge, the vector rotates by an
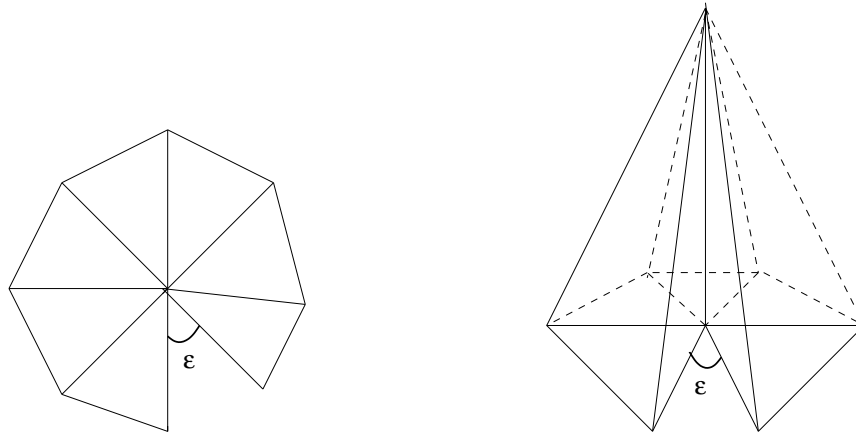
Figure 2.3: On a 2-dimensional triangulated manifold, the curvature is concentrated on vertices and on a 3-dimensional skeletonised manifold the curvature is concentrated on edges.
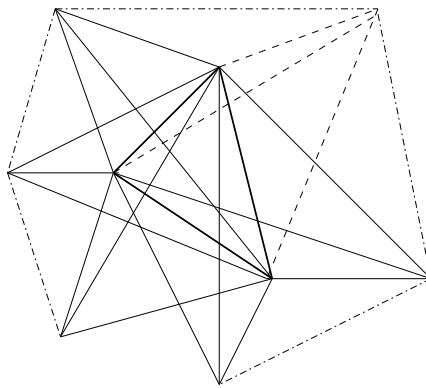
Figure 2.4: The curvature of a skeletonised 4-dimensional manifold is concentrated on 2-d simplices or triangles.

angle equal to the deficit of that hinge once it returns to its starting point as shown in figure (2.5).
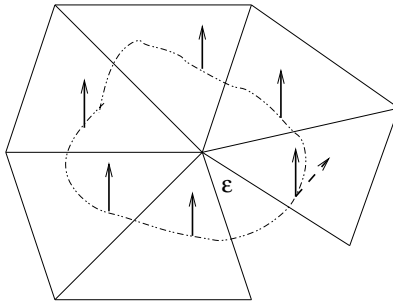
Figure 2.5: A vector parallel transported around a loop enclosing a bone comes back to its initial position rotated by an angle equal to the deficiency of that bone.

The situation however, is slightly more complicated in a 4-dimensional skeletonised manifold. Suppose we are to parallel transport a vector, in a 4-d skeletonised spacetime, around a loop enclosing this triangular bone. This vector can be broken into two orthogonal components, one lying in the plane of the triangular bone and the other perpendicular to it. Parallel transporting the vector around a loop enclosing the triangular bone results in the rotation of the component that is perpendicular to the triangular bone. The amount of rotation is equal to the deficiency of the bone. The issue of parallel transport of a vector, along a path enclosing a triangular bone in 4-dimensions, will be discussed in detail in chapter (6)

2.1.1   Descretised Action and Regge's Equation

The gravitational action in General Relativity is given by:

$$I_g = \frac{1}{16\pi} \int \mathcal{L}_\mathcal{G} \; d^4x \tag{2.1}$$

with the Lagrangian density, $\mathcal{L}_\mathcal{G} = R \sqrt{-g}$, where R stands for the scalar curvature and g for the determinant of the metric. This action is usually accompanied by an action

corresponding to an energy-momentum source. Thus, the general form of the Lagrangian density in General Relativity which is used in the so-called Einstein-Hilbert action is written as:

$$\mathcal{L}_{\mathcal{EH}} = \mathcal{L}_{\mathcal{G}} + \mathcal{L}_{\mathcal{M}} \tag{2.2}$$

This action is then to be varied with respect to the metric components, $g_{\alpha\beta}$, to obtain the familiar Einstein's equations given by:

$$R_{\alpha\beta} - \frac{1}{2}R\, g_{\alpha\beta} = \kappa\, T_{\alpha\beta} \tag{2.3}$$

where $\kappa = 8\pi G$ and the cosmological constant is assumed to be zero.

Regge showed that the relativistic action in its descretised form can be written as:

$$I = \frac{1}{8\pi} \sum_k A_k\, \epsilon_k \tag{2.4}$$

where A_k is the volume content of the kth hinge and ϵ_k is the deficiency associated with this hinge. To find the analogue of Einstein's field equations, one is to vary this action with respect to the edge lengths that indeed play the role of the metric in the discretised limit. Regge showed that if the dimension of a manifold is larger than two, one can remarkably carry out this variation as if the deficiencies were constants [Regge 1961]. Similarly, in the continuum the variation of the Ricci tensor does not contribute to the equations of motion [Stephani 2008].

In a 2-dimensional manifold, the curvature is concentrated on vertices or points which do not have any volume content. The action for this case in fact produces the discrete form of the Gauss-Bonnet theorem:

$$\sum_k \epsilon_k = 2\pi\chi \tag{2.5}$$

where χ is the Euler characteristic and is given by $\chi = 2 - 2g$ with g representing

the genus[2]. Thus for a 2-dimensional skeletonised manifold, the action is a topological invariant. This result is of course in good agreement with the continuum limit expression of the action given by [Hamber 2007]:

$$\frac{1}{2} \int R\sqrt{-g}\, d^2x = 2\pi\chi \tag{2.6}$$

In a 3-dimensional skeletonised manifold, the deficiencies are concentrated on edges, l_k, and thus the action is given by:

$$^{(3)}I = \frac{1}{8\pi} \sum_k l_k\, \epsilon_k \tag{2.7}$$

where $^{(3)}I$ stands for the discretised action in three dimensions. Varying Regge's action with respect to edge lengths for this case results in:

$$\sum_k \frac{\partial l_k}{\partial l_p} \epsilon_k = 0 \quad \Rightarrow \quad \epsilon_k = 0 \tag{2.8}$$

Consequently, all 3-dimensional skeletonised manifolds are flat. This is indeed the discrete analogue of the fact that Einstein's equation have only trivial solutions in three dimensions [Sorkin 1975].

Regge derived the skeletonised version of the field equations for a manifold equipped with a positive-definite metric by taking the variation of equation (2.4) with respect to an arbitrary edge-length l_p. He showed that in this case the vacuum field equations are given by:

$$\frac{1}{2} l_p \sum_k \cot \theta_{pk}\, \epsilon_k = 0 \tag{2.9}$$

where θ_{pk} is the angle facing edge l_p in the kth triangle sharing edge l_p and ϵ_k is the deficinecy of the kth triangle as shown in figure (2.6). In chapter (3), we will re-derive appropriate Regge equations to be used in PIES. The revised Regge equations account for Causality in this evolutionary scheme.

---

[2]Roughly speaking, genus is the number of holes in a manifold
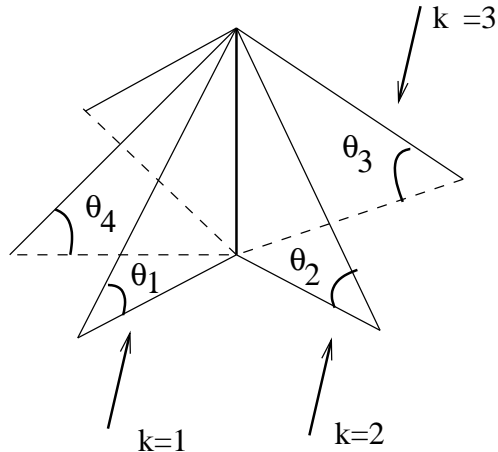
Figure 2.6: To obtain a discrete analogue to Einstein's equation, Regge's action is varied with respect to the length of a certain edge. For a 4-dimensional triangulated manifold, all the triangular bones, sharing the particular edge chosen, are included in the action.

2.2 The Action must always be real

As shown in equation (2.4), two quantities appear in the action: the area content of the bone and the deficiency residing on this bone. On a manifold with Minkowskian signature, which we take it to be $(-+++)$, there are two main types of bones that one usually has to deal with in analysing a problem using Regge Calculus. A space-like bone is a bone constructed from only space-like edges, while a time-like bone is one with one or more of its edges time-like. Switching to the language of coordinates for a moment, the bivector representing the area of a time-like bone, which one might assume to lie in the (t, z) plane, falls in the (x, y) plane and thus it corresponds to a real quantity:

$$\vec{L} = \vec{u} \times \vec{v} \tag{2.10}$$

where $\vec{u}$ and $\vec{v}$ are two edges of a triangular bone, one running in the t direction and the other in the z direction. If a vector is parallel transported around a loop enclosing this bone, its x and y components undergo a rotation while its t component remains unchanged. Thus such a vector will undergo a rotation by an angle equal to the deficiency

of the bone. Of course this angle must be real as it represents a rotation. From this simple analysis, it is clear that the area of a time-like bone must always be taken to be real. To achieve this purpose, Regge proposed to *define* the length of $\vec{L}$ to be given by:

$$4L_{tl}^2 = (\vec{v} \cdot \vec{u})^2 - (\vec{v})^2(\vec{u})^2 \tag{2.11}$$

It is not hard to see that using this definition L_{tl} indeed always turns out to be a real
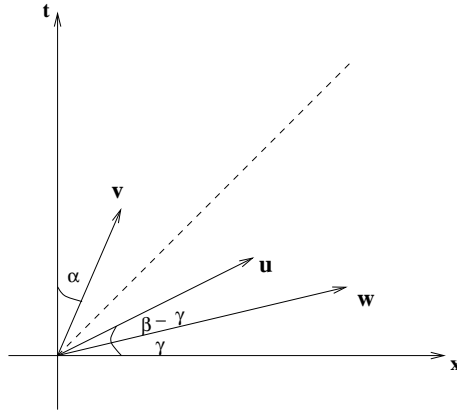
Figure 2.7: Time-like vector $\vec{v}$ as well as space-like vectors $\vec{u}$ and $\vec{w}$ shown in an arbitrary coordinate system where the x-axis and t-axis are taken to be orthogonal. The angle between $\vec{u}$ and the x-axis is β while the one between $\vec{w}$ and x-axis is γ.

quantity. To see this, let us take $\vec{v}$ to be time-like and $\vec{u}$ to be space-like and in the frame of a certain observer be given by (the choice of observer is completely irrelevant as eventually, only the dot product of the two vectors is important for us and the value of the dot product is independent of the frame in which it is calculated) as shown in figure (2.7):

$$\vec{v} = |v|(\cosh \alpha \hat{t} + \sinh \alpha \hat{x})$$
$$\vec{u} = |u|(\sinh \beta \hat{t} + \cosh \beta \hat{x})$$

The dot product of these two vectors is then clearly given by:

$$\vec{u} \cdot \vec{v} = |u||v| \sinh (\alpha - \beta)$$

Using this dot product in equation (2.11) yields:

$$4L_{tl}^2 = |u|^2|v|^2 \sinh^2(\alpha - \beta) + |u|^2|v|^2 = |u|^2|v|^2 \cosh^2(\alpha - \beta) \qquad (2.12)$$

where the change in the sign of the second term comes from the fact that since $\vec{v}$ is time-like, and thus $|\vec{v}|^2 = -|v|^2$.

Similarly, the bivector corresponding to a space-like edge is imaginary. This type of bone can be thought as residing in the (x, y) plane. In this case, the temporal component of a vector, parallel-transported around a loop enclosing such bone, undergoes a rotation corresponding to a boost. Therefore, the deficiency of this type of bone is imaginary. Again, to keep the action real, one is left with no choice but to assign an imaginary area to a space-like bone. To achieve this purpose, the area of a space-like bone with edges, $\vec{u}$ and $\vec{w}$ is defined in the customary way as:

$$4L_{sl}^2 = (\vec{w})^2(\vec{u})^2 - (\vec{w} \cdot \vec{u})^2 \qquad (2.13)$$

This definition produces an imaginary action as can be seen through the following analysis. Once again, one can write $\vec{u}$ and $\vec{w}$ as follows (in a given frame):

$$
\begin{aligned}
\vec{u} &= |u|(\sinh\beta\hat{t} + \cosh\beta\hat{x}) \\
\vec{w} &= |w|(\sinh\gamma\hat{t} + \cosh\gamma\hat{x})
\end{aligned}
$$

The dot product of the two space-like vector is then evidently given by:

$$\vec{w} \cdot \vec{u} = |w||u| \cosh(\gamma - \beta)$$

Inserting this into equation (2.13) and simplifying, yields:

$$4L_{sl}^2 = |w|^2|u|^2 - |w|^2|u|^2 \cosh^2(\gamma - \beta) = -|w|^2|u|^2 \sinh^2(\gamma - \beta) \qquad (2.14)$$

which is clearly always negative and thus results in an imaginary bivector.

Keeping these conventions in mind, in appendix (B), we will seek a general method of calculating the area of a variety of time-like bones that can be constructed in Minkowski plane. To our knowledge, there does not exist a comprehensive treatment of the area of "Minkowskian triangles" in the literature. The advantage of the formulae obtained in appendix (B) is that they produce the area of a time-like bone given only the length of the edges, the sole piece of information at hand for skeletonised space-times.

2.2.1   Calculating the Deficit Angle

From the above discussion, it is clear that one piece of data required in writing the Regge equation is the deficit angle. To calculate the deficit angle concentrated on a subsimplex of co-dimension two, we need to find the dihedral angle subtended by the faces of each of the simplices hanging at this bone. The deficit angle concentrated on hinge p, where k simplices meet, is then given by:

$$\epsilon_p = 2\pi - \sum_k \theta_k \tag{2.15}$$

where θ_k is the dihedral angle between two (n-1)-dimensional faces of the kth simplex hanging at bone p.

For a 2-dimensional skeletonised manifold, we need to calculate the angle between the two edges of each of the triangles meeting at the vertex under consideration. The trigonometric sine of the angle between two edges of a triangle in terms of its edge lengths is given by:

$$\sin\theta = \frac{2A}{l_1 l_2} \tag{2.16}$$

where A is the area of the triangle in terms of its edge lengths which is in turn given by Heron's formula:

$$A = \sqrt{P\left(P - l_1\right)\left(P - l_2\right)\left(P - l_3\right)} \tag{2.17}$$

In equation (2.17), P is half of the perimeter of the triangle and l_1, l_2 and l_3 are the edge lengths of the triangle. For higher dimensional Euclidean simplices the volume content can be determined using a Cayley-Menger determinant which is the modern version of Heron's formula. In particular, the volume of an n-simplex is given by:

$$v_n^2(s) = \frac{(-1)^{n+1}}{(n!)^2 \, 2^n} \begin{vmatrix} 0 & 1 & 1 & \dots \\ 1 & 0 & l_{01}^2 & \dots \\ 1 & l_{10}^2 & 0 & \dots \\ 1 & l_{20}^2 & l_{21}^2 & \dots \\ \dots & \dots & \dots & \dots \\ 1 & l_{n0}^2 & l_{n1}^2 & \dots \end{vmatrix}$$

A formula similar to equation (2.16) can be used in higher dimensions as well. In particular, in n dimensions, the trigonometric sine of the dihedral angle, subtended by the $(n-1)$-dimensional faces f and f' with volume contents $V_{n-1}(f)$ and $V_{n-1}(f')$, is given by :

$$\sin \theta(f, f') = \frac{n}{n-1} \frac{V_n(s) V_{n-2}(h)}{V_{n-1}(f) V_{n-1}(f')} \tag{2.18}$$

where $V_n(s)$ is the volume of the n-simplex and $V_{n-2}(h)$ stands for the volume content of the bone [Hamber 2007]. This formula however is not of much use as it only determines the sine of the angle and thus the angle cannot be measured unambiguously.

There exists however a more practical method in the literature [Hartle 1984] for the calculation of the dihedral angle. As was mentioned earlier, any n-simplex is specified by its $n+1$ vertices, $(0, 1, ..., n)$. Any simplex can then be spanned by n vectors, e_i's, as shown in figure (2.8). The *volume n-form* associated with an n-simplex is then defined
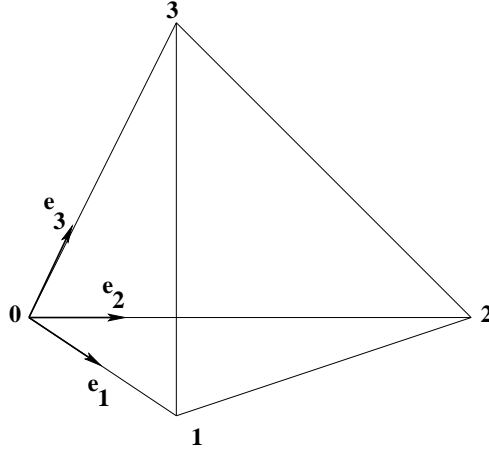
Figure 2.8: A simplex of dimension n can always be spanned by the n vectors.

as[3]:

$$\omega_n = e_1 \wedge e_2 \wedge ...e_n \tag{2.19}$$

The volume V_n of an n-simplex is simply the norm of ω_n and is given by:

$$V_n^2 = (\frac{1}{n!})^2 \ \det(e_i.e_j) \tag{2.20}$$

where

$$e_i.e_j = \frac{1}{2}(l_{0i}^2 + l_{0j}^2 - l_{ij}^2) \tag{2.21}$$

The dot product between two volume n-forms is defined as:

$$\omega_n.\omega_n' = (\frac{1}{n!})^2 \ \det(e_i.e_j') \tag{2.22}$$

Finally, the dihedral angle between two simplices with corresponding volume n-forms, ω_n and ω_n' is given by:

$$\cos\theta = \frac{\omega_n \cdot \omega_n'}{V_n \ V_n'} \tag{2.23}$$

To obtain the correct sign for $\cos\theta$, one has to construct the volume n-forms as follows: if ω_{n-1} is the volume form of the hinge, then the corresponding volume forms of the

---

[3]$\wedge$ represents the exterior product. The value of the exterior product of two 1-forms, p_1 and p_2, on the pair of vectors $\vec{v}_1, \vec{v}_2 \in \mathcal{R}^n$ is defined to be the oriented area of the image of the parallelogram with sides $p_1(\vec{v}_1)$ and $p_2(\vec{v}_2)$ on the p_1, p_2 plane [Arnold 1997].

n-simplices, the dihedral angles between which is sought, is given by:

$$\omega_n = \omega_{n-1} \wedge e \qquad \text{and} \qquad \omega'_n = \omega_{n-1} \wedge e' \qquad (2.24)$$

where e and e' are the appropriate vectors to build the n-simplices from the hinge. Using the formulae mentioned in this section, the dihedral angle between any two n-dimensional simplices sharing a sub-simplex of co-dimension two can be found. Finally, by using equation (2.15), one can obtain the deficiency corresponding to a certain sub-simplex of co-dimension two.

2.3   Binachi Identities in Regge Calculus

In the General Theory of Relativity, the Bianchi identities read:

$$R_{\alpha\beta\mu\nu;\,\lambda} + R_{\alpha\beta\nu\lambda;\,\mu} + R_{\alpha\beta\lambda\mu;\,\nu} = 0 \qquad (2.25)$$

where $R_{\alpha\beta\mu\nu}$ is the Riemann tensor and ";" represents the covariant derivative. One important consequence of the Bianchi identities lies in the fact that they imply, the Einstein's tensor, defined as: $G_{\mu\nu} = R_{\mu\nu} - \frac{1}{2}R\,g_{\mu\nu}$, is divergence free (here $R_{\mu\nu}$ is the Ricci tensor, R is the curvature scalar and $g_{\mu\nu}$ is the metric). Another important ground where Bianchi identities play a vital role is in the context of degrees of freedom. Einstein's field equations as given by:

$$G_{\alpha\beta} = 8\pi G\, T_{\alpha\beta} \qquad (2.26)$$

are indeed a system of 10 coupled differential equations. These equations are to be solved for the components of the metric, $g_{\alpha\beta}$, given an energy-momentum source represented by $T_{\alpha\beta}$. However, $g_{\alpha\beta}$, are the components of the metric in *some coordinate system*. Consequently, a change in the coordinate system induces a change in these components. As there are four coordinate functions, there exist four arbitrary functional degrees of freedom among the ten components of $g_{\alpha\beta}$. It should then be impossible to determine the 10 components of the metric from any set of initial data since the coordinate system to the

future of this moment can be changed arbitrarily. Indeed Bianchi identities guarantee this property for Einstein's equation. The fact that Einstein's tensor is divergence free, i.e. $G^{\alpha\beta}{}_{;\beta} = 0$, implies that there are four differential identities, one for each value of α. Consequently, only six of the Einstein's equations are independent.

Regge showed that there exists discrete analogues to Bianchi identities [Regge 1961] for skeletonised space-times. In particular, for a 4-dimensional skeletonised space-time, the Bianchi identities imply that the product of the rotation matrices corresponding to all the triangular hinges meeting at an edge is the identity transformation [Barrett et al. 1997]. The fact that the Bianchi identities have a counter-part in Regge Calculus means that one enjoys the freedom to choose the lapse and shift[4] arbitrarily when employing a (3+1)-evolutionary method in the context of Regge Calculus. In section (2.5), we will explain, in more detail, the consequences of the existence of a counter-part for the Bianchi identities in the context of Regge Calculus.

2.4   (3+1)-Evolutionary Methods in Regge Calculus

A number of different (3+1)-evolutionary methods have been introduced in the context of Regge calculus. The so-called "Prism Methods", used by Collins and Williams and later by Brewin, employed non-simplicial blocks to triangulate the space-time. In particular, these methods used tetrahedral blocks to tessellate the 3-dimensional hypersyrfaces and connected the corresponding vertices, on two consecutive space-like slices, by time-like edges. The 4-dimensional blocks formed in this procedure are in fact non-simplicial blocks. The use of non-simplicial blocks required the introduction of additional pieces of

---

[4]The Lapse function and the Shift vector are two important notions used in the ADM formalism first developed by Arnowitt, Deser and Misner. The ADM formalism is a Hamiltonian formulation of General Relativity in which the space-time is foliated into a family of spatial hypersurfaces. Roughly speaking, lapse and shift describe how two consecutive spatial laminations of space-time are connected together. The equations of motion of the lapse function and the shift vector can be specified arbitrarily corresponding to the freedom in laying out a coordinate system in space-time [Misner, Thorne & Wheeler (1972)].

information such as diagonals of the blocks or some of the angles between the edges of the blocks. Two types of equations arise in such approaches: "Evolution Equations" corresponding to the variation carried out with respect to space-like edges and "Constraint Equations" corresponding to the variations carried out with respect to time-like edges. In addition to the disadvantage of using non-simplicial blocks, the main shortcoming of these methods is that the two above-mentioned types of equations are coupled such that it is impossible to obtain local solutions [Barrett et al. 1997].

A different kind of (3+1)-evolutionary method in the context of Regge Calculus was introduced by Barrett et al. based on a much earlier work by Sorkin [Sorkin 1975]. This method is known as "Parallelisable Implicit Evolution Scheme for Regge Calculus" [Barrett et al. 1997] and is considered to be the most successful (3+1)-evolutionary method currently at hand. Using this approach, a given tessellated hypersurface can be evolved by evolving one vertex at a time or in parallel for those vertices which are not directly joined by an edge. One big advantage of this method is that it allows for advancement of any triangulation with an arbitrary underlying topology. The procedure is such that, independent of the order of advancement of vertices, each vertex has a unique predecessor and successor and thus the triangulation of the 3-dimensional hypersurfaces remains intact. This approach will be described in detail in the next section.

2.5   Parallelisable Implicit Evolution Scheme for Regge Calculus

Consider a time evolution problem in Regge Calculus and suppose that the connection matrix is known entirely up to and including a given triangulated space-like hypersurface. "Parallelisable Implicit Evolution Scheme" (PIES), otherwise known as the "Sorkin Triangualtion Algorithm" then offers us an algorithm to advance each and every vertex

of this $(n-1)$-dimensional triangulated hypersurface into the future. It is easiest to see the algorithm at work for a (2+1)-dimensional space-time. Figure (2.9) shows a spatial 2-dimensional triangulated surface. To advance vertex A to the next surface, to be built
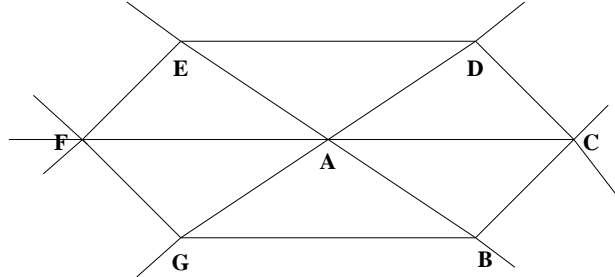
Figure 2.9: A 2-dimensional surface obtained from foliating a 3-dimensional space-time at a single moment of time.

"above" the one shown in (2.9), introduce a new vertex A' "above" A, in particular in the third dimension or temporal direction. Vertices A and A' are then to be connected by a "vertical edge". It is important to note that this vertical edge does not have to be orthogonal to the initial hypersurface. As will be explained in detail in chapter (4), this edge must be chosen so that it lies within the future null cone of vertex A. In addition, vertex A' is to be connected to all vertices on the initial surface which were connected to A directly. Thus vertices B, C, D, E, F, G are to be connected to A' by the so-called "diagonal edges" (The unprimed vertices are all assumed to reside on the same surface). This results in a tent-like structure built above the initial surface as shown in figure (2.10). The next step is to evolve another vertex, for instance vertex B, into the future. Following a similar procedure, we introduce a vertex B' in the third dimension and then connect all the vertices on the initial surface (which were directly connected to B) to B'. Moreover, we have to connect A' to B'. $A'B'$ is indeed the first edge on the next surface, the evolved version of AB. This step is shown in figure (2.11).

Suppose now that a given vertex is connected to N other vertices on the initial
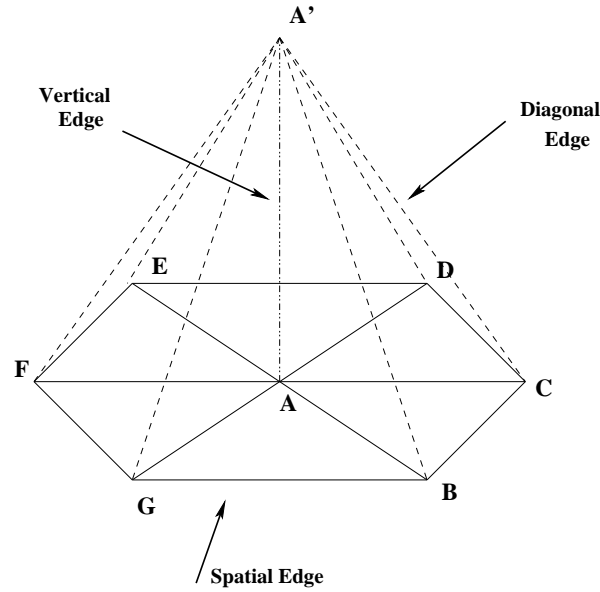
Figure 2.10: Evolution of vertex A according to the Sorkin Triangulation Algorithm or PIES. Vertex A' is introduced above A in the temporal direction. The edge that connects A to A' is known as the "Vertical Edge" in the literature. Also shown in the figure are the "Diagonal Edges" as described in the text.
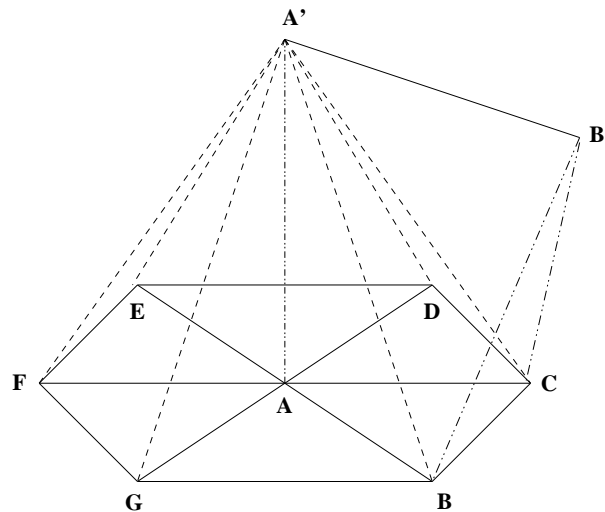
Figure 2.11: $A'B'$ is indeed the evolved version of AB. The rest of the vertices can be evolved using the same procedure.

hypersurface. Evolving this vertex introduces $N + 1$ news edges: the vertical edge as well as N diagonal edges. The construction is such that there exists a spatial edge with known length corresponding to a diagonal edge. Therefore one, in principle, can solve exactly for the diagonal edges. It has however been shown that this approach leads to ill-conditioned algebraic systems [Hartle 1984]. This is where the Bianchi identities come to the rescue. The fact that the Bianchi identities have an analogue in Regge Calculus allows us to choose the length of four of the newly introduced edges arbitrarily. Thus, at each vertex, one has the freedom to choose the length of four of the edges that go between a hypersurface and its evolved version. This indeed corresponds to the freedom in the choice of lapse and shift. The above-mentioned construction can be immediately generalised to (3+1) dimensions. The construction here, however, is slightly more complicated as shown in figure (2.12).
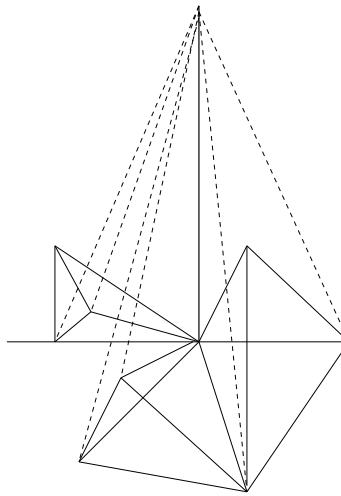
Figure 2.12: The Evolution of a vertex according to Sorkin's Triangulation in $(3 + 1)$ dimensions. In a $(3 + 1)$-dimensional evolutionary problem, the tetrahedra comprising the initial hypersurface each become a base to a 4-simplex.

In their seminal paper on the PIES, Barrett et al. only briefly discuss the issue of

causality and place a few restrictions on the type of edges as will be discussed in more detail in the next chapter. *Barret et al. however insist on the fact that these causality conditions are very likely not sufficient and the issue of causality in "Parallelisable Implicit Evolution Scheme for Regge Calculus" clearly requires much more investigation.* Indeed they express the fact that they are not sure whether the restrictions imposed on the edges will satisfy the Courant condition. A deep investigation into the issue of causality indeed formed a major part of this thesis as will be explained in detail over the next few chapters.

2.6   Previous Applications of the Parallelisable Implicit Evolution Scheme for Regge Calculus

The Parallelisable Implicit Evolution Scheme for Regge Calculus has been employed to examine the evolution of the spatially closed Friedmann-Lamaître-Robertson-Walker (FLRW) universe [Barrett et al. 1997, De Felice & Fabri 2000]. As will be described in more detail, it did not however produce the expected results. We believe the reason this algorithm has not been successful is that it does not account for causality properly. Over the next few chapters, we will show how to include causality into PIES. The revised algorithm will be illustrated by a numerical example and will be shown to resolve a major barrier faced by Barrett et al.

Chapter 3

Inclusion of Causality in the PIES

3.1 Introduction

In his seminal paper, Regge derives an analogue to Einstein's equation valid for a *Riemannian manifold* from the following action:

$$I_R = \sum_k A_k \epsilon_k \tag{3.1}$$

Regge's original equation however, is not very useful when it comes to General Relativity (GR) as GR is concerned with *pseudo-Riemannian* manifolds. The common belief among the practitioners of Regge Calculus has been that the Lorentzian signature can be incorporated in Regge's equation by tagging time-like quantities with an "imaginary" $i = \sqrt{-1}$. Inclusion of Lorentzian signature however, is not as trivial as commonly thought. Taking the derivative of square roots of negative edges in such cases may result in change of sign as the following simple example shows [Miller 1995]:

$$i = \sqrt{-1} = \sqrt{\frac{1}{-1}} = \frac{1}{\sqrt{-1}} = \frac{1}{i} = -i \tag{3.2}$$

Such errors might become crucial, especially when one considers a (3+1)-evolutionary scheme in the context of Regge Calculus. It was mentioned earlier that the Sorkin triangulation is believed to be the most successful (3+1)-evolutionary method for skeletonised

manifolds currently at hand. The Lorentzian signature has been included in this method using the above-mentioned approach of tagging time-like edges with imaginary $i's$. In this chapter, we re-derive the relevant Regge equations as used in PIES, for a Lorentzian manifold, from scratch. The equations obtained in this section prevent errors such as the one in equation (3.2). Another crucial issue that has not been properly addressed in the relevant literature is the inclusion of Causality into PIES. In this chapter, we explain how causality can be incorporated into Sorkin's evolutionary method.

In this chapter, we revise the relevant Regge equations, as used in PIES, so that they include causality. We do this for both a time-like and a space-like bone. One important quantity that is used in our analysis in this chapter, is the area of a triangular bone in a pseudo-Riemannian 4-dimensional skeletonised space-time. It is computationally important to find a single formula (that can easily be used in a computer code) from which the area of any type of triangular bone is given in terms of its edge lengths. To prevent the interruption of the main discussion of this chapter, the derivation of the area formulae and other related materials are presented as an appendix.

3.2   Area of a Bone and the Issue of Causality

In their seminal paper on PIES, Barrett et al. argue that since in this approach one tries to obtain the information about the newly introduced edges from the knowledge of the triangulation of the initial spatial hypersurface, the tent-like structure formed above a chosen vertex on a spatial hypersurface must reside within the future domain of dependence of this hypersurface. Thus, as shown in figure (3.1), the diagonal edges must be space-like while the vertical edge can in principle be time-like, null or space-like. The restriction as imposed by Barrett et al. is more a "No Collision" requirement than a causality requirement. What this condition does is that by making the diagonal edges
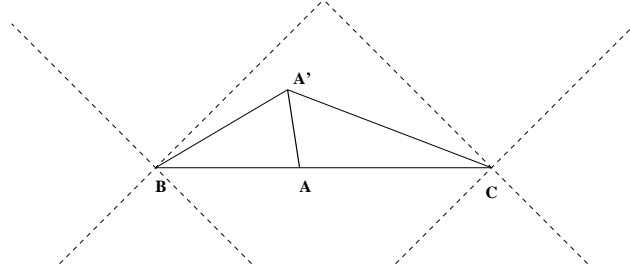
Figure 3.1: An illustration of PIES in a (1+1) skeletonised space-time. The dashed line segments represent the null cones of vertices B and C. Barrett et al. require that the diagonal edges such as BA' be space-like while the evolutionary paths of vertices, such as AA' can be time-like, space-like or null. This condition only prevents the time-like evolutionary paths of vertices not to collide. This condition is a "No Collision" condition which results in a piece-wise linear congruence of non-intersecting paths of evolving vertices.

space-like, it prevents the time-like paths of evolving vertices from colliding in the future. In that sense, it prevents future singularities to occur.

To include causality without violating the above-mentioned condition, one has to look at the past null cone of the evolved counterpart of a vertex. Figure (3.2) shows the situation in a (1+1)-dimensional space-time. It is quite clear that not the entire 1-dimensional piece-wise linear space is within the past null cone of vertex A'.

It is best to discuss causality in a (3+1)-dimensional skeletonised space-time. Consider triangle $\triangle CAB$ in figure (3.3); suppose that CA is a space-like edge on a triangulated 3-dimensional spatial hypersurface. Following the PIES algorithm, assume vertex B is the evolved version of vertex C. Edge BC is time-like but edges AB and CA are space-like as prescribed by the algorithm. CA resides on the initial hypersurface while BC and AB go between the two hypersurfaces. The length of edge BC can be chosen arbitrarily corresponding to the freedom in the choice of lapse. This edge-length will later be used
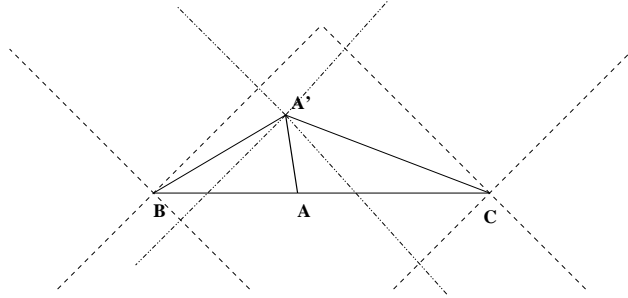
Figure 3.2: Only the information within the past null cone of A' could have affected it. The null cones of A', B and C are represented with dashed lines.

to derive the length of unknown diagonal edges, using Regge Equations. The null cone of vertex B intersects CA at point P. This null cone divides the time-like bone $\triangle CAB$, into a triangle with two space-like and one null edge (NSS) and a triangle with one time-like, one space-like and one null edge (NST). Clearly, only the (NST) part of the bone is in the past domain of dependence of vertex B and could have had any influence on B. Thus to account for causality, we have to include this fact in the action.

To include causality in PIES, instead of the entire area of the bone in Regge action, given by equation (3.1), only the part of area which is within the past null cone of vertex B must be included in the action. In particular, in writing the relevant Regge equations obtained by varying the area of a bone with respect to CB, one has to carry out this variation for the area of the (NST) triangle, $\triangle CBP$.

We now carry out this variation for a time-like bone as well as a space-like bone. In what follows, we will be using the results obtained in appendix (B).
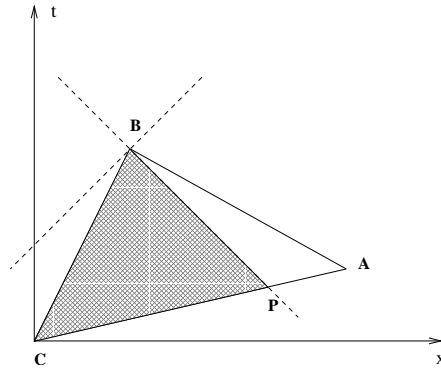
Figure 3.3: Triangle $\triangle CBA$ is a SST triangle and is broken into a NSS triangle, $\triangle PAB$, and a NST triangle, $\triangle CBP$, via the null cone of vertex B, here drawn with dashed lines.
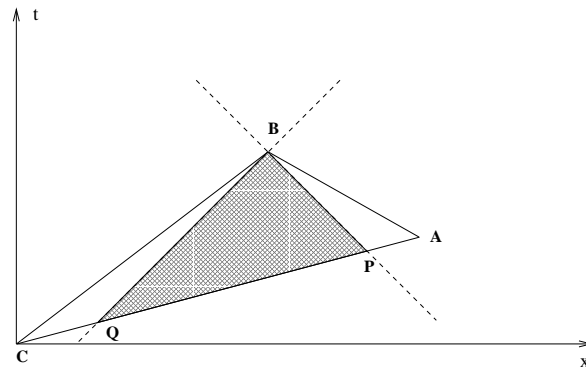
Figure 3.4: Triangle $\triangle CBA$ is a SSS triangle and is broken into two NSS triangles, $\triangle PAB$ and $\triangle CBQ$, and a NNS triangle, $\triangle BPQ$ via the null cone of vertex B, here drawn with dashed lines.
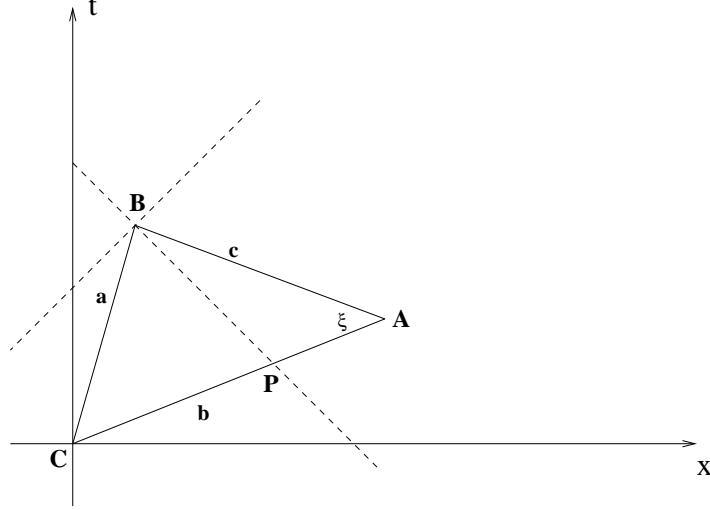
Figure 3.5: The time-like bone $\triangle CAB$ is divided into a NST and a NSS triangle by the null line passing through B.

3.2.1   Variation of a Time-Like Bone with respect to a Time-Like edge

Consider the time-like bone $\triangle CAB$ in figure (3.5). In this triangle we have:

$$A_{\triangle CBP} = A_{\triangle CAB} - A_{\triangle APB}$$

Where $A_{\triangle CBP}$ represents the area of triangle $\triangle CBP$ and so on. From (B.18), one can write:

$$A_{\triangle CBP} = A_{\triangle CAB} - \frac{A_{\triangle CAB}}{2b^2}(a^2 + b^2 + c^2) + \frac{4A_{\triangle CAB}^2}{2b^2}$$

where a, b and c are the edges lengths of triangle $\triangle CAB$, as shown in figure (3.5). Varying the area of $\triangle CBP$ with respect to a, the time-like edge of $\triangle CAB$, one has:

$$\frac{\partial A_{\triangle CBP}}{\partial a} = \frac{\partial A_{\triangle CAB}}{\partial a}(1 - \frac{a^2 + b^2 + c^2}{2b^2} + \frac{4A_{\triangle CAB}}{b^2}) - \frac{a}{b^2}A_{\triangle CAB} \qquad (3.3)$$

but as shown in appendix (B)

$$\frac{\partial A_{\triangle CAB}}{\partial a} = \frac{1}{2}a\frac{(b^2 + a^2 + c^2)}{4A_{\triangle CAB}} = \frac{1}{2}a\,\coth\xi$$

Inserting this in equation (3.3) results in:

$$\frac{\partial A_{\triangle CBP}}{\partial a} = \frac{1}{2}a\,(\coth\xi)(1 - \frac{c}{b}\cosh\xi + \frac{2c}{b}\sinh\xi) - \frac{a}{b^2}A_{\triangle CAB}$$

where we have used

$$4A_{\triangle CAB}/b^2 = (2c/b)\sinh\xi \qquad \text{and} \qquad (c/b)\cosh\xi = (b^2 + a^2 + c^2)/2b^2.$$

One can simplify this equation by replacing $A_{\triangle CAB}$ with $\frac{1}{2}b\,c\sinh\xi$ to obtain:

$$\frac{\partial A_{\triangle CBP}}{\partial a} = \frac{1}{2}a\,(\coth\xi - \frac{c}{b}\,e^{-2\xi}\operatorname{csch}\xi) \tag{3.4}$$

Finally, generalising equation (3.4) for all the bones hanging at edge a, one obtains the relevant Regge equation that must be used in a "causal PIES":

$$\sum_n \frac{1}{2}a\Big[\coth\xi_n - \frac{c_n}{b_n}\,e^{-2\xi_n}\operatorname{csch}\xi_n\Big]\epsilon_n = 0 \tag{3.5}$$

where the sum is over all the bones meeting at the time-like edge "a" and ξ_n is the angle opposite to "a" in the nth bone hanging at edge "a". ϵ_n stands for the deficiency associated with bone n.

3.2.2 Variation of a Space-Like Bone with respect to a Space-Like edge

We now examine the Regge equations associated with a space-like bone. In figure (3.6), the area of the space-like bone, $\triangle CAB$, can be written as:

$$A_{\triangle CAB} = A_{\triangle APB} + A_{\triangle PBQ} + A_{\triangle BQC} \tag{3.6}$$

and thus:

$$\frac{\partial A_{\triangle PBQ}}{\partial c} = \frac{\partial A_{\triangle CAB}}{\partial c} - \frac{\partial A_{\triangle ABP}}{\partial c} - \frac{\partial A_{\triangle BCQ}}{\partial c}$$

$\triangle ABP$ and $\triangle BCQ$ are both (NSS) triangles and their areas, as shown in appendix (B.0.3) are given by:

$$A_{\triangle ABP} = \frac{i}{4}(c^2 - |\overline{AP}|^2) \quad \text{and} \quad A_{\triangle BCQ} = \frac{i}{4}(a^2 - |\overline{CQ}|^2)$$
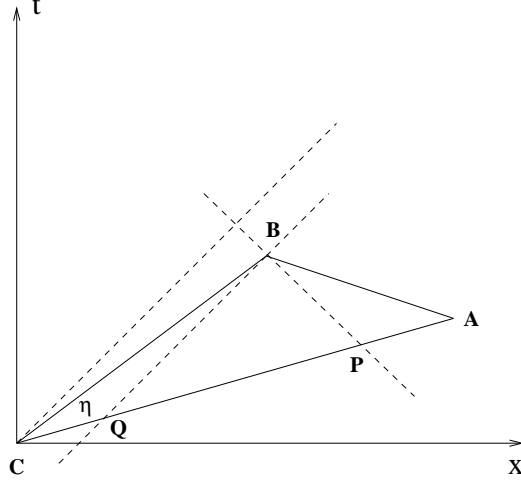
Figure 3.6: In space-like bone $\triangle CAB$, drawing the null cone of B produces three triangles. The angle between $\overline{CA}$ and the x-axis is β while the angle between $\overline{CB}$ and x-axis is α.

where $i = \sqrt{-1}$.

$$\frac{\partial A_{ABP}}{\partial c} = \frac{ic}{2} \tag{3.7}$$

$$\frac{\partial A_{BCQ}}{\partial c} = 0 \tag{3.8}$$

On the other hand, from appendix (B.0.1), the area of $\triangle CAB$ is given by:

$$A^2_{\triangle CAB} = -\frac{1}{16}(a^4 + b^4 + c^4 - 2a^2b^2 - 2a^2c^2 - 2b^2c^2)$$

whence:

$$\frac{\partial A_{\triangle CAB}}{\partial c} = \frac{c}{8A_{\triangle CAB}}(a^2 + b^2 - c^2) \tag{3.9}$$

Using (3.7), (3.8) and (3.9) in (3.6) yields:

$$\frac{\partial A_{\triangle BPQ}}{\partial c} = \frac{c}{8A_{\triangle CAB}}(a^2 + b^2 - c^2) - \frac{ic}{2} \tag{3.10}$$

In triangle $\triangle CAB$,

$$\begin{cases} \overline{CA} = b\left(\sinh\beta\,\hat{t} + \cosh\beta\,\hat{x}\right) \\ \overline{CB} = a\left(\sinh\alpha\,\hat{t} + \cosh\alpha\,\hat{x}\right) \end{cases}$$

$$\overline{CA} \cdot \overline{CB} = ab \cosh \eta \tag{3.11}$$

thus:

$$\cosh \eta = \frac{a^2 + b^2 - c^2}{2ab}$$

In addition, equation (B.1) reads:

$$\sinh^2 \eta = \frac{-4A^2_{\triangle CAB}}{a^2 b^2}$$

Consequently,

$$\coth \eta = \frac{i(a^2 + b^2 - c^2)}{4A_{\triangle CAB}}$$

It is important to note that $\coth \eta$ is a real quantity and the imaginary ι appearing in the numerator of the above equation cancels with the imaginary ι that is built in the area of triangle $\triangle CAB$. Using this result in (3.10) yields:

$$\frac{\partial A_{\triangle BPQ}}{\partial c} = -\frac{ic}{2} (\coth \eta + 1)$$

The Regge equation corresponding to a (SSS) edge is then given by:

$$\sum_n \frac{\partial A_n}{\partial c} \epsilon'_n = -\frac{ic}{2} \sum_n (\coth \eta_n + 1) \, \epsilon'_n = 0 \tag{3.12}$$

where η_n is the angle opposite to edge c in triangle n hanging at this edge and ϵ'_n is the *imaginary* deficit angle corresponding to this bone. It is important to observe that the first term in (3.12) cannot by itself be zero. This means that in an empty curved skeletonised space-time, a space-like edge has both space-like and time-like bones hanging at it.

3.3   Conclusion

In this chapter, we showed how to account for causality in a (3+1)-evolutionary scheme for skeletonised space-times, first introduced by Barrett et al [Barrett et al. 1997]. Both the time-like and space-like types of bones, as classified by Regge, were considered extensively and a new convention concerning the areas of triangles with at least one null side

was set. The Regge equations corresponding to variation of a time-like bone with respect to a time-like edge and the variation of a space-like bone with respect to a space-like edges were obtained. An important observation was made regarding space-like edges. It was shown that in a skeletonised analogue of a curved space-time a space-like edge *cannot* have only space-like bones hanging at it and a combination of both space-like and time-like edges must hang at this bone.

Chapter 4

A Skeletonised Model of the FLRW Universe

4.1 Introduction

If a numerical method is to produce reasonable solutions to Einstein's equation, it must be able to reproduce the known analytical solutions, fairly well. The spatially closed Friedmann-Lemaître-Robertson-Walker (FLRW) Universe is among the most famous solutions to Einstein's equation that is obtained analytically. In this chapter, we show that a skeletonised FLRW universe, using the *revised* PIES algorithm, evolves in a fairly close manner to the corresponding analytical solution. More importantly, we show that the inclusion of causality resolves the problem of "Stop Point" as observed by previous practitioners of Regge Calculus. In section (4.2) of this chapter we briefly review the FLRW solution. We describe the general characteristics of two of the standard triangulations of a 3-sphere in section (4.3). Before approximating the spatially closed FLRW solution using the revised Regge equations, we will discuss the notion of time in the context of Sorkin triangulation and describe a difficulty associated with this notion in section (4.4). We propose an approach towards resolving the ambiguities associated with the notion

of time in Regge Calculus. Section (4.5) describes the initial value problem as well as the evolution problem of FLRW universe in the context of the PIES. Finally, in section (4.7), we will compare the exact spatially closed FLRW model with the same solution as obtained using Sorkin Triangulation. Section (4.8) wraps up this chapter with some concluding remarks. In this chapter, the gravitational constant, G, as well as the speed of light, c, is taken to be equal to one: $c = G = 1$. The cosmological constant, Λ, is set to zero.

4.2   The Friedmann-Lemaître-Robertson-Walker Universe

It is believed that the universe, on its largest scales, at a given moment of time, is spatially homogeneous and isotropic. Homogeneity refers to the fact that the universe looks the same from every point and isotropy implies that the universe, at a given point, looks the same in every direction. Indeed this belief, that goes by the name of "Cosmological Principle", is a revised version of the "Copernican Principle". The "Copernican Principle" insists that the space-time is homogeneous and isotropic, a more precise statement of the fact that we do not occupy any specific position in the Universe. The "Cosmological Principle" is the foundation of the standard model of cosmology. The fact that the deviations from regularity of the Cosmic Micro-Wave Background are on the order of 10^{-5} or smaller is perceived by many to be a strong support for the isotropy of the universe.

Put into more rigourous form, isotropy states that for any two vectors, $\vec{u}$ and $\vec{v}$, in the tangent space of a point P of a manifold M, there exists an isometry of the manifold that takes $\vec{u}$ to $\vec{v}$. Homogeneity states that for any two points in such a manifold, there always exists an isometry that takes one point to the other; in other words, the metric of the manifold is the same everywhere. If the spatial hypersurfaces of a space-time, at a given

instant, are both isotropic and homogeneous then these spatial hypersurfaces are called "maximally symmetric". Schur's lemma [Kobayashi & Nomizu 1963] states that these maximally symmteric spatial slices have uniform curvature. The Weyl tensor associated with the 3-metric of these spatial slices always vanishes and it is possible to show that the Riemann tensor can be written as:

$$R_{abcd} = \frac{R}{k(k-1)}(\gamma_{ac}\,\gamma_{bd} - \gamma_{ad}\,\gamma_{bc}) \tag{4.1}$$

where k is the dimension of the hypersurfaces (which is of course three for a 4-dimensional space-time), R is the Ricci scalar associated with these hypersurfaces and γ_{ij} represents the 3-metric [Carroll 2004].

It is possible to show that the most general form of a metric for a space-time with maximally symmetric spatial slices is the Robertson-Walker (RW) metric given by:

$$ds^2 = -dt^2 + a^2(t)\left(\frac{dr^2}{1-kr^2} + r^2(d\theta^2 + \sin^2\theta\,d\phi^2)\right) \tag{4.2}$$

where $a(t)$ is known as the "Scale Factor" and roughly describes how big the slices of the universe are at a given moment of time. k is a constant representing the curvature. Assuming the topology is trivial, the spatial slices are 3-spheres if $k = 1$, flat if $k = 0$ and hyperbolic if $k = -1$. A more economical representation of the RW metric can be obtained using the following change of variable:

$$d\chi^2 = \frac{dr^2}{1-kr^2} \tag{4.3}$$

This results in a more compact and useful form of the RW metric given by:

$$ds^2 = -dt^2 + a^2(t)\left(d\chi^2 + f^2(\chi)(d\theta^2 + \sin^2\theta d\phi^2)\right) \tag{4.4}$$

In equation (4.4), $f(\chi)$ is a function that can take on one of the following three forms:

$$f(\chi) = \begin{cases} \sin\chi & k = 1 \\ \chi & k = 0 \\ \sinh\chi & k = -1 \end{cases}$$

The time coordinate used in the RW metric is known as the "Cosmological Time" and is measured by the so-called comoving observers. These are observers who stay at a fixed coordinate (r, θ, ϕ). The lapse of their proper time is taken to be equal to the lapse of comoving time. Incidentally, the only observers that perceive the universe as being isotropic are these comoving observers. It is important to further clarify what one means by the expression "Cosmological Time". The notion of a cosmological time or universal time is not unambiguously defined in General Relativity. The so-called "Weyl's Postulate" however provides us with a means of defining a notion of universal time:

> Suppose the worldlines of galaxies form a bundle or more precisely a congru-ence of timelike geodesics that are non-intersecting except for a singularity possibly in the past or in the future or both. Then these worldlines are diverg-ing from a singularity in the past and possibly converging to one in the future. Each of these geodesics passes through one regular point. Then we assume that there exists a set of orthogonal spacelike hypersurfaces to these geodesics. We could parametrise these hypersurfaces with a parameter t which without loss of generality could be chosen to be the proper time along the geodesics [Islam 1992].

The evolution of a universe, endowed with the RW metric, is determined through Einstein's equation,

$$G^{\mu\nu} = 8\pi\, T^{\mu\nu} \tag{4.5}$$

It is customary to take the energy-momentum source to be a perfect fluid represented by:

$$T^{\mu\nu} = (\rho + P)u^{\mu}u^{\nu} + Pg^{\mu\nu} \tag{4.6}$$

where $\vec{u}$ is the four velocity of the particles of the perfect fluid, ρ is the energy-momentum density and P stands for pressure. Inserting the RW metric into Einstein's equation along with the perfect fluid as the energy momentum source yields the famous Friedmann

equations given by:

$$\left(\frac{\dot{a}}{a}\right)^2 = \frac{8\pi}{3}\rho - \frac{k}{a^2} \tag{4.7}$$

$$\frac{\ddot{a}}{a} = -\frac{4\pi}{3}(\rho + 3P) \tag{4.8}$$

In this chapter, we concentrate on the spatially closed FLRW universes with spatial slices having trivial topology and of course the geometry of a three sphere. From this point on, we set $k = 1$ in equation (4.2). These universes are also known as spherical FLRW universes and we will be using this term throughout the rest of this chapter. Setting the pressure, P, equal to zero in the perfect fluid expression gives the equation for dust. The solution to Friedmann equation for a spherical FLRW universe filled with dust is a cycloid given by the following parametric equations:

$$\begin{cases} a = \frac{1}{2}a_{max}(1 - \cos\eta) \\ \\ \tau = \frac{1}{2}a_{max}(\eta - \sin\eta) \end{cases} \tag{4.9}$$
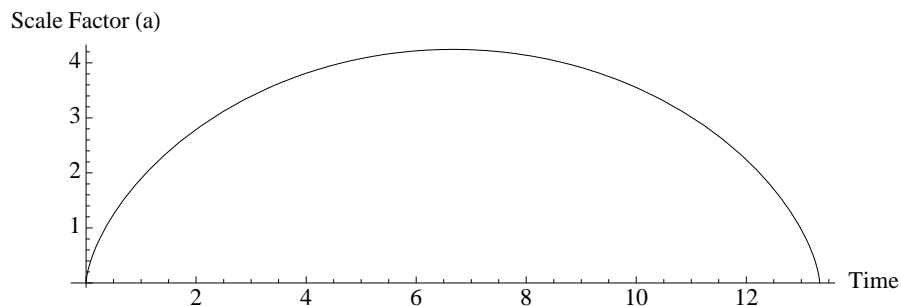
Figure 4.1: The Evolution of a Spherical FLRW Universe with total mass M=10. The maximum value attained by the scale factor is $a_{max} = 4.24413$ and this occurs at $\tau = 6.667$.

Such a universe starts out at a singularity, expands, reaches a maximum size at a_{max} and then starts contracting to collapse to a singularity as shown in figure (4.1).

The maximum value of the scale factor is very closely related to the total mass of this universe and is given by:

$$a_{max} = \frac{4M}{3\pi} \tag{4.10}$$

It is important to note that the notion of the total mass-energy of a spherically closed FLRW universe has no well-defined meaning. The reason is that there exists no platform outside the universe where an observer can stand and measure the attraction of this mass via Keplerian orbits [Misner, Thorne & Wheeler (1972)]. The only reason that the symbol M is interpreted as the total mass of the universe is that during the evolution of a matter dominated universe, the product of "mass-energy density" and volume remains a constant. This constant is represented by symbol M:

$$\rho \cdot 2\pi^2 a^3 = M$$

and it is the value of this constant that is referred to as the total mass of the universe [Misner, Thorne & Wheeler (1972)].

4.3   Standard Triangulations of a 3-sphere

It is clear that the very first step in implementing PIES is the introduction of an appropriate lattice. As we intend to use a (3+1)-evolutionary method based on Regge Calculus, we seek a skeletonisation of a 3-dimensional hypersurface. In the particular case under consideration, the spatial hypersurfaces are 3-spheres. Here, we examine the evolution of the FLRW using two of the standard triangulations of a 3-sphere: the 5-cell and the 16-cell models. One important property of these standard models is that the number of tetrahedrons meeting at each edge of these lattices is the same. This indeed corresponds to the isotropy requirement of the FLRW universe. In what follows, we first give a detailed description of these two standard triangulations of 3-sphere and then will use these two lattices to examine the evolution of a skeletonised FLRW universe.

4.3.1 5-Cell Triangulation of S^3

A 5-cell or Pentatope, represented in figure (4.2), also known as α_4, is the 4-dimensional counterpart of a planar triangle and a solid tetrahedron. It has 5 tetrahedral cells, 10
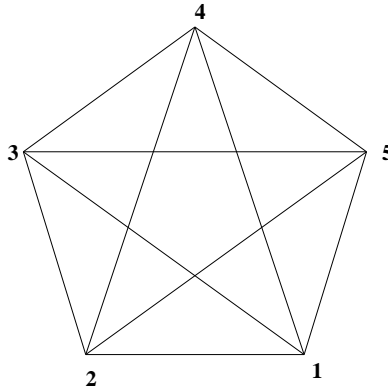
Figure 4.2: A 5-Cell or Pentatope

faces, 10 edges and 5 vertices. The Schläfli symbol [1] for this polychoron is $\{3, 3, 3\}$. Three tetrahedral cells meet at every edge and from each vertex, there emanates four edges. The easiest way to think about this 4-simplex is to imagine that one tetrahedron sits in the middle and on each face of this central tetrahedron one of the four remaining tetrahedra is assembled such that none of the faces of the central tetrahedron is exposed. The apexes of the four external tetrahedra are then identified as a single point in the 4th dimension. The 3-surface of the pentatope is topologically equivalent to a 3-sphere and this hypersurface is considered as the simplest triangulation of a 3-sphere, just as the surface of a solid tetrahedron is a triangulation of a 2-sphere. Similarly, the perimeter of a triangle can be perceived as a piece-wise linear model of a circle. This particular triangulation can be used along with PIES to model a $S^3 \times R$ space-time.

---

[1]The Schläfli symbol of a regular polychoron is given by $\{p, q, r\}$, where $\{p\}$ represents the type of polygonal face, $\{p, q\}$ represents the type of cells and r represents the number of cells meeting at an edge.

4.3.2   16-Cell Triangulation of S^3

The 16-cell or Hexadecachoron is another regular convex polychoron whose hypersurface is considered a standard triangulation for a 3-sphere. It is also known as β_4 in the literature. This 4-dimensional dipyramid is bounded by 16 tetrahedral cells and has 32 triangular faces, 24 edges, and 8 vertices. The Schläfli symbol of the 16-cell model is given by $\{3,3,4\}$. At each vertex, 8 tetrahedra, 12 triangles and 6 edges meet. At every edge, 4 tetrahedra and 4 triangles meet [Coxeter 1973]. In addition to the Pentatope, we will use the surface of this polychoron as the underlying lattice to approximate the spatial hypersurfaces of the FLRW universe.
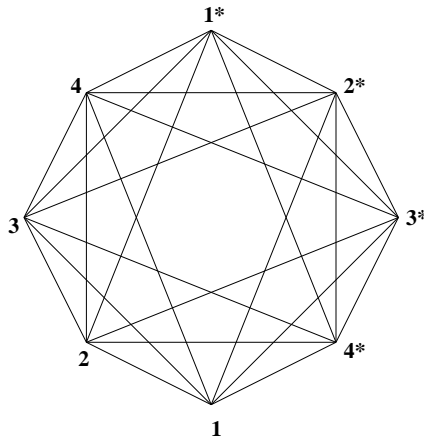
Figure 4.3: A 16-Cell or Hexadecachoron

4.4   The Time-Function in the Parallelisable Implicit Evolutionary Method

One of the most important pieces of required information in solving any second order differential equation is the initial conditions. For a second order differential equation, one requires two pieces of initial conditions, the value of the sought-after function at a given point and its rate of change at that point. Switching to the language of Newtonian

Mechanics, to solve a second order differential equation, one requires both the position and the velocity of an object at a given time.

The Sorkin triangulation method does not introduce the initial data in a time evolution problem comprehensively. In fact, the algorithm is such that it only uses the information on a 3-dimensional *hypersurface*, not a 4-dimensional *thick slice* of spacetime(sandwiched between two consecutive hypersurfaces), to produce the next 3-dimensional hypersurface [Tuckey 1993]. The recipe does not tell one how *fast* the initial slice has evolved to the newly obtained slice. To compare the at-hand situation with the procedure of solving a second order differential equation, in Sorkin triangulation method, one has the value of a function at a given point but not its rate of change at that point.

It is well known that the notion of *measured proper time*, in prism evolutionary methods, is ambiguous. In particular, depending on where an observer is located in a lattice, different times are measured. Some possible cases have been initially explored in the literature [Collins & Williams 1973]. To obtain their choice of time function, Collins and Williams embedded their pentatope universe in a 4-dimensional Euclidean space. More specifically, for the pentatope model in their evolutionary scheme, Collins and Williams explored three possible time functions: elapsed time for a test particle located at the centre of a tetrahedron, elapsed time for a test particle located at a tetrahedron vertex and finally the elapsed time for a test particle that at the moment of time-symmetry lies on the intersection of the 3-sphere of the analytical solution and the corresponding pentatope of the lattice universe. The first choice gives the smallest elapsed time and the second choice gives the largest elapsed time. According to Collins and Williams, any other choice of time function, including the third choice, gives an elapsed time larger than the first choice and smaller than the second choice. The critical issue of elapsed time in a lattice universe was not much explored in the few papers that were written on

skeletonised FLRW universes after that of Collins and Williams. All other works used either the first choice or the second choice of time as presented by Collins and Williams, depending on which one produced a better fit, and did not elaborate on the crucial issue of time.
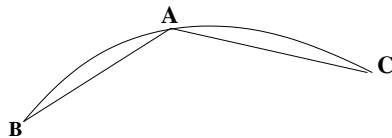
Figure 4.4: An arc segment is approximated using two line segments

Indeed none of the above-mentioned time functions can be taken to represent a global time as defined in the case of the analytical solution using the Weyl postulate. Each of the time functions as defined by Collins and Williams are only the time of a particular observer which is by no means a *preferred* observer. To gain a better understanding of the problem facing us, let us consider the evolution of a 1-dimensional surface. Suppose the curve shown in figure (4.4) is approximated by the two line segments BA and AC and all the information pertaining to this discretisation is at hand. We aim to evolve this structure according to the Sorkin triangulation algorithm. We choose to evolve vertex A first. In principle, according to the algorithm, we can move along any straight line segment, emanating from vertex A, within the future null cone of this vertex. As was discussed earlier, one is free to choose the length of this vertical edge connecting vertex A to its evolved counter-part, say A'. It is well known that, in the continuum, the length of a time-like geodesic represents the time elapsed on the clock of the observer moving along that geodesics. The situation is not much different here as it is clear that the physics of a skeletonised space-time in Regge Calculus is very similar to Special Relativity. Any line segment within the null cone of vertex A, emanating from A, is indeed a piece of a geodesic and its norm represents the elapsed time for an observer moving along this

line segment. In the particular example shown in figure (4.5), one can choose to advance vertex A along any of the paths g_1, g_2, g_3 or g_4. The elapsed time of all such observers are related via Lorentz transformations. In principle, one of these observers measures a time that is either identical or closely related to the lapse of time of a comoving observer, however, it is not possible to identify this observer among the infinite number of observers whose paths are geodesics, starting at vertex A. Since there is not a unique comoving observer at each vertex, but a class of such observers, there is no unique comoving time, but a whole class of choices of comoving time.
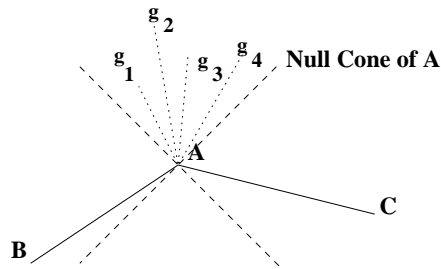
Figure 4.5: One may choose to advance vertex A along any of the geodesics g_1, g_2, g_3 and g_4. Each of these geodesics is the path of a certain observer and each of them measure his own proper time.

One is not even able to define a comoving observer in a manner similar to the Weyl postulate, by using orthogonality of the observer's path to the spatial hypersurface. First of all, the notion of an orthogonal vector at a cone singularity is not well defined. Suppose now that one tries to come up with a definition of an orthogonal vector at a vertex. It is not possible to generalise such a definition to all vertices so to obtain a notion of comoving time. To perceive this, suppose one seeks an orthogonal vector, at vertex A, in the example shown in figure (4.5). One may take the vector average of the two vectors $\vec{V}$, orthogonal to BA, and $\vec{W}$, orthogonal to AC at vertex A and defines this average to be the orthogonal vector at vertex A as shown in figure (4.6). This however is only

a local solution and does not necessarily result in the same elapsed time for all vertices. In particular, there is no guarantee that using the same definition of normals at all the vertices results in equal lapse of time at all the vertices. It is of course well known that
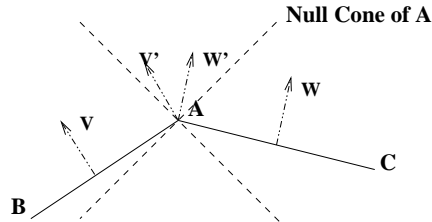
Figure 4.6: Vector $\vec{V}$ is orthogonal to edge BA and vector $\vec{W}$ is orthogonal to edge AC. One may define a normal at vertex A by taking a weighted average of them and measure the lapse of time using this normal. There is however no guarantee that this "Local" solution results into the same lapse of time for every vertex.

one property of comoving observers is that their lapse of proper time is equal and thus this approach does not provide one with a general solution.

A precise analysis of the analytical solution showed that indeed the correct elapsed time must be equal to the 4-volume of the 4-dimensional structure formed in between two 3-dimensional spatial slices divided by the 3-volume of the base. Indeed the resulting expression plays the role of the altitude of this structure. The particular nature of the Sorkin triangulation algorithm however, makes it extremely hard to even recognise the form of this structure. This 4-dimensional object can take on many forms, depending on how one chooses to start the evolution and how the choices of lapse and shift, for each vertex, differs from that of other vertices. An extensive search of current literature did not even reveal a formula through which one can calculate the 4-volume of a structure with two pentatopes of different sizes at the two ends (this object is indeed the higher dimensional replica of a trapezium and a truncated pyramid. The objects formed in the process of Sorkin evolution of course have much more complicated shapes).

Consequently, we commenced a search for possible *measures* of time for the evolution of the FLRW universe using Sorkin Triangulation. Our quest has shown that there exists a family of different time-functions with an undetermined constant coefficient. It must be emphasised that the time-functions obtained, as discussed below, do not represent the proper time or the comoving time. They all however, can be taken to be related to the lapse of time correctly.

The first hint for the correct form of the time-function came from an approach towards quantum gravity known as the "Sum-over-Histories Framework for Gravity" [Sorkin 1994]. It is well known that in this approach the 4-volume can be taken as a measure of time. As was mentioned, it is very difficult to calculate the total volume of a 4-dimensional slice generated using Sorkin algorithm. We however chose the 4-volume of a 4-simplex, that forms upon evolving a certain vertex, as a measure of time. Such a 4-simplex has its base on the old hypersurface and two of its vertices are the particular vertex under consideration and its evolved counter-part and thus always has one time-like edge and nine space-like edges. This volume, represented by δV_4, when scaled by the edge length of the hypersurface that is being evolved (up to an undetermined constant), can be taken as a measure of time as it embraces many features of the initial hypersurface as well as the particular edges used in the course of evolution.

Another appropriate choice of time-function can be taken to be the difference between the 3-volumes of two consecutive spatial 3-dimensional surfaces, scaled by the edge length of the hypersurface. Again, up to an undetermined constant coefficient, the fit produced using this time-function is in good agreement with the analytical solution. Calling the difference between the 3-volumes of two consecutive hypersurfaces δV_3, we have:

$$\delta V_3 = 2\pi^2(a_1^3 - a_2^3)$$

so that

$$t \propto \frac{2\pi^2}{a_1}(a_1^3 - a_2^3)$$

where a is the effective radius associated with the lattice edge lengths of the two consecutive spatial hypersurfaces.

Finally, another measure of the elapsed time could be obtained using a combination of the above-mentioned time-functions. The reason is that the first of these two time-functions certainly has a component in the temporal direction and the second one measures the spatial change of volume and thus combining them in the form of

$$t \propto (\frac{1}{a^2})(\delta V_3)^{\alpha}(\delta V_4)^{(1-\alpha)}$$

certainly produces another measure of time. Here α is an unknown constant power. In section (4.7), we will present the evolution of the 5-Cell and 16-Cell models using the first two choices of time-fucntions as presented above.

4.5   Construction of the Skeletonised FLRW Universe

In this chapter, we show the evolution of the 5-cell and the 16-cell model as obtained through the revised Regge equations for the PIES when plotted against the time functions described in the previous section. The details of the calculations are given over the next two sections. All the previous attempts to evolve a skeletonised spatially closed FLRW universe, using Prism Methods or PIES, have failed. Most notably, Brewin and Barrett et al., studied the evolution of the spatially closed skeletonised FLRW universe extensively, using Regge equations, as introduced by Regge in his seminal paper [Brewin 1987, Barrett et al. 1997].

Their results showed that the evolution of simplicial analogues to spatially closed FLRW universes *stops* well before such universes collapse to zero spatial volume. This
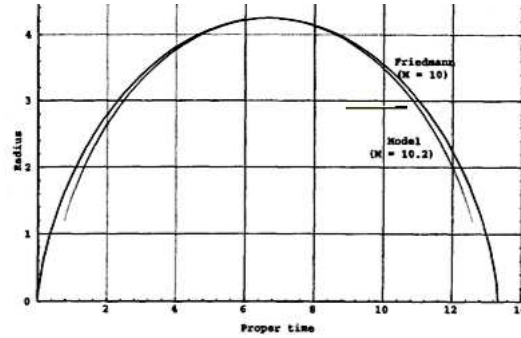
Figure 4.7: The Evolution of the spherical FLRW Universe using the 600-cell triangulation of 3-sphere as obtained by Barrett et al. The evolution stops well before reaching zero spatial volume [Barrett et al. 1997].

problem is usually called the "Stop Point" problem. In particular, Barrett et al. noticed that the point of stop is independent of the length of time-like intervals between two consecutive spatial hyper-surfaces.

Independent of the choice of time function, there is an important characteristic that distinguishes our approximations from the ones performed before. *The evolution of our solution does not stop at a certain volume and the universe collapses to zero spatial volume.* This is a strong indication that the inclusion of causality, as was discussed in chapter (3), removes the obstacle faced by those who used the original form of Regge equation to reconstruct the FLRW universe.

To see how well the revised Regge equations in the Sorkin triangulation approximate the analytical spherical FLRW solution, we take the surfaces of the 5-cell and 16-cell triangulations to represent the skeletonised counter-parts of the 3-sphere. In addition, we take the usual perfect fluid assumption of FLRW universe to be represented by particles of dust. On each vertex of each of the above lattices, we assemble a particle of dust and we take these dust particles to have identical masses.

The code used in the reconstruction of the spherical FLRW universe was developed in Mathematica. The flowchart as well as the code, corresponding to one step of evolution, are included in appendices (D) and (E). The details of obtaining the required parameters used in the code is given over the next few sections.

4.5.1   Construction of the Initial Hypersurface at the Moment of Time-Symmtry

The first step in comparing the skeletonised spherical FLRW universe with the analytical solution is the construction of the triangulated hypersurface at the moment of "Time Symmetry". A 4-geometry is said to be time-symmetric if there exists a space-like hypersurface at all points of which the extrinsic curvature vanishes [Misner, Thorne & Wheeler (1972)]. Before solving the initial value problem, it is necessary to define the notion of "Effective Radius": the "Effective Radius" of the skeletonised universe, denoted by a_e, is found by equating the total volume of a spatial hypersurface of the lattice universe with that of a 3-sphere:

$$2\pi^2 a^3 = k\,\frac{l^3}{6\sqrt{2}}$$

(4.11)

where k is the number of tetrahedral cells.

The next step is to solve the initial value problem at the instant of time-symmetry. It is well known that the initial value problem, for a space-time with an instant of time-symmetry, reduces to [Misner, Thorne & Wheeler (1972)]:

$$^{(3)}R = 16\pi \text{ (energy-density)}$$

(4.12)

where $^{(3)}R$ stands for the 3-dimensional (spatial) Ricci tensor. When written in the context of skeletonised space-times, equation (4.12) has the following appearance

[De Felice & Fabri 2000]:

$$\sum_j \epsilon_{ij} \, l_{ij} = 16\pi \, \frac{M_e}{n} \tag{4.13}$$

where n is the number of vertices of the underlying simplicial complex. The sum is over all the vertices j, joined to vertex i by an edge of length l_{ij}. ϵ_{ij} is the defect over each edge l_{ij} (It is important to note that here, we are looking at a 3-dimensional lattice and thus the defects are concentrated on edges). In any of the standard triangulations of a 3-sphere with Schläfli symbol $\{p, q, r\}$, the number of tetrahedral cells meeting at an edge is equal to r. The dihedral angle between any two faces of an equilateral tetrahedron is equal to arccos(1/3) or approximately 71°. Thus the defect on each edge of a given standard triangulation is:

$$\epsilon = 2\pi - r \ \arccos(1/3)$$

In addition, each vertex is connected to C other vertices (where $C = 4$ for the 5-cell model and $C = 6$ for the 16-cell) and thus equation (4.13), becomes:

$$C \, l_{max} \, (2\pi - r \ \arccos(1/3)) = 16\pi \, \frac{M_e}{n} \tag{4.14}$$

In this equation, l_{max} is the edge length of the skeletonised universe at the moment of time symmetry. This maximum edge length can be obtained using equation (4.11) in reverse by setting $a = a_{max}$, where a_{max} is the scale factor of the analytical solution at the moment of time symmetry. Next by using equation (4.14), one can find the "Effective Mass", M_e, that must be put in the skeletonised universe so that its volume at the moment of time-symmetry is equal to that of the analytical solution.

4.5.2 Evolution of the Initial Hypersurface

With these pieces of initial data at hand, we will now set out to evolve the skeletonised FLRW universe using the revised Regge equation in Sorkin triangualtion. As was mentioned in chapter (2), the fact that the Bianchi identities have a counter-part in Regge Calculus allows us to choose the length of four of the unknown edges arbitrarily. The

length of the remaining edges can be found using corresponding revised Regge equations.

In this section however, we undertake a slightly different approach from what was just described to examine the evolution of the skeletonised FLRW universes. As we intend to test whether the revised PIES algorithm solves the problem of "Stop Point", we make similar assumptions to those made by Barrett et al.[Barrett et al. 1997]. For more discussion on the assumptions, the reader is referred to the paper by Barrett et al. [Barrett et al. 1997]. Following Barrett et al., we assume that there exist homogenous and isotropic solutions to the relevant Regge equations for the lattice universes under consideration. This is indeed equivalent to the assumptions that (i) all diagonal edges at each step are equal, (ii) all the "vertical" time-like edges going between any two consecutive hypersurfaces are equal and finally, (iii) all the edge lengths of a given spatial hypersurface are equal. The assumption about the vertical time-like edges can be seen as a choice of lapse. The assumptions about the diagonal edges as well as the spatial edges however, certainly involve assumptions about the dynamics of the system and are more than a choice of shift.
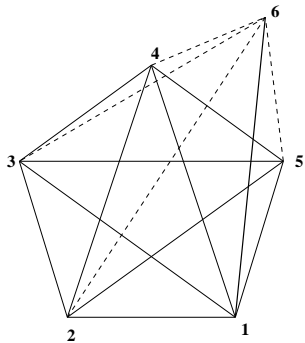
Figure 4.8: First Step in the Evolution of a Pentatope Universe. Vertex [1] evolves to vertex [6].
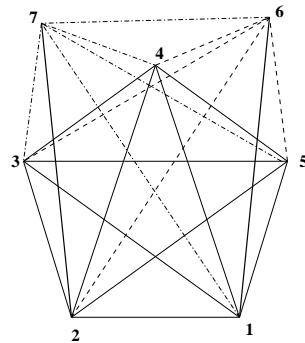
Figure 4.9: Second Step in the Evolution of a Pentatope Universe. Vertex [2] evolves to vertex [7].

Using the above-mentioned assumption of the existence of homogeneous and isotropic

solutions, the evolutions of the 5-cell and the 16-cell universes run very similarly. Thus, we choose to describe the evolution of the pentatope universe in detail and we dispense with details of the 16-cell model calculation. The evolution of the lattice universe consists of two major steps:

In the first step according to the algorithm, we choose a vertex, say vertex [1] in the pentatope universe as shown in figure (4.8), and introduce a new vertex above it; call it [6]. Vertex [6] is then to be connected to [1] by a time-like edge of norm, say ν. This is known as the vertical edge, although it does not have to be orthogonal to the hypersurface. In addition, the algorithm prescribes that all other vertices that are directly connected to vertex [1] on the initial hypersurface must be connected to vertex [6] via space-like edges. The length of these unknown edges will be obtained by solving the corresponding Regge equations. To evolve the pentatope universe, we assume that the length of the time-like vertical edge is given. Given the length of the spatial edges on an initial hypersurface and assuming that all the diagonal edges are equal, we can obtain the length of the diagonal edges by solving the relevant Regge equations.

Next, we pick another vertex on the initial hypersurface, for instance [2], and in a procedure identical to that described earlier for evolution of [1] to [6], evolve [2] into another vertex, say [7]. This step, however, involves an extra task of connecting [6] to [7]. Again, using the assumption of homogeneity and isotropy of the universe, the new diagonal edges introduced in the process of evolving [2] to [7] are taken to have the length of the diagonal edges introduced in the previous step, obtained through Regge equations. The only remaining unknown, appearing in our revised Regge equation, is [67]. The length of [67] can now be acquired by solving the corresponding Regge equation. Since we are assuming that each hypersurface is an equilateral pentatope, finding the length of [67] indeed is the end of an evolutionary step. One can in principle continue this

procedure until the spatial volume of the pentatope universe collapses to zero. We will now describe how the relevant Regge equations, for each step must be obtained.

4.5.3   Lattice Action and the Relevant Regge Equations

The first step in writing the corresponding Regge equations for the lattice universe is to write the relevant Regge action. As was mentioned earlier, we choose to represent the usual perfect fluid assumption of the analytical FLRW universe by dust. In particular, we place one dust particle on each of the vertices of the skeletonised universe at a given instant of time. Each particle is assumed to have a mass of M_e/n where M_e is the *effective mass* of the lattice universe as was described earlier and n is the number of vertices of the lattice. The corresponding action for the skeletonised FLRW universe is then given by (in the units $c = G = 1$):

$$I = \frac{1}{8\pi} \sum_k A_{causal_k} \epsilon_k + \sum_j \frac{M}{n} \nu_j \tag{4.15}$$

where ν_j is the norm of the time-like edge connecting a vertex to its evolved counterpart. The term A_k in the above equation represents the "Causal Area Content" of all those bones with defect ϵ_k on them. In utilising PIES for the evolution of the pentatope universe, two types of bones are distinguishable: (i) time-like bones with two space-like and a time-like edge, in particular a spatial edge, a diagonal edge and a vertical edge (ii) space-like bones with two space-like diagonals and one spatial edge. As we proceed, it will become clear that, for the numerical examples under consideration, we will only be using the time-like bones.

The total action as given by equation (4.15), in principle, can be varied with respect to three types of edges: vertical, spatial and diagonal. The particular assumption of the existence of homogeneous and isotropic solutions however allows us to acquire the desired

solution using only the set of equations that are obtained by variation of the action with respect to the vertical time-like edge. In particular, the variation of the action with respect to a typical vertical edge, ν_i for instance, results in:

$$\frac{1}{8\pi} \sum_k \frac{\partial A_k}{\partial \nu_i} \epsilon_k = \frac{M_e}{5} \tag{4.16}$$

The left-hand side of equation (4.16) is indeed the variation of a time-like bone with respect to a time-like edge. The corresponding equation for this variation was obtained in chapter (3) where we showed how causality can be accounted for. In the next section, we calculate the required parameters for the evolution of the skeletonised universes and customise equation (4.16) for both the 5-Cell and the 16-Cell models.

4.6 Calculation of the Required Parameters

Once the total mass of a spherical FLRW universe is given, the maximum scale factor as well as moment of time symmetry can be obtained. Here we choose to reproduce the evolution of a spherical FLRW universe with total mass of $M = 10$. The maximum scale factor for this universe is given by $a_{max} = \frac{4M}{3\pi} = 4.24413$. The universe attains the maximum volume at $\tau = 6.6667$.

4.6.1 The 5-Cell Universe

Using equation (4.11), for the pentatope universe to achieve the same maximum 3-volume as the above analytical model at the moment of time symmetry, we find $l_{max} = 13.6814$. From this value of l_{max}, using equation (4.14):

$$4\,l_{max}\left(2\pi - 3\ \arccos(1/3)\right) = 16\pi\,\frac{M_e}{5} \tag{4.17}$$

the effective mass for the pentatope universe is equal to $M_e = 14.1005$. Using equation (3.5) of chapter (3), for a pentatope, we have:

$$\sum_{k=1}^{4} \frac{1}{2}\nu\left(\coth \xi_k - \frac{d_k}{l_k}\,e^{-2\xi_k}\,\text{csch}\,\xi_k\right)\epsilon_k = \frac{8\pi}{5}M \tag{4.18}$$

where ξ_k is the hyperbolic angle facing the vertical edge, with respect to which the variation is carried out, in the kth triangle hanging at this vertical edge. Since the initial pentatope is taken to be equilateral, and we are also assuming that each 3-dimensional hypersurface will keep the shape of an equilateral pentatope throughout the evolution, the defect on each of the four triangles hanging at the vertical edge is the same. By the same token, one concludes that all hyperbolic angles, ξ_k, facing the vertical edge, are also equal.

We now have the required equations to evolve the pentatope universe. In the first step of evolution, the unknown is the length of the diagonal edges which can be obtained using equation (4.18). In the second step, the same equation can be used but this time, the unknown is the triangulation edge length of the evolved hypersurface.

4.6.2 The 16-Cell Universe

Following the steps taken for the 5-Cell model, we can obtain the maximum edge length as well as the equivalent mass for the 16-Cell universe. Using equation (4.11), the maximum edge length of the 16-cell model, at the moment of time symmetry, is given by $l_{max} = 9.2843$. From this, using equation (4.14):

$$6\, l_{max}\, (2\pi - 4\ \arccos(1/3)) = 16\pi\, \frac{M_e}{8} \tag{4.19}$$

the total effective mass for the 16-Cell model turns out to be $M_e = 12.0517$. The relevant Regge equation for this triangulation of the 3-sphere is given by:

$$\sum_{k=1}^{6} \frac{1}{2}\nu \left(\coth \xi_k - \frac{d_k}{l_k}\, e^{-2\xi_k}\ \mathrm{csch}\, \xi_k\right)\epsilon_k = \pi M \tag{4.20}$$

4.7 Discussion of the General Space of Solutions

The general space of solutions is very similar for the 5-Cell and the 16-Cell models and thus we start with a general discussion of the roots. To visualise the evolutionary steps

taken, we choose to discuss the example of the pentatope as shown in figures (4.8) and (4.9). In the first step of evolution, vertex [1] is evolved to vertex [6]. The length of [16] is taken to be known using our freedom in the choice of lapse. The length of the diagonal edges that connect vertices [2], [3], [4] and [5] to [6] are unknown. As we seek homogeneous and isotropic solutions, we take all these edge lengths to be equal and denote them by d. Using the Regge equation obtained by varying the action with respect to the time-like edge, [16], one can obtain the length of space-like diagonal edges, d. This Regge equation has two roots. One that is smaller than the edge length of the hypersurface which is being evolved and one that is larger. The smaller root results in a solution corresponding to a space-time that is contracting and the larger one results in a solution that expands indefinitely. As we were examining the contraction of the space-time from the point of time-symmetry on, we were interested in a solution that contracts. Choosing the smaller root to represent the value of the diagonal edges, we may proceed to the next step. Evolving vertex [2] to [7] introduces a number of new edges. Again, as the sought-after solution is required to be homogeneous and isotropic, we take the diagonal edge lengths to be equal to the value obtained in the previous step. The only unknown then is edge [67], the evolved counterpart of edge [12]. Once again, by using the Regge equation obtained by varying the action with respect to the time-like edge, [27], we find the length of edge [67]. This equation also produces two solutions which are both acceptable as they are both contracting. This indeed finishes one full step of evolution as by finding the length of edge [67], we know all the edge lengths of the next spatial foliation or skeletonised hypersurface which is an equilateral pentatope.

The difference between the two spatial roots, obtained in the second step, is less than or of the order of 10^{-2}. The graphs of the larger roots for both the 5-cell and the 16-cell are shown in figures (4.10), (4.11), (4.12) and (4.13). The total number of steps taken to produce the 5-cell graph is 18800 and for the 16-cell graph is 14135. The last value

of the scale factor for the 5-cell model in the graphs shown in figures (4.10) and (4.12) is 2% of the maximum scale factor. For the case of the 16-cell graphs shown in figures (4.11) and (4.13), the last value of the scale factor is 1.1% of the maximum scale factor. *It is quite evident that independent of the choice of time-function, both the 5-cell and the 16-cell universes evolve towards zero spatial volume. This is indeed the most important consequence of the inclusion of causality into PIES and the most notable contribution of this thesis to the field of evolutionary methods in Regge Calculus.* The solution associated with both of the spatial roots however shows a *curious* feature. As the spatial edge length gets closer to zero, it takes more and more steps to make progress. This is reminiscent of collapse towards the singularity of a blackhole. In both cases however, with the use of a good computer, one can satisfactorily get close to zero. Of course, like any other numerical method, we expect that this numerical approximation breaks at some point but the fact that the course of evolution follows the analytical model closely and the stop point is not at about 1/4 of the maximum spatial volume (as others found) is an indication that the modified PIES is a remarkable numerical method.
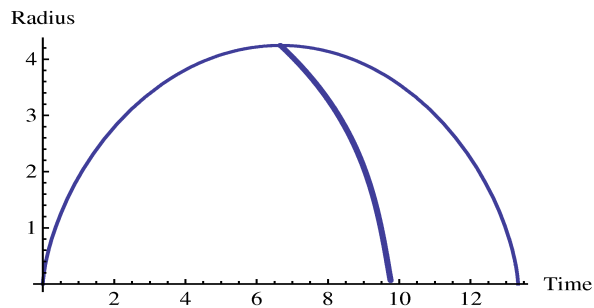
Figure 4.10: The larger root of the 5-Cell model. The time function is taken to be $\frac{1}{20a}\delta V_4$.
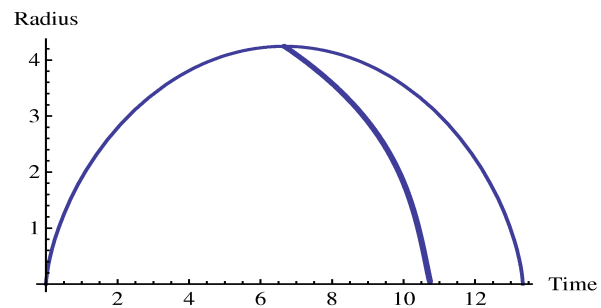
Figure 4.11: The larger root of the 16-Cell model. The time function is taken to be $\frac{1}{4a}\delta V_4$.
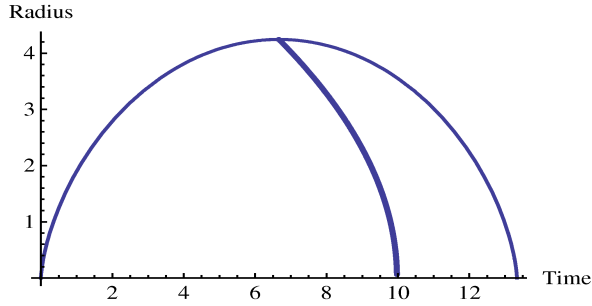
Figure 4.12: The larger root of the 5-Cell model. The time function is taken to be $0.02 \frac{2\pi^2}{a_1}(a_1^3 - a_2^3)$.
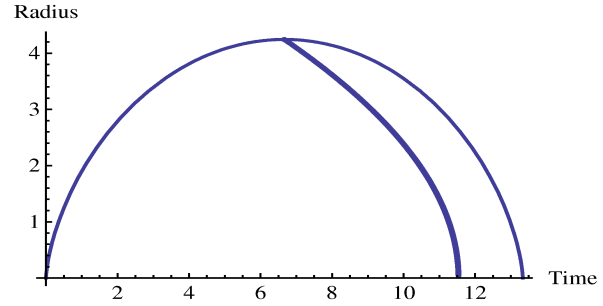
Figure 4.13: The larger root of the 16-Cell model. The time function is taken to be $0.02 \frac{2\pi^2}{a_1}(a_1^3 - a_2^3)$.

4.8   Conclusion

The successful reconstruction of the spherical FLRW universe is evidently a confirmation for the importance of accounting for causality properly in PIES. The inclusion of causality into Parallelisable Implicit Evolution Scheme has indeed perfected the best evolutionary scheme currently at hand in the context of Regge Calculus. This method can now be effectively employed to examine the evolution of manifolds devoid of symmetry or with non-trivial topology. The issue of elapsed time, however is an aspect that requires further investigation. The ambiguities associated with the notion of time were discussed earlier in this chapter. In the particular case considered in this chapter, it was possible to introduce measures of time and as the analytical solution was known, we were able to discern the correctness of the results. A definition of a global time in skeletonised space-times however is essential; otherwise it is impossible to interpret the findings using Regge calculus properly. This issue is certainly worth of further study.

Chapter 5

Triangle Inequalities in the Minkowski Plane

5.1 Introduction

Minkowski geometry is sometimes perceived as the twin of Euclidean geometry. The former is equipped with a metric of semi-definite signature, i.e. $(-, +, +..., +)$ while the latter's metric has a positive definite signature, i.e. $(+, +, ..., +)$. It is well known that the Minkowskian geometry (also known as the Lorentzian geometry), in four dimensions, is the best mathematical tool to describe the Special Theory of Relativity. Although the difference between the Minkowskian and Euclidean geometries appears to be minor at first glance, the simple difference in the metric signature is indeed the underlying cause of the dramatic differences between these two geometries. The so-called paradoxes of the Special Theory of Relativity all emanate from the fact that the underlying geometry of the space-time is Minkowskian rather than the familiar Euclidean geometry.

One of the most prominent characteristics of the plane Euclidean geometry is the validity of the "Triangle Inequality", stating that the norm of the sum of two vectors

is smaller or equal to the sum of their norms . Geometrically, this statement implies that the length of one of the edges of a triangle is always smaller than the sum of the other two edge lengths. A similar statement is true in plane Minkowskian geometry for a certain class of triangles and goes with the name "Reverse Triangle Inequality". However, the properties of the Minkowskian geometry give rise to a number of such inequalities as will be explored in detail over the succeeding sections. The purpose of this chapter is to introduce and prove a number of these inequalities that hold for triangles residing on a Minkowski plane. To our knowledge, except for the "Reverse Triangle Inequality", none of the inequalities presented in this chapter, have been explored in the literature before.

In addition to the geometrical interest, such inequalities constitute an essential part of finite element methods, such as Regge Calculus in the General Theory of Relativity where the space-time is represented by a lattice. In particular, the fact that the relevant edge lengths of a certain simplex, for instance a tetrahedron, satisfy the Euclidean triangle inequality guarantees that the geometry of the space confined within this tetrahedron is Euclidean. Similarly, to ensure that the geometry inside the simplices used to build a lattice space-time is Minkowskian, one has to ensure that the length of any three edges that form a triangle in a Minkowski plane satisfy the relevant triangle inequalities in Minkowskian geometry. More specifically, in gradually building the space-time lattice in "Parallelisable Implicit Evolutionary Method", or any other evolutionary method in the context of Regge Calculus, one has to ensure that these inequalities are satisfied at each stage of evolution.

5.2   Preliminaries

Let L^2 be the vector space R^2 provided with the Minkowskian (Lorentzian) inner product:

$$\vec{v} \cdot \vec{u} = v_1 u_1 - v_2 u_2$$

where $\vec{v} = (v_1, v_2)$ and $\vec{u} = (u_1, u_2)$.

In L^2 a vector $\vec{v}$ is space-like if $\vec{v} \cdot \vec{v} > 0$, time-like if $\vec{v} \cdot \vec{v} < 0$ and null if $\vec{v} \cdot \vec{v} = 0$. The norm of a vector $\vec{v}$, $||\vec{v}||$, is defined by $\sqrt{|\vec{v} \cdot \vec{v}|}$ and is evidently always positive. Let $\vec{e_1} = (1, 0)$ and $\vec{e_2} = (0, 1)$. A vector $\vec{v}$ is called "future-directed" if $\vec{v} \cdot \vec{e_2} > 0$. Furthermore, a vector $\vec{u}$ is called "right-directed" (respectively "left-directed") if $\vec{u} \cdot \vec{e_1} > 0$ (respectively $\vec{u} \cdot \vec{e_1} < 0$) [Birman & Nomizu 1984].

As stated in appendix (A), by Minkowski plane we mean a plane with $(-, +)$ signature or equivalently, a plane with a space-like normal. Such a plane contains time-like, space-like and null lines.

Earlier, we mentioned that the celebrated "triangle inequality" in Euclidean geometry has a counter-part in Minkowskian geometry known as the "Reverse Triangle Inequality". This inequality is valid for pure space-like triangles by which we refer to a triangle built
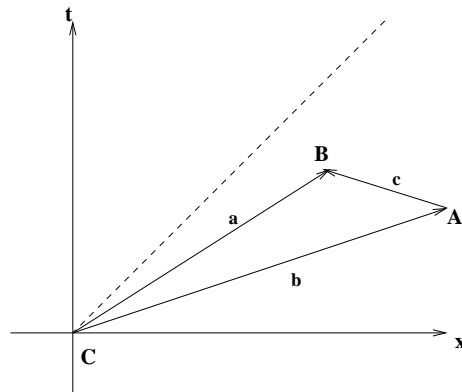
Figure 5.1: A Pure Space-Like Triangle. The Reverse Triangle Inequality states: $a > b+c$

out of only future-directed space-like edges. The "Reverse Triangle Inequality" states that the sum of lengths of the two edges of a pure space-like triangle is smaller than the length of their sum. It is well known that the "Reverse Triangle Inequality" is valid for

pure time-like triangles as well. By a pure time-like triangle we refer to a triangle built out of only future-directed time-like edges.

As was mentioned in the previous chapter, a pure space-like triangle however is not the only possible type of triangle that can be built on a Minkowski plane. One, in principle, can use a number of different combinations of time-like, space-like and null edges to build a triangle. To our knowledge, there do not exist triangle inequalities that relates the edge lengths of these triangles with mixed edges.

This chapter is devoted to presenting a number of triangle inequalities in Minkowskian geometry for triangles with mixed edges. In section (5.3), we describe two inequalities that hold for triangles built out of two space-like and a time-like edge (SST triangles). In section (5.4), another two inequalities that hold true in triangles with two space-like and one null edge (NSS triangles) are introduced.

One note is in place with regards to the conventions used in this chapter. The label of a vector without an arrow at the top of it is meant to refer to the norm of that vector and therefore u refers to the norm of vector $\vec{u}$. We also follow the convention of calling the norm of an edge in a triangle with the lower case character corresponding to the label of the opposite vertex of that triangle. Finally, in all the figures, the dashed lines are meant to present the null lines.

5.3   Triangle Inequalities for a SST Triangle

For the proof of proposition 1 in SST triangles, we introduce the notion of a "twin triangle" to a certain SST triangle. To build a twin triangle to a SST triangle, $\triangle CAB$, we introduce a "twin" vector to the right-directed space-like vector $\vec{CA}$, say $\vec{CA'}$ as shown in
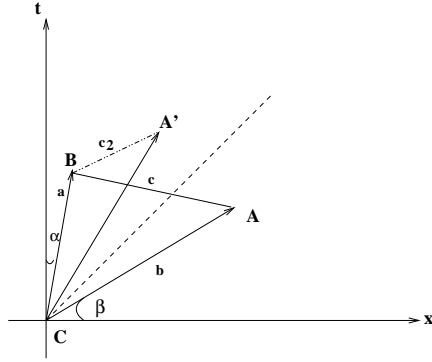
Figure 5.2: $\vec{CA'}$ is the "twin" vector of $\vec{CA}$.

figure (5.2). By a "twin" vector, we mean $\vec{CA'}$ to be a *time-like* vector having the same norm as $\vec{CA}$ such that the angle between $\vec{CA'}$ and the t-axis is equal to that between $\vec{CA}$ and the x-axis. As shown in figure (5.2), a new triangle $\triangle CBA'$ is formed. Depending on the construction of triangle $\triangle CBA$, $\vec{BA'}$, can be either time-like or space-like. The following lemma states the required conditions for $\vec{BA'}$ to be time-like.

Lemma If $-\frac{|\vec{CB}|}{|\vec{CA}|}\frac{\vec{CA}\cdot\vec{CM}}{\vec{CB}\cdot\vec{CM}} > 1$, then $\vec{BA'}$ is time-like. Here, $\vec{CM}$ is the right-directed null vector associated with the null cone of vertex C.

Proof. Suppose that in an arbitrary coordinate system vectors $\vec{CA}$ and $\vec{CB}$ are given by:

$$
\begin{cases}
\vec{CA} &= b\left(\sinh\beta\,\hat{t} + \cosh\beta\,\hat{x}\right) \\
\vec{CB} &= a\left(\cosh\alpha\,\hat{t} + \sinh\alpha\,\hat{x}\right) \\
\vec{CM} &= m\left(\hat{t} + \hat{x}\right)
\end{cases}
\tag{5.1}
$$

where m is an arbitrary scalar

We now show that the stated condition in this lemma is equivalent to $\alpha > \beta$ where α is the angle between $\vec{CB}$ and the t-axis while β is the angle between $\vec{CA}$ and the x-axis as shown in figure (5.2). To see this, we take the dot product of vectors $\vec{CA}$ and $\vec{CB}$

with $\vec{CM}$, using the representations stated in equation (5.1). We have

$$
\begin{aligned}
\vec{CA} \cdot \vec{CM} &= m\,b\,(\cosh\beta - \sinh\beta) = m\,b\,e^{\beta} \\
\vec{CB} \cdot \vec{CM} &= -m\,a\,(\cosh\alpha - \sinh\alpha) = -m\,a\,e^{\alpha}
\end{aligned}
$$

and thus

$$
-\frac{|\vec{CB}|}{|\vec{CA}|}\frac{\vec{CA}\cdot\vec{CM}}{\vec{CB}\cdot\vec{CM}} = \frac{-a}{b}\frac{m\,b\,e^{-\beta}}{-m\,a\,e^{-\alpha}}
$$

but as stated in the lemma

$$
-\frac{|\vec{CB}|}{|\vec{CA}|}\frac{\vec{CA}\cdot\vec{CM}}{\vec{CB}\cdot\vec{CM}} = \frac{e^{\alpha}}{e^{\beta}} > 1
$$

Consequently,

$$
e^{\alpha} > e^{\beta} \Rightarrow \alpha > \beta \qquad\qquad \blacksquare
$$

We now prove that, if $\alpha > \beta$, then $\vec{BA'}$ is time-like.

In triangle $\triangle CBA$ we have:

$$
\vec{AB} = \vec{CB} - \vec{CA}
$$

Squaring both sides of the above equation and noting that $\vec{AB}$ is space-like (so $|\vec{AB}|^{2} > 0$), we have:

$$
AB^{2} = -CB^{2} + CA^{2} - 2\,CA\ CB\ \sinh(\alpha - \beta) > 0
$$

which in turn means:

$$
CA^{2} - CB^{2} > 2\,CA\ CB\ \sinh(\alpha - \beta)
$$

and since $\alpha > \beta$, $2\,CA\ CB\ \sinh(\alpha - \beta) > 0$. Thus one can square both sides of the above equation to find:

$$
(CA^{2} - CB^{2})^{2} > 4\,CA^{2}\ CB^{2}\ \sinh^{2}(\alpha - \beta)
$$

which can be rewritten as:

$$
(CA^{2} - CB^{2})^{2} > 4\,CA^{2}\ CB^{2}\ \cosh^{2}(\alpha - \beta) - 4\,CA^{2}\ CB^{2}
$$

and finally get:

$$(CA^2 + CB^2)^2 > 4\,CA^2\ CB^2\ \cosh^2(\alpha - \beta)$$

taking the square root of this last equation[1] yields:

$$2\,CA\ CB\ \cosh^2(\alpha - \beta) - CA^2 - CB^2 < 0 \tag{5.2}$$

but equation (5.2) indeed implies that $\vec{BA'} \cdot \vec{BA'} < 0$ which in turn means if $\alpha > \beta$, $\vec{BA'}$ is always time-like. In this case, the twin triangle is a pure time-like triangle.   ■

We will now state an inequality that holds for SST triangles with a pure time-like twin:

Proposition 1.   In a SST triangle with a pure time-like twin triangle, $b > c + a$. In other words, the norm of the right-directed space-like edge is always larger than the sum of the norms of the time-like and the left-directed space-like edge.

Proof.   As triangle $\triangle CBA'$ is a pure time-like triangle the "Reverse Triangle Inequality" holds for it:

$$b > a + c_2 \tag{5.3}$$

where $|\vec{BA'}| = c_2$.

We know that:

$$\begin{cases} \triangle CBA' : & \vec{BA'} = \vec{CA'} - \vec{CB} \Rightarrow & c_2^2 = a^2 + b^2 - 2a\,b\,\cosh(\alpha - \beta) \\ \triangle CAB : & \vec{AB} = \vec{CB} - \vec{CA} \Rightarrow & c^2 = b^2 - a^2 - 2\,a\,b\,\sinh(\alpha - \beta) \end{cases} \tag{5.4}$$

and thus:

$$c_2^2 - c^2 = 2\,b\,(b - a\,e^{-(\alpha - \beta)}) \tag{5.5}$$

---

[1]Note that all the variables appearing on both sides of this inequality are indeed positive. CA and CB are norms of vectors which are defined to be positive and the hyperbolic cosine is always larger than 1. Thus, in taking the square root, the direction of the inequality sign does not change.

The fact that $\alpha > \beta$, implies that: $e^{-(\alpha-\beta)} < 1$ and thus:

$$a\,e^{-(\alpha-\beta)} \quad < \quad a$$

$$b - a\,e^{-(\alpha-\beta)} \quad > \quad b - a$$

but from the second expression of equation (5.4) it is clear that since $\vec{AB}$ is space-like and $\alpha > \beta$, then $b > a$. Using this fact, one concludes that $b - a\,e^{-(\alpha-\beta)} > b - a > 0$.

It is then clear that:

$$c_2^2 - c^2 > 0 \tag{5.6}$$

Since c_2 and c are norms of edges, by definition, they are positive and thus the above equation implies:

$$c_2 > c \tag{5.7}$$

Combining (5.7) and (5.3), one arrives at:

$$b > c + a. \qquad \blacksquare$$

Proposition 2.   In a SST triangle, it is always possible to show that: $c < a + b$. In other words, in a SST triangle, the norm of the left-directed space-like edge is always smaller than the sum of the norms of the time-like and the right-directed space-like edge.

Proof.   To prove the inequality stated in proposition 3, we pursue a rather different line of argument. The null vector $\vec{CM}$ in figure (5.3) can always be written as:

$$\vec{CM} = m\,(\hat{t} + \hat{x})$$

where m is a positive scalar. In the reference frame of a certain observer, the edges of
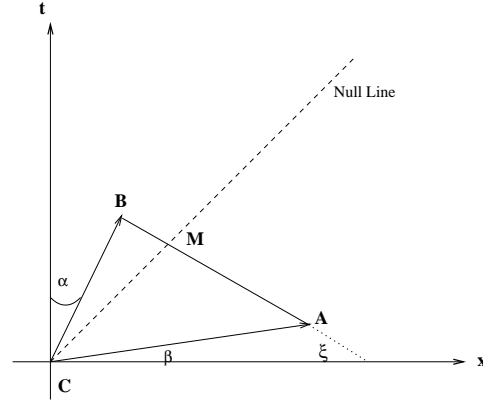
Figure 5.3: Vector $\vec{CM}$ is null.

the triangle $\triangle CBA$ have the following coordinate representation:

$$\begin{cases} \vec{CB} = a\left(\cosh\alpha\,\hat{t} + \sinh\alpha\,\hat{x}\right) \\ \vec{CA} = b\left(\sinh\beta\,\hat{t} + \cosh\beta\,\hat{x}\right) \\ \vec{AB} = c\left(\sinh\xi\,\hat{t} - \cosh\xi\,\hat{x}\right) \end{cases}$$

Taking the dot product of $\vec{CA}$ and $\vec{CB}$ with the null vector $\vec{CM}$, one has:

$$\vec{CB} \cdot \vec{CM} = a\,m\left(\sinh\alpha - \cosh\alpha\right) = -a\,m\,e^{-\alpha} \tag{5.8}$$

$$\vec{CA} \cdot \vec{CM} = b\,m\left(\cosh\beta - \sinh\beta\right) = b\,m\,e^{-\beta} \tag{5.9}$$

Subtracting the above two equations yields:

$$(\vec{CA} - \vec{CB}) \cdot \vec{CM} = a\,m\,e^{-\alpha} + b\,m\,e^{-\beta} \leq m\left(a + b\right)$$

but $(\vec{CA} - \vec{CB}) = -\vec{AB}$ which in turn implies:

$$-\vec{AB} \cdot \vec{CM} \leq m(a + b) \tag{5.10}$$

on the other hand, one has:

$$-\vec{AB} \cdot \vec{CM} = -m\,c\left(-\sinh\xi - \cosh\xi\right) = m\,c\,e^{\xi} \tag{5.11}$$

Combining equations (5.10) and (5.11), one arrives at:

$$c\,e^{\xi} < (a + b)$$

Noting the fact that since $\xi > 0$ then $e^\xi > 1$, the above equation in turn implies:

$$c < a + b. \qquad \blacksquare$$

5.4 Triangle Inequalities for a NSS Triangle

Before stating propositions (3) and (4) concerning inequalities in triangles with two space-like and one null edge, we need to introduce the notion of two co-directed vectors as well as two anti-directed vectors. Two vectors $\vec{u}$ and $\vec{v}$ are called co-directed if $sgn\,(\vec{v}.\vec{e_1}) = sgn\,(\vec{u}.\vec{e_1})$ and $sgn\,(\vec{v}.\vec{e_2}) = sgn\,(\vec{u}.\vec{e_2})$. They are called anti-directed if one or neither of these two conditions hold.
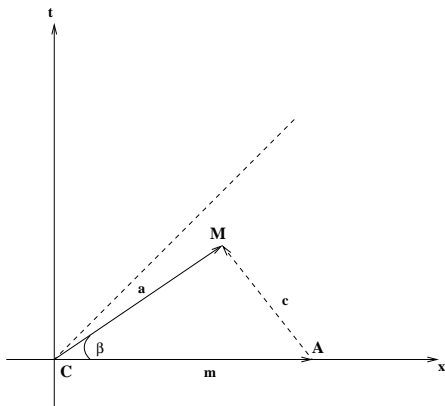
Figure 5.4: $\vec{CA}$ and $\vec{CM}$ are co-directed but they are both anti-directed with respect to $\vec{AM}$.
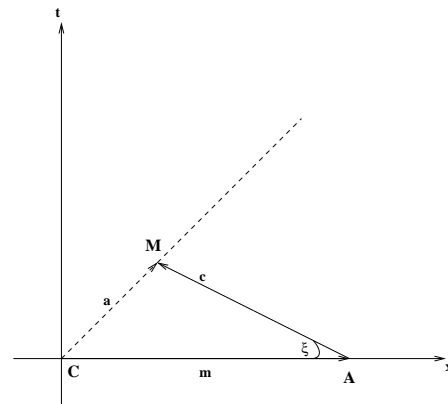
Figure 5.5: $\vec{CA}$ and $\vec{AM}$ are anti-directed but $\vec{CA}$ and $\vec{CM}$ are co-directed.

Another important notion that will be used in the next proposition concerns space-like vector. We call a vector $\vec{v}$ *more space-like* than $\vec{u}$, if $\vec{v} \cdot \vec{e_1} > \vec{u} \cdot \vec{e_1}$.

Finally, it is beneficial to divide the NSS triangles, constructed from only future-directed vectors, into two main groups: those with two co-directed space-like vectors and those with two anti-directed space-like vectors. Proposition (4) concerns the first group of NSS triangles and proposition (5) concerns the second group.

Proposition 3.   In a NSS triangle with two co-directed space-like edges, the length of the more space-like vector is always larger than the length of the less space-like vector.

Proof.   This inequality is rather intuitive as seen in figure (5.4). It is intuitively clear that for the difference of two future directed space-like vectors to be null, the "more space-like vector" must have a larger length.

To see this rigourously however, it is handy to have the coordinate description of the edges constituting triangle $\triangle CAM$ in the frame of reference of a certain observer. Without loss of generality, let us assume that vector $\vec{CA}$ lies along the x-axis:

$$\begin{cases} \vec{CA} = m\,\hat{x} \\ \vec{CM} = a\,(\sinh\beta\,\hat{t} + \cosh\beta\,\hat{x}) \\ \vec{AM} = c\,(\hat{t} - \hat{x}) \end{cases}$$

In triangle $\triangle CAM$, one can write:

$$\begin{cases} \vec{CM} = \vec{CA} + \vec{AM} \\ \vec{CA} = \vec{CM} - \vec{AM} \end{cases}$$

Taking the dot product of each of the above two expressions with itself and using the shorthand notation introduced in figure (5.4), one arrives at:

$$\begin{cases} a^2 = m^2 - 2\,m\,c \\ m^2 = a^2 + 2\,a\,c\,e^{\beta} \end{cases}$$

where β is the angle between $\vec{CM}$ and the x-axis. Adding the above two equations and eliminating $2\,c$, one obtains:

$$a\,e^{\beta} = m$$

Since $\beta > 0$, then $e^{\beta} > 1$ and thus

$$m > a \qquad or \qquad |\vec{CA}| > |\vec{CM}|. \qquad\qquad \blacksquare$$

Proposition 4.   In a NSS triangle with two anti-directed space-like edges, the length of the space-like vector which is co-directed with the null vector is always larger than the length of the space-like vector which is anti-directed with respect to the null vector.

Proof   Pursuing the same line of reasoning as above in NSS triangle $\triangle CAM$, shown in figure (5.4), one has:

$$\begin{cases} \vec{CA} = \vec{CM} - \vec{AM} \\ \vec{AM} = \vec{CM} - \vec{CA} \end{cases}$$

Taking the dot product of each of the above two expressions with itself, one obtains:

$$\begin{cases} m^2 = c^2 + 2\,a\,c\,e^{\xi} \\ c^2 = m^2 - 2\,a\,m \end{cases}$$

Adding up the above two expressions, eliminating $2\,a$ and rearranging, one arrives at:

$$c\,e^{\xi} = m$$

which in turn implies:

$$c < m \qquad or \qquad |\vec{AM}| < |\vec{CA}|. \qquad\qquad \blacksquare$$

5.5 Conclusion

In this chapter, we proved a number of inequalities for triangles with mixed edges on Minkowski plane. We do not claim that we have presented all the triangle inequalities that might hold between the edge lengths of triangles with mixed edges on a Minkowski plane. However, this work is an important step in correctly building lattice space-times in evolutionary methods in the context of Regge Calculus.

An interesting and at the same time reassuring point is that in triangles with null sides, the arbitrary scalar, introduced to facilitate the proofs, does not appear in the final inequality. This of course is what one expects as the scalar chosen to represent the null vectors is completely aribitrary.

Chapter 6

Raychaudhuri's Equation in Regge Calculus

6.1 Introduction

Raychaudhuri's equation has long been of significant importance in the proof of singularity theorems. In addition, it has also been used in other relativistic fields such as gravitational lensing, cracking of self-gravitating objects, etc (for a recent review see [Ellis 2007]). Raychaudhuri's equations represent the evolution of the quantities that characterise a flow. These consist of expansion, shear and rotation of a congruence of time-like (null) curves. The significance of the Raychaudhuri's equations lie in the fact that it clearly reveals the attractive nature of gravity in the absence of shear and vorticity. To best of our knowledge this equation has never been considered in the realm of Regge Calculus [Regge 1961].

Our purpose in this chapter is to find an analogue to Raychaudhuri's equation in the context of Regge Calculus. Such a treatment is essential as it enables us to correctly interpret the dynamical results obtained using Regge Calculus. It also provides insight

into the nature of collapse into a singular state in a skeletonised space-time. Moreover, comparing the continuous results of General Relativity with their counter-parts in Regge Calculus, will give us a better insight into the advantages and shortcomings of this finite element method.

This chapter is organised as follows: In section (6.2), we briefly review Raychaudhuri's equations in continuum. Section (6.3) examines the behaviour of geodesics in skeletonised space-times. In section (6.5.1), we derive analogues to expansion and shear for (2+1)-dimensional lattice space-times. Section (6.6) covers a derivation of similar nature for (3+1)-dimensional skeletonised space-times. We close this chapter with some concluding remarks.

In this work, we assume that the space-times under consideration are close to Minkowskian, i.e. the amount of curvature residing on each bone is very small (weak field limit). In addition, our derivations are valid for a congruence of *time-like geodesics*.

6.2 Raychaudhuri's equation in the Continuum

To contrast the Raychaudhuri equation with its Regge Calculus analogue, it is useful to review this equation in the continuum first. As was mentioned earlier, Raychaudhuri's equations describe the evolution of expansion, shear and vorticity of a congruence of time-like (null) curves. The equation corresponding to the evolution of expansion parameter has however received more attention and it is in fact this equation that goes with the name of Raychaudhuri's equation (it is sometimes also known as Riccati equation [Kar & SenCupta 2007]); we will also follow this convention. In what follows, we will concentrate on time-like curves and later on will only consider time-like geodesics.

For a flow of time-like curves, with 4-velocity vector field, $\vec{v}$, and acceleration $a^\alpha = v^\alpha{}_{;\beta} v^\beta$, the Raychaudhuri equation is given by:

$$\frac{d\theta}{d\tau} = -\frac{1}{3}\theta^2 - 2\sigma^2 + 2\omega^2 + a^\alpha{}_{;\alpha} - R_{\alpha\beta}v^\alpha v^\beta \tag{6.1}$$

In the above equation $\theta = v^\alpha{}_{;\alpha}$ represents expansion. The shear scalar is represented by σ where $\sigma^2 = \sigma_{\alpha\beta}\sigma^{\alpha\beta}$ and

$$\sigma_{\alpha\beta} = v_{(\alpha;\beta)} - a_{(\alpha}v_{\beta)} - \frac{1}{3}\theta h_{\alpha\beta}$$

with

$$h_{\alpha\beta} = g_{\alpha\beta} - v_\alpha v_\beta/(v_\sigma v^\sigma)$$

being the projection tensor. Finally, $\omega^2 = \omega_{\alpha\beta}\omega^{\alpha\beta}$ is the vorticity or rotation where

$$\omega_{\alpha\beta} = v_{[\alpha;\beta]} - a_{[\alpha}v_{\beta]}$$

If the energy-matter content of the space-time is a perfect fluid, given by

$$T^{\mu\nu} = (P + \rho)u^\mu u^\nu + P g^{\mu\nu},$$

the last term on the right hand side of equation (6.1) can be replaced by $-\frac{1}{2}\kappa(\rho + 3P)$ using Einstein's Equation. Provided that $\rho + 3P \geq 0$, for a congruence of time-like geodesics, clearly, it is only vorticity that opposes collapse. The sign of acceleration is indefinite (of course when considering time-like geodesics, the acceleration term vanishes). Shear, energy density and pressure all promote collapse.

We close this section by reminding the reader of the Focusing Theorem. The focusing theorem, an important consequence of Raychaudhui's equation, states that if the strong energy condition holds, i.e. $\rho + 3P \geq 0$, a time-like geodesic congruence that is hypersurface orthogonal (i.e. $\omega_{\alpha\beta} = 0$) will contract and collapse to a singularity during a finite amount of time.

6.3 Geodesics in Regge Calculus

One can obtain much insight into the structure of a skeletonised space-time by examining the behaviour of two initially parallel geodesics, enclosing a bone. The derivation of analogues to expansion and shear scalar is much simplified by this preliminary consideration. We should mention that, in all the derivations presented in this chapter, we take the congruence of the geodesics to be irrotational. The space-time curvature is not continuous in Regge calculus but, as stated earlier, is concentrated on $(n-2)$-dimensional bones. As the geometry is flat within simplices, geodesics are straight lines. When a geodesic moves from one simplex to the next, the transition is such that the angle between the geodesic and the normal to the entrance face is equal to that between the geodesic and the normal to the exit face. [Chakrabarti et al. 1999]. Figure (1) shows this clearly for a skeletonised 2-dimensional manifold. Here the building blocks are triangles and the curvature is concentrated on vertices or 0-dimensional simplices (clearly, for a 2-dimensional skeletonised manifold, face corresponds to edge) .
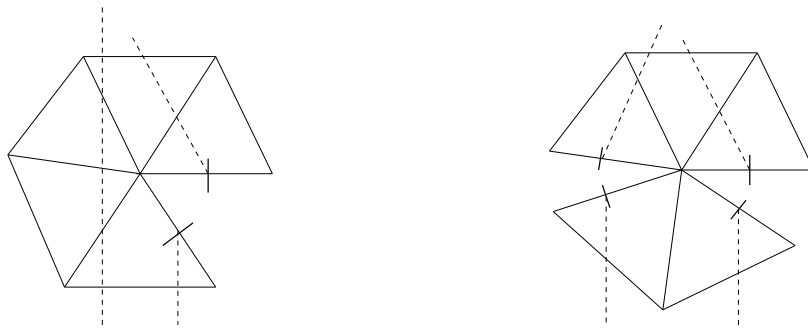
Figure 6.1: The paths of two initially parallel geodesics on a triangulated 2-d manifold, enclosing a vertex. As shown, representation is not unique, however, the total rotation of the two geodesics with respect to their initial paths always equals the deficiency of the enclosed bone.

Two initially parallel geodesics will remain parallel unless they enclose a bone. The rotation of one of the geodesics with respect to the other is equal to the deficit an-

gle concentrated on the enclosed bone. There is however no unique representation for the behaviour of the geodesics [Chakrabarti et al. 1999]. One can take one of the two geodesics to remain unchanged and the other one to rotate by an angle equal to the deficiency of the enclosed bone. Equally, one can take each of the two geodesics to rotate, with respect to its initial path, by an angle equal to half of the deficiency of the enclosed bone as shown in the right panel of figure (6.1). It is important to point out that such rotation is only revealed upon examining two geodesics enclosing a bone. Looking at one single geodesic will not uncover this rotation (and in turn the curvature). This of course is reminiscent of the continuum case. The curvature of a manifold is only revealed by considering the paths of two initially parallel geodesics.

To conclude this section we note that, if one considers two initially parallel rays that enclose a number of vertices between them, one can always think of one of the two geodesics to rotate with respect to the other by an angle that is equal to the sum of deficit angles on the bones enclosed [Chakrabarti et al. 1999].

6.4 Expansion of Two non-Parallel Geodesics in Flat Space-Time

To analyse the evolution of a congruence of time-like geodesics in a skeletonised space-time, consider the two geodesics, g_1 and g_2, shown in figure (6.2). We initially assume that these two geodesics do not enclose any bones on their way, thus the the expansion (contraction) considered here arises merely from the paths of the two geodesics.

If extended, these two geodesics will cross each other at an angle α. Suppose that the proper time is measured along geodesic g_1. In addition, suppose that the distance between
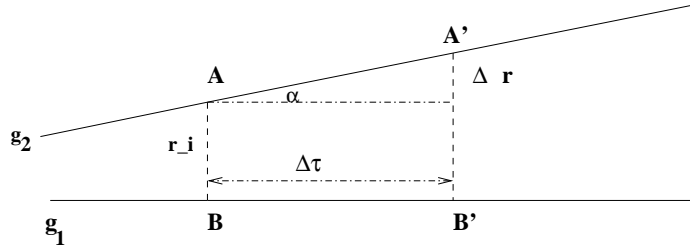
Figure 6.2: Paths of Two Non-Parallel Geodesics in a Flat Space-Time

the two geodesics, at a given proper time, is defined to be the length of a perpendicular line segment to g_1, starting from point B on g_1, and extended until crossing g_2 at point A. If there exists no curvature, then after proper time $\Delta\tau$ has elapsed along g_1, the distance between the two geodesics is increased by Δr given by:

$$\Delta r = \Delta\tau \tan\alpha \tag{6.2}$$

thus

$$\overline{A'B'} = \overline{AB} + \Delta\tau \tan\alpha \tag{6.3}$$

The fact that we choose our congruences of geodesics to be irrotational guarantees that any two geodesics, chosen from a given congruence, are coplanar. *Therefore, this result is always true independent of the dimension of the flat space-time under consideration.*

6.5 Raychauduri's Equation in (2+1)-Dimensional Skeletonised Space-Times

To find an analogue to Raychaudhuri's equation in the framework of Regge Calculus, it is easier to first examine expansion and shear in a (2+1)-dimensional space-time. The curvature of a 3-dimensional skeletonised manifold is concentrated on 1-dimensional edges. In general, this bone can be oriented in three different positions with respect to the plane
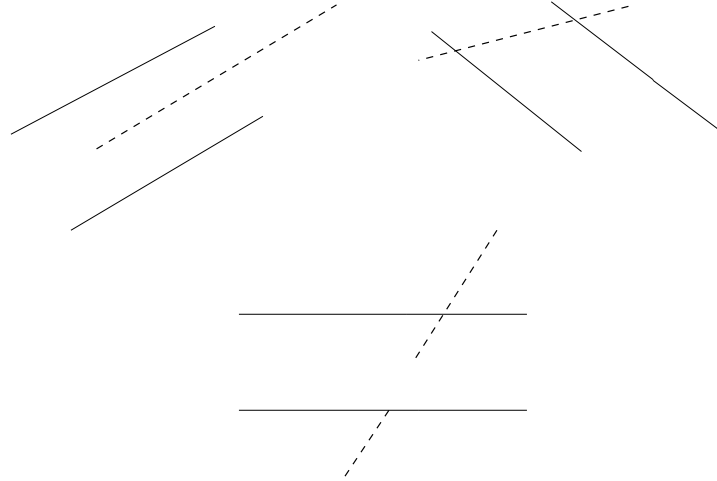
Figure 6.3: Possible orientation of a bone with respect to the plane of two geodesics in (2+1)-dimensions.

that passes through any two geodesics enclosing this bone:

 (i) The bone is parallel or anti-parallel to this plane (the case where the bone lies in the same plane is also classified as a special case belonging to this category).

 (ii) The bone is orthogonal to the plane passing through the two geodesics.

 (iii) The bone pierces through the plane passing through the two geodesics, making an arbitrary angle with the geodesic under consideration (or a beam parallel to them passing through the perforation location).

Different orientations of a bone with respect to the plane of two geodesics is shown in figure (6.3). The particular orientation described in (i) does not result in any deviation in the path of any of the two geodesics. Obviously, the second case in the above list is a special case of the third one and thus we will examine the third case in detail. In both three and four dimensional cases, we will assume that the deficiency corresponding to each bone is small and the bones enclosed are all parallely oriented (weak field limit) [Regge 1961].

6.5.1 Distance between two geodesics in (2+1) Skeletonised Space-Times

Suppose now that the two geodesics g_1 and g_2 enclose a bone of positive deficiency ϵ, represented by a unit vector $\vec{P}$ chosen on this bone, as shown in figure (6.4). As the proper time is measured along g_1, $\overline{O_1O_2}$ and $\overline{O_1'O_2'}$ are taken to be perpendicular to g_1. Without loss of generality, we assume that upon enclosing bone $\vec{P}$ geodesic g_1 rotates towards g_2 and g_2 continues on its old path. We have chosen the unit vector $\vec{AO_2'}$ on g_1 to represent this geodesic (Note that the results obtained below remain unchanged, if one chooses to measure the proper time along g_2 while keeping it on its initial path). The
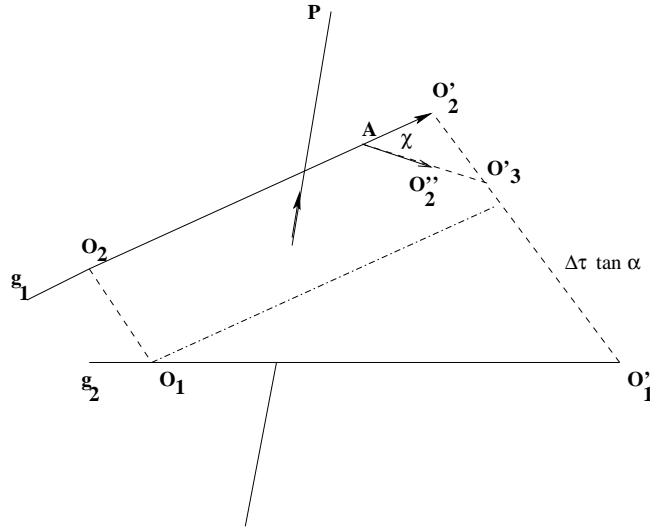
Figure 6.4: Paths of Two Geodesics Enclosing a Bone of Deficiency ϵ in (2+1)-dimensions

distance between g_1 and g_2 after proper time $\Delta\tau$ elapses on g_1 is given by: $\overline{O_1'O_3'}$. This change of distance between g_1 and g_2 in turn is given by:

$$\overline{O_1'O_3'} = \overline{O_1O_2} + \Delta\tau \tan\alpha - \overline{O_2'O_3'} \qquad (6.4)$$

where the last term comes from the distortion caused by the deficiency on the $\vec{P}$. Upon passing by $\vec{P}$, vector $\vec{AO_2'}$ undergoes a rotation, by an angle ϵ, with $\vec{P}$ as the axis of the rotation. Calling the rotated $\vec{AO_2'}$, $\vec{AO_2''}$, it is easy to see that the length of $\vec{AO_2''}$ is not

necessarily equal to $\overline{AO_3'}$. To calculate $\overline{O_2'O_3'}$, it is enough to find the angle between $\vec{AO_2'}$ and $\vec{AO_2''}$. As we are considering the rotation of vector $\vec{AO_2'}$ around axis $\vec{P}$, we have:

$$\vec{AO_2''} = \vec{P} \times (\vec{AO_2'} \times \vec{P}) \cos \epsilon + (\vec{P} \times \vec{AO_2'}) \sin \epsilon + \vec{P}(\vec{AO_2'} \cdot \vec{P}) \tag{6.5}$$

We take the dot product of both sides of equation (6.5) by $\vec{AO_2'}$ to get:

$$\begin{aligned} \vec{AO_2'} \cdot \vec{AO_2''} &= \vec{AO_2'} \cdot [\vec{P} \times (\vec{AO_2'} \times \vec{P})] \cos \epsilon \\ &+ \vec{AO_2'} \cdot (\vec{P} \times \vec{AO_2'}) \sin \epsilon + \vec{AO_2'} \cdot \vec{P}(\vec{AO_2'} \cdot \vec{P}) \end{aligned} \tag{6.6}$$

which can be written as:

$$\begin{aligned} \vec{AO_2'} \cdot \vec{AO_2''} &= \vec{AO_2'} \cdot [\vec{AO_2'}(\vec{P} \cdot \vec{P}) - \vec{P}(\vec{P} \cdot \vec{AO_2'})] \cos \epsilon \\ &+ \vec{P} \cdot (\vec{AO_2'} \times \vec{AO_2'}) \sin \epsilon + \vec{AO_2'} \cdot \vec{P}(\vec{AO_2'} \cdot \vec{P}) \end{aligned} \tag{6.7}$$

Of course $\overline{AO_2'} = \overline{AO_2''}$ and we have chosen both of them to be unit vectors. Thus, simplifying equation (6.7) yields:

$$\vec{AO_2'} \cdot \vec{AO_2''} = \vec{AO_2'} \cdot (\vec{AO_2'} - \vec{P} \cos \phi) \cos \epsilon + (\vec{AO_2'} \cdot \vec{P}) \cos \phi$$

Calling the angle between the two vectors $\vec{AO_2'}$ and $\vec{P}$, ϕ, and noting that χ is the angle between $\vec{AO_2'}$ and $\vec{AO_2''}$ as shown in figure (6.4), we can simplify the above equation to obtain:

$$\cos \chi = (1 - \cos^2 \phi) \cos \epsilon + \cos^2 \phi = \sin^2 \phi \, \cos \epsilon + \cos^2 \phi \tag{6.8}$$

It is easy to see that:

$$\frac{\overline{O_2'O_3'}}{\overline{AO_2'}} = \tan \chi \quad \Rightarrow \quad \overline{O_2'O_3'} = \tan \chi \tag{6.9}$$

Therefore, $\overline{O_1'O_3'}$ is given by:

$$\overline{O_1'O_3'} = \overline{O_1'O_2'} - \overline{O_2'O_3'}$$

$$\overline{O_1'O_3'} = \overline{O_1O_2} + \Delta\tau \, \tan \alpha - \tan \chi \tag{6.10}$$

where $\tan \chi$ can be obtained as follows. Equation (6.8) reads:

$$\cos \chi = \sin^2 \phi \, \cos \epsilon + \cos^2 \phi \tag{6.11}$$

Since ϵ is very small (weak field limit), we expand $\cos\epsilon$ around zero and write:

$$\cos\chi = \sin^2\phi\left(1 - \frac{\epsilon^2}{2}\right) + \cos^2\phi = 1 - \frac{\epsilon^2}{2}\sin^2\phi \qquad (6.12)$$

and thus

$$\cos^2\chi = \left(1 - \frac{\epsilon^2}{2}\sin^2\phi\right)^2 = 1 - \epsilon^2\sin^2\phi + H.O.(\epsilon^4) \qquad (6.13)$$

which in turn yields:

$$\tan^2\chi = \frac{\epsilon^2\sin^2\phi}{1 - \epsilon^2\sin^2\phi} \qquad (6.14)$$

$$\tan^2\chi = \epsilon^2\sin^2\phi(1 - \epsilon^2\sin^2\phi)^{-1} \qquad (6.15)$$

$$\tan^2\chi = \epsilon^2\sin^2\phi + H.O.(\epsilon^4) \qquad (6.16)$$

Using this result in equation (6.10), we obtain:

$$\overline{O_1'O_3'} = \overline{O_1O_2} + \Delta\tau\,\tan\alpha - \epsilon\sin\phi \qquad (6.17)$$

where α is the angle between the two geodesics, ϵ is the deficiency of the bone and ϕ is the angle between $\vec{P}$ and geodesic g_1.

6.5.2 Expansion and Shear in (2+1)-dimensional Skeletonised Space-Times

Figure (6.5) depicts the circular cross section of a congruence of time-like geodesics. Three geodesics are shown in this figure. We make the following assumptions:

$$\begin{cases} \text{Angle between } \vec{P} \text{ and } g_2: & \phi \\ \text{Angle between } \vec{P} \text{ and } g_3: & \xi \\ \text{Angle between } g_1 \text{ and } g_2: & \alpha \\ \text{Angle between } g_1 \text{ and } g_3: & \beta \end{cases}$$

After time $\Delta\tau$ elapses on g_1, using the results obtained in the previous section, we have:

$$\begin{cases} \overline{O_1'O_2'} = \overline{O_1O_2} + \Delta\tau\tan\alpha - \epsilon\sin\phi \\ \overline{O_1'O_3'} = \overline{O_1O_3} + \Delta\tau\tan\beta - \epsilon\sin\xi \end{cases}$$
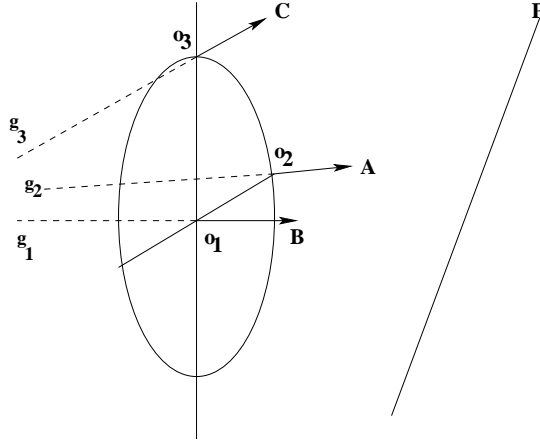
Figure 6.5: The Circular Cross Section of a Congruence of Geodesics in a (2+1)-dimensional Skeletonised Space-time

where $\overline{O_1O_2} = \overline{O_1O_3} = r_I$ and r_I stands for the initial radius of the circular cross section. Taking the average of $\overline{O_1'O_2'}$ and $\overline{O_1'O_3'}$ to find the average expansion, one finds:

$$a = \frac{\overline{O_1O_2} + \overline{O_1O_3}}{2} = r_I + \frac{\Delta\tau}{2}(\tan\alpha + \tan\beta) - \frac{\epsilon}{2}(\sin\phi + \sin\xi) \tag{6.18}$$

and thus the expansion is given by:

$$\theta = \frac{\Delta\tau}{2}(\tan\alpha + \tan\beta) - \frac{\epsilon}{2}(\sin\phi + \sin\xi) \tag{6.19}$$

The first term on the right hand side of equation (6.19) represents an average expansion caused by the paths of the geodesics and the fact that we chose them not to be parallel. This expansion was explained in detail in section (6.5.1) while the second term on the right hand side represents an average contraction caused by the deficiency of the bone. Of course if the bone deficiency is negative, this term also represents expansion.

To obtain the shear scalar, we subtract the average expansion, a, from $\overline{O_1'O_2'}$ and $\overline{O_1'O_3'}$ to obtain:

$$\begin{cases} \overline{O_1'O_2'} - a = \frac{\Delta\tau}{2}(\tan\alpha - \tan\beta) - \frac{\epsilon}{2}(\sin\phi - \sin\xi) = \sigma \\ \overline{O_1'O_3'} - a = -\left(\frac{\Delta\tau}{2}(\tan\alpha - \tan\beta) - \frac{\epsilon}{2}(\sin\phi - \sin\xi)\right) = -\sigma \end{cases}$$

where σ indeed plays the role of the shear scalar. Again, had we chosen the congruence to be a congruence of initially parallel geodesics, the term $\frac{\Delta\tau}{2}(\tan\alpha - \tan\beta)$ would not have appeared in the expression for σ. The second term in the expression of σ however represents the net effect of the curvature residing on the bone.

6.6   Raychaudhuri's Equation in (3+1)-Dimensional Skeletonised Space-Times

We will now attempt to find an analogue to expansion and shear scalar in a (3+1)-dimensional skeletonised space-time. In a skeletonised 4-dimensional manifold, the curvature resides on triangles, where a number of 4-simplices meet. A vector that is parallel transported around a loop enclosing an isolated triangle rotates by an angle equal to the deficiency of this triangle. In this process, the projection of this vector on the triangle remains unchanged and only the orthogonal component of this vector is rotated [Wheeler 1964].
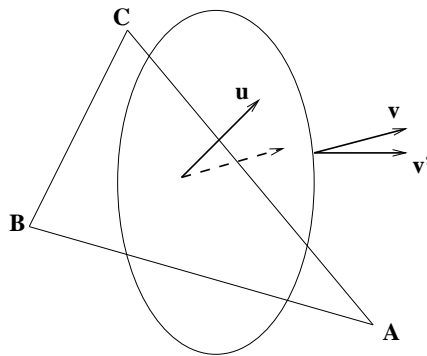
Figure 6.6:   Vector $\vec{v}$ is parallel transported around a loop enclosing Triangular bone ABC.

Let's examine the change in a vector $\vec{v}$, parallel transported around a loop that encloses a triangular bone with deficiency ϵ, as shown in figure (6.6). Suppose vector $\vec{u}$ is

the normal to this triangular bone. One can then break vector $\vec{v}$ into two orthogonal components, one parallel to $\vec{u}$ and the other perpendicular to it:

$$\vec{v} = \vec{u} \times (\vec{v} \times \vec{u}) + \vec{u}(\vec{u} \cdot \vec{v}) \tag{6.20}$$

where the first term on the right hand side of equation (6.20) is orthogonal to $\vec{u}$ and will be denoted by $\vec{v_\perp}$ and the second term on the right hand side of equation (6.20) is parallel to $\vec{u}$ and will be denoted by $\vec{v_{||}}$. We take the axis of rotation to be:

$$\vec{P} = \frac{\vec{v_\perp}}{|\vec{v_\perp}|}$$

as this is the simplest choice arising from the definition of parallel transport of the component that is perpendicular to the plane of the triangular bone, along a path encircling the bone. Upon rotation, we get:

$$\vec{v'_{||}} = \frac{\vec{v_\perp}}{|\vec{v_\perp}|} \times (\vec{v_{||}} \times \frac{\vec{v_\perp}}{|\vec{v_\perp}|}) \cos \epsilon + (\frac{\vec{v_\perp}}{|\vec{v_\perp}|} \times \vec{v_{||}}) \sin \epsilon \tag{6.21}$$

which can be written as:

$$\vec{v'_{||}} = \left[\vec{v_{||}}(\frac{\vec{v_\perp}}{|\vec{v_\perp}|} \cdot \frac{\vec{v_\perp}}{|\vec{v_\perp}|}) - (\vec{v_{||}} \cdot \frac{\vec{v_\perp}}{|\vec{v_\perp}|})\frac{\vec{v_\perp}}{|\vec{v_\perp}|} \right] \cos \epsilon + (\frac{\vec{v_\perp}}{|\vec{v_\perp}|} \times \vec{v_{||}}) \sin \epsilon \tag{6.22}$$

Simplifying the above expression:

$$\vec{v'_{||}} = \vec{v_{||}} \cos \epsilon + (\frac{\vec{v_\perp}}{|\vec{v_\perp}|} \times \vec{v_{||}}) \sin \epsilon \tag{6.23}$$

If ϵ is small, by expanding $\cos \epsilon$ and $\sin \epsilon$, we can write:

$$\vec{v'_{||}} = \vec{v_{||}} + (\frac{\vec{v_\perp}}{|\vec{v_\perp}|} \times \vec{v_{||}})\epsilon \tag{6.24}$$

It is then clear that $\vec{v'}$ is given by:

$$\vec{v'} = \vec{v'_{||}} + \vec{v_\perp} = \vec{v_{||}} + \vec{v_\perp} + (\frac{\vec{v_\perp}}{|\vec{v_\perp}|} \times \vec{v_{||}})\epsilon \tag{6.25}$$

which in turn reads:

$$\vec{v'} = \vec{v} + (\frac{\vec{v_\perp}}{|\vec{v_\perp}|} \times \vec{v_{||}})\epsilon \tag{6.26}$$

Thus, the change in the length of vector $\vec{v}$, after rotation, is given by:

$$|\vec{v'} - \vec{v}| = |\vec{v_{||}}|\epsilon = (|\vec{v}| \cos \phi)\epsilon \tag{6.27}$$

where ϕ is the angle between $\vec{u}$, the normal to the bone, and $\vec{v}$.

6.6.1 Expansion in (3+1)-dimensional Skeletonised Space-Times

To obtain the expansion for a (3+1)-dimensional manifold, one follows a similar procedure to that under-taken in section (6.5.1). There are however subtle differences between the two which will be explained in this section. As was discussed earlier, in an irrotational congruence of geodesics, independent of the dimension of a skeletonised space-time, one can always pass a plane through any two geodesics of this congruence. The construction here is similar to what we had in section (6.5.1) with the difference that the bone in this case is a triangular one as shown in figure (6.7). Again, suppose that the proper time is
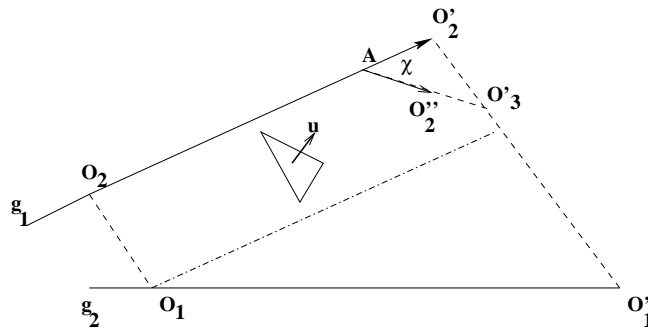
Figure 6.7: Paths of Two Geodesics Enclosing a Bone of Deficiency ϵ in (3+1)-dimensions

measured along geodesic g_1 and that the distance between the two geodesics is taken to be the length of the line perpendicular to g_1. After time $\Delta\tau$ elapses, the distance between g_1 and g_2 is $\overline{O'_1 O'_3}$. If initially, the distance between the two geodesics is assumed to be $\overline{O_1 O2}$, then:

$$\overline{O'_1 O'_3} = \overline{O_1 O_3} + \Delta\tau \tan \alpha - \overline{O'_2 O'_3} \tag{6.28}$$

where again the second term in the above equation is an expansion arising from the original paths of the geodesics and the last term is a contraction due to enclosing a bone with positive deficiency. α is the angle between the two geodesics if extended until they cross. One is then to find $\overline{O_2'O_3'}$. To reach this goal, it is enough to find angle χ, the angle between $\vec{AO_2'}$ and $\vec{AO_2''}$. Using equation (6.23), we have:

$$\vec{AO_2''} \cdot \vec{AO_2'} = \cos \chi = \cos^2 \phi \cos \epsilon + \sin^2 \phi \tag{6.29}$$

where we have used the fact that $\vec{AO_2'}$ is a unit vector. As ϵ is a small quantity, we can re-write the above equation as:

$$\cos \chi = \cos^2 \phi (1 - \frac{\epsilon^2}{2}) + \sin^2 \phi = 1 - \frac{\epsilon^2}{2} \cos^2 \phi \tag{6.30}$$

Taking on the same strategy as before, we find:

$$\cos^2 \chi = (1 - \frac{\epsilon^2}{2} \cos^2 \phi)^2 = 1 - \epsilon^2 \cos^2 \phi + H.O.(\epsilon^4) \tag{6.31}$$

$$\sin^2 \chi = 1 - \cos^2 \chi = \epsilon^2 \cos^2 \phi \tag{6.32}$$

Thus:

$$\tan^2 \chi = \epsilon^2 \cos^2 \phi (1 - \epsilon^2 \cos^2 \phi)^{-1} \tag{6.33}$$

$$\tan^2 \chi = \epsilon^2 \cos^2 \phi + H.O.(\epsilon^2) \tag{6.34}$$

from which one finally arrives at:

$$\tan \chi = \epsilon \cos \phi \tag{6.35}$$

Since:

$$\frac{\overline{O_2'O_3'}}{\overline{AO_2'}} = \tan \chi \tag{6.36}$$

again, noting that $\vec{AO_2'}$ is a unit vector and using equation (6.35), we have:

$$\overline{O_2'O_3'} = \epsilon \cos \phi \tag{6.37}$$

Inserting this last result into equation (6.29), the expansion in a (3+1) dimensional space-time is:

$$\overline{O_1' O_3'} = \overline{O_1 O_3} + \Delta\tau \, \tan\alpha - \epsilon \cos\phi \qquad (6.38)$$

where, $\Delta\tau$ is the time elapsed between the two measurements of the distance between the two geodesics, ϵ is the deficiency of the enclosed triangular bone and ϕ is the angle between g_1 and the normal to this bone.

6.6.2   Shear in (3+1)-dimensinal Skeletonised Space-times
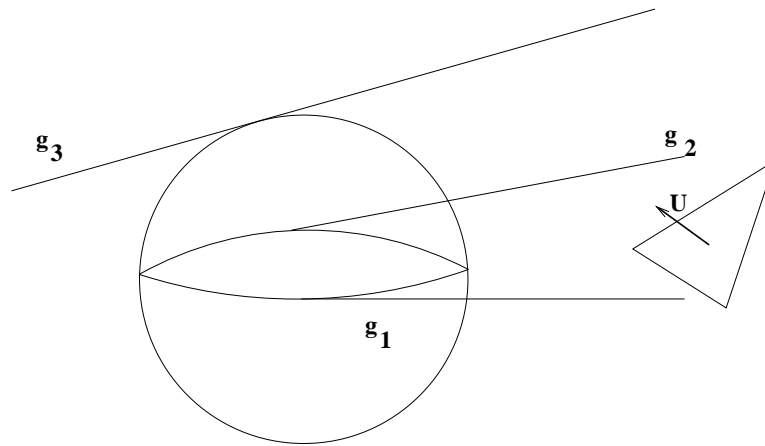
Figure 6.8: The cross section of a congruence of time-like geodesics in a (3+1)-dimensional space is a sphere. The bones in this skeletonised space-time are triangles.

Figure (6.8) depicts the spherical cross section of a congruence of time-like geodesics. As in the (2+1)-dimensional case, let's make the following assumptions:

$$\begin{cases} \text{Angle between } \vec{U} \text{ and } g_2: & \phi \\ \text{Angle between } \vec{U} \text{ and } g_3: & \xi \\ \text{Angle between } g_1 \text{ and } g_2: & \alpha \\ \text{Angle between } g_1 \text{ and } g_3: & \beta \end{cases}$$

where $\vec{U}$ is the normal to the triangular bone enclosed by the three geodesics shown. Again, we choose the representation where g_1 remains unaffected and g_2 and g_3 rotate

with respect to it. After time $\Delta\tau$ elapses, using equation (6.38), we have equations:

$$
\begin{cases}
\overline{O_1'O_2'} = \overline{O_1O_2} + \Delta\tau\tan\alpha - \epsilon\cos\phi \\
\overline{O_1'O_3'} = \overline{O_1O_3} + \Delta\tau\tan\beta - \epsilon\cos\xi
\end{cases}
$$

Again, as the initial cross section is spherical, $\overline{O_1O_2} = \overline{O_1O_3} = R_I$, where we have chosen R_I to denote the initial distance between g_1 and g_2 and g_3. Taking the average of $\overline{O_1'O_2'}$ and $\overline{O_1'O_3'}$, one finds

$$
a = \frac{\overline{O_1'O_2'} + \overline{O_1'O_3'}}{2} = R_I + \frac{\Delta\tau}{2}(\tan\alpha + \tan\beta) - \frac{\epsilon}{2}(\cos\phi + \cos\xi) \tag{6.39}
$$

and thus the average expansion is found to be:

$$
\theta = \frac{\Delta\tau}{2}(\tan\alpha + \tan\beta) - \frac{\epsilon}{2}(\cos\phi + \cos\xi) \tag{6.40}
$$

Following a similar approach to that of section (6.5.2), we find that the shear scalar σ is given by the equations:

$$
\begin{cases}
\overline{O_1'O_2'} - a = \frac{\Delta\tau}{2}(\tan\alpha - \tan\beta) - \frac{\epsilon}{2}(\cos\phi - \cos\xi) = \sigma \\
\overline{O_1'O_3'} - a = -\left(\frac{\Delta\tau}{2}(\tan\alpha - \tan\beta) - \frac{\epsilon}{2}(\cos\phi - \cos\xi)\right) = -\sigma
\end{cases}
$$

6.7 Conclusion

In this chapter, we examined the average expansion and shear scalar in (2+1) and (3+1)-dimensional space-times in the weak field limit. The general form of these flow characteristics contain trigonometric functions of the angles between the geodesics and the bones in (2+1)-dimensional case. In the case of (3+1)-dimensional skeletonised space-times, the expressions of expansion and shear scalar contain the trigonometric functions of the angles between the geodesics and the normal to the triangular bones. Of course this behaviour is not far from what one expects from Regge Calculus. It is however clear that generalising the expressions for average expansion and shear scalar in the presence of multiple bones is quite involved.

Chapter 7

Conclusion and Future Work

In this thesis, the "Parallelisable Implicit Evolutionary Scheme for Regge Calculus", a (3+1)-evolutionary method in the context of Regge Calculus, was analysed. Causality was an aspect that was not included in the PIES properly. Following a detailed analysis, we showed how causality can be accounted for in this scheme. Ambiguities associated with the notion of time in this formalism were addressed. The revised algorithm was used to reproduce the spherical FLRW universe with the surfaces of the 5-Cell and the 16-Cell polytopes as the underlying lattices. Three appropriate time functions for the numerical example were introduced. It was shown that the revised algorithm produced a good approximation to the spherical FLRW universe. *The most important conclusion however was that, independent of the choice of the time function, the revised algorithm resolves the problem of stop point, as faced previously by others employing the PIES.*

One important issue that is in need of further investigation is the issue of exact lapse of time in PIES. In particular, it is important to find an algorithm through which one can calculate the 4-volume of the 4-dimensional structure sandwiched between two consecutive spatial foliations. Another issue certainly worthy of further consideration is to reproduce and follow the evolution of other exact solutions to Einstein's equations using

the PIES. Such considerations provide ample opportunities to understand the cons and pros of PIES better. Of interest are solutions which are less symmetric compared to FLRW such as Binachi Universes which are homogeneous but anisotropic.

Undoubtedly, we are living during a glorious era for Astronomy. A number of different projects and space telescopes are providing us with quite impressive data about the universe we live in. A curious feature of this universe is its shape or topology. One crucial application of the revised PIES algorithm is to examine the evolution of a universe with non-trivial topology. It is of most interest to follow the evolution of such universes and explore the possibility of having a universe with non-trivial topology yet compatible with current observational data.

A part of this thesis was devoted to considering triangle inequalities in the framework of Minkowskian geometry. A number of triangle inequalities for triangles made with a combination of time-like, space-like and null edges were obtained. These inequalities are the counter-parts of the "Reverse Triangle Inequality" which holds for triangles constructed out of only space-like (time-like) edges. Such inequalities are essential in ensuring the correct construction of a skeletonised space-time especially when employing (3+1)-evolutionary methods in the context of Regge Calculus. In particular, to ensure that the geometry inside a given simplex is Minkowskian, one has to ensure that the relevant inequalities are satisfied. *We obtained inequalities that hold in SST triangles as well as NSS triangles.* We plan to further study these inequalities in the future and examine whether it is possible to express them using the sign of a Cayley-Menger determinant as is done in the case of Euclidean triangles.

Finally, in this thesis, the Raychaudhuri equation in the context of Regge Calculus was examined. The discretised counterparts of average expansion and shear scalar were

derived for both (2+1)-dimensional and (3+1)-dimensional space-times in the weak field limit. As expected, in the (2+1)-dimensional case, the trigonometric functions of the angles between the edge bones and the geodesics appear in the discretised expressions of average expansion and shear scalar. In the case of a (3+1)-dimensional space-times, a similar situation arises. In particular, the trigonometric functions of the angles between the geodesics and the normal to the triangular bones appear. The results of this chapter clearly show that the expressions for average expansion and shear scalar will be quite complicated when the congruence of geodesics encloses a number of bones.

Appendix A

A Note about the Minkowski Plane

All the area calculations, presented in appendix (B), are based on the geometric interpretation of the cross product. To be more specific, in Euclidean geometry, the norm of the cross product between two vectors $\vec{u}$ and $\vec{v}$ represents the area of the parallelogram spanned by them. Since the notion of area is meaningful in both Euclidean and Minkowskian geometry, one can interpret the norm of the cross product of two future directed vectors of the same type as the surface area of the parallelogram spanned by them [Yaglom 1979]. As we will show later, one cannot always use this notion directly to find the surface area of a time-like bone. Before starting our search for formulae for the areas of different types of bones in a 4-dimensional space-time, it is essential to first clarify what we mean by the expression "Minkowski Plane". We also need to treat the notion of angle in a Minkowski plane comprehensively.

A Minkowskian plane is a plane with a space-like normal. The geometry of this plane is the so-called Minkowskian or Lorentzian geometry represented by the following metric:

$$ds^2 = dt^2 - dx^2$$

The angles between the vectors of this plane are hyperbolic angles defined with respect to the Lorentzian length of the arc of the unit hyperbola confined between them (in op-
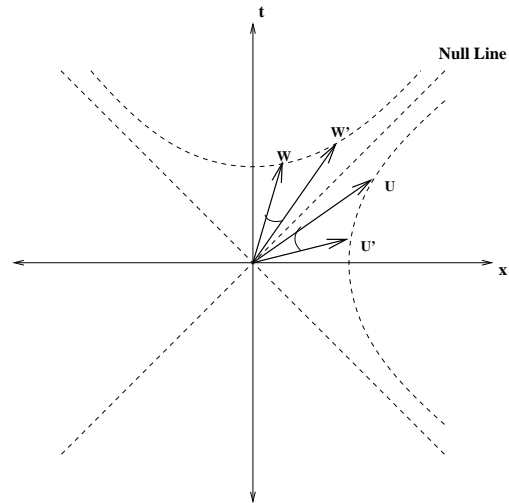
Figure A.1: Hyperbolic Angle in Minkowski Plane. It is quite easy to see why a hyperbolic angle between a space-like and a time-like vector is not defined. They obviously cannot confine a hyperbolic arc between them.

position to a circular angle as defined in a Euclidean plane with reference to a circle). As shown in figure (A.1), a hyperbolic angle in a Minkowskian plane is only defined between either two time-like or two space-like vectors. The reason is that the arc of a unit hyperbola can only be confined between either two time-like or two space-like vectors. As is evident from figure (A.1), it is impossible for a time-like and a space-like vector to confine part of a hyperbolic arc between them. Consequently, an angle between a space-like and a time-like vector is not defined. Thus, for example, no angle is defined in a triangle with one null side, one time-like side and one space-like side. In a triangle with two space-like and a time-like edge, only one angle is defined: the hyperbolic angle between the two space-like edges.

To prevent any possible confusion over this definition, let us look at an example where the above definition might become confusing. Figure (A.2) depicts a 3-dimensional space equipped with a metric of Lorentzian signature. It is important to distinguish between
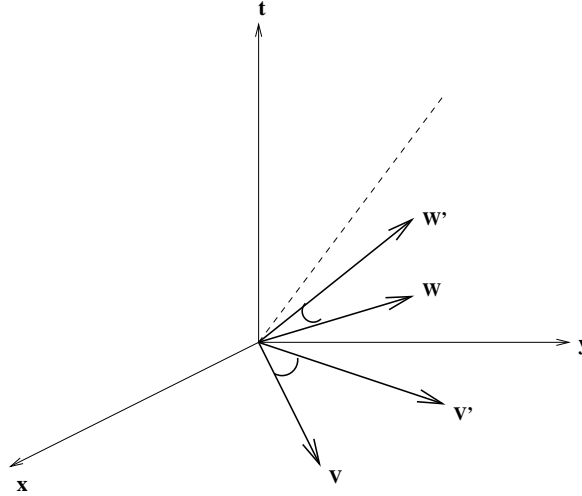
Figure A.2: A 3-dimensional space equipped with a metric of signature $+1$ which we choose to represent by $(-++)$. $\vec{W}$ and $\vec{W}'$ are in the $x - y$ plane while vectors $\vec{V}$ and $\vec{V}'$ are in the $y - t$ plane. The $x - y$ plane is space-like, i.e. it has a time-like normal, while the $y - t$ plane is time-like, i.e. it has a space-like normal.

the two types of angles subtended by the pair of space-like vectors, $\vec{V}$ and $\vec{V}'$, and the pair of space-like vectors, $\vec{W}$ and $\vec{W}'$. Although vectors $\vec{V}$ and $\vec{V}'$ are space-like, they span a sub-space with a positive definite signature or in other words a plane with a time-like normal. The $x - y$ plane where $\vec{V}$ and $\vec{V}'$ reside is a space-like surface and thus the angle between these two space-like vectors is circular as is the case with any angle in Euclidean geometry (which is incidentally the flat geometry with positive definite signature). The status of $\vec{W}$ and $\vec{W}'$ is however, rather different. $\vec{W}$ and $\vec{W}'$ span a time-like plane, characterised by semi-definite signature which we choose to represent with $(-+)$. The normal to the $y - t$ plane, the plane spanned by $\vec{W}$ and $\vec{W}'$, is space-like. The angle between $\vec{W}$ and $\vec{W}'$ is then *hyperbolic* and is based on the Lorentzian length of the arc of the unit hyperbola confined between them.

Appendix B

Areas of Triangles on the Minkowski Plane

In this appendix, we choose to represent a vector AB, which is an edge of a triangle $\triangle CAB$, with $\overline{AB}$ instead of $\vec{AB}$ as this notation is more convenient for the purpose of this appendix. In addition, in this appendix, we follow the convention of calling the norm [1] (taken to be a real and positive quantity) of an edge in a triangle with the lower case character corresponding to the label of the opposite vertex of that triangle. Finally, all the vectors used in construction of the triangles are assumed to be future directed [Birman & Nomizu 1984].

B.0.1 Area of a SSS Triangle

Figure (B.1) shows the space-like triangle $\triangle CAB$. As per our earlier discussion on the cross product, the area of $\triangle CAB$ is given by:

$$4A^2_{\triangle CAB} = |\overline{CA} \times \overline{CB}|^2$$

---

[1]The norm of a vector $\vec{u}$, used in this paper, is based on the definition given by Dray [Birman & Nomizu 1984] and is taken to be $|\vec{u}| = \sqrt{|\vec{u} \cdot \vec{u}|}$.
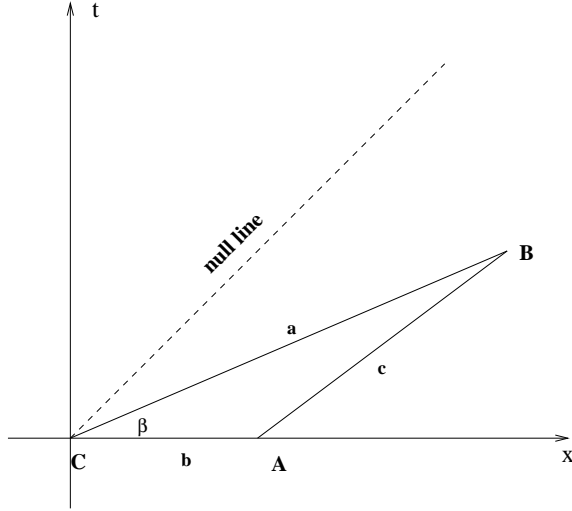
Figure B.1: A Space-Like Triangle.

but

$$|\overline{CA} \times \overline{CB}|^2 = \overline{CA}^2\overline{CB}^2 - (\overline{CA} \cdot \overline{CB})^2$$

which in turn yields

$$A^2_{\triangle CAB} = -\frac{1}{4}b^2\,a^2\sinh^2\beta \tag{B.1}$$

$A_{\triangle CAB}$ is evidently imaginary as required. It is desirable to have this area only in terms of edge lengths as this is all the information at hand in a skeletonised space-time. It is easy to see that

$$\sinh^2\beta = \frac{(a^2 + b^2 - c^2)^2}{4a^2b^2} - 1$$

which in turn yields the familiar Heron formula [Heath 1921] given by:

$$A_{\triangle CAB} = \frac{1}{4}\sqrt{(b + a + c)(a + c - b)(b + c - a)(b + a - c)} \tag{B.2}$$

Using a Cayley-Menger determinant [Sommerville 1958], this can be written as:

$$A^2_{\triangle CAB} = -\frac{1}{16}\begin{vmatrix} 0 & 1 & 1 & 1 \\ 1 & 0 & b^2 & a^2 \\ 1 & b^2 & 0 & c^2 \\ 1 & a^2 & c^2 & 0 \end{vmatrix}$$

B.0.2   Area of a SST Triangle

Figure (B.2) shows the time-like bone $\triangle CAB$ with two space-like and one time-like edge.

To find the area of a SST bone, one can always use the cross product of the two space-like
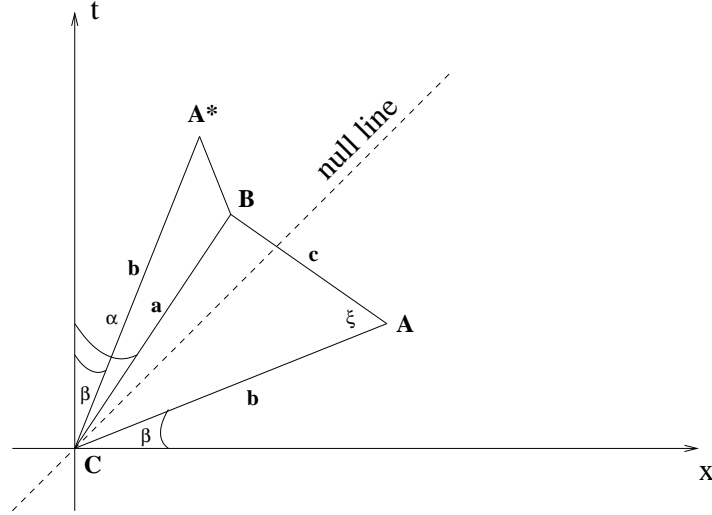
Figure B.2: $\overline{CA}^*$ is the time-like twin of $\overline{CA}$. The angle between $\overline{CB}$ and the t-axis is α and thus the angle between $\overline{CA}^*$ and $\overline{CB}$ is $(\alpha - \beta)$.

edges in a manner that was described earlier. In particular the area of the SST triangle $\triangle CAB$ is given by:

$$A_{\triangle CAB} = \frac{1}{2}\, b\, c\, \sinh \xi$$

To obtain the value of $\sinh \xi$ in the above equation, take the dot product of the following equation with itself:

$$\overline{CA} + \overline{AB} \;\; = \;\; \overline{CB} \tag{B.3}$$

$$b^2 + c^2 - 2\,b\,c\,\cosh \xi \;\; = \;\; -a^2 \tag{B.4}$$

Thus, $\sinh \xi$ is given by:

$$\sinh^2 \xi = \frac{(b^2 + c^2 + a^2)^2 - 4\,b^2\,c^2}{4\,b^2\,c^2}$$

Finally, the area of the SST triangle $\triangle CAB$ is given by:

$$A^2_{\triangle CAB} = \frac{1}{16}\left((a^2 + c^2 + b^2)^2 - 4c^2 b^2\right) \tag{B.5}$$

We have however discovered another method to arrive at this result. In this method, the area is obtained using a time-like and a space-like edge. In addition to being a new method, one advantage of this approach is in that it finds an interpretation for the angle between a space-like and a time-like edge.

As was stated earlier in appendix (A), the notion of angle between a time-like and a space-like vector is not geometrically meaningful. To employ a time-like and a space-like vector to find a triangular area, we first need to find an appropriate geometrical definition for the dot product between a time-like and a space-like vector. Although the dot product between such two vectors is defined in terms of their components, this does not yield a suitable geometrical definition for the angle between the two vectors. To get around this problem, we introduce the notion of a "twin" time-like vector to a space-like vector. Without loss of generality, take a space-like vector $\overline{CA}$ and a time-like vector $\overline{CB}$, as shown in figure (B.2), to be given by:

$$\begin{cases} \overline{CA} &= |\overline{CA}|(\cosh \alpha \hat{t} + \sinh \alpha \hat{x}) \\ \overline{CB} &= |\overline{CB}|(\sinh \beta \hat{t} + \cosh \beta \hat{x}) \end{cases}$$

in a given coordinate system. It is clear that

$$\overline{CA} \cdot \overline{CB} = |\overline{CA}||\overline{CB}| \sinh(\alpha - \beta) \tag{B.6}$$

Define the time-like twin vector, $\overline{CA}^*$, to $\overline{CA}$ such that

$$|\overline{CA}| = |\overline{CA}^*| = b$$

and the angle between $\overline{CA}^*$ and the t-axis is equal to that between $\overline{CA}$ and x-axis as shown in figure (B.2). Define a new binary operation, $\diamond$, as follows:

$$\overline{CA}^* \diamond \overline{CB} = b\, a \sinh(\alpha - \beta) \tag{B.7}$$

Comparing equations (B.6) and (B.7), it is clear that:

$$\overline{CA}^{*} \diamond \overline{CB} = \overline{CA} \cdot \overline{CB}$$

with the added bonus that the difference between angles α and β in equation (B.7) is now geometrically meaningful, as $(\alpha - \beta)$ is now the angle between two time-like vectors.

If $\vec{u}$ is the space-like edge and $\vec{v}$ is a time-like edge of a time-like bone, it was mentioned earlier that Regge defined the area of this bone to be:

$$4A^2 = (\vec{u} \cdot \vec{v})^2 - \vec{u}^2 \vec{v}^2 \tag{B.8}$$

Using equation (B.7) in Regge's formula for the area of the time-like bone, the area of $\triangle CAB$ is given by:

$$4A^2_{\triangle CAB} = (\overline{CA}^{*} \diamond \overline{CB})^2 + (\overline{CA}^{*})^2 \, \overline{CB}^2 = b^2 \, a^2 \cosh^2(\alpha - \beta) \tag{B.9}$$

which is evidently always real.

It is again desirable to write this area only in terms of the edge lengths. To get the formula of the area of $\triangle CAB$ only in terms of its edge lengths, notice that $\triangle CA^*B$ is a pure time-like triangle [Birman & Nomizu 1984]. The area of $\triangle CA^*B$ is given by: $\frac{1}{2}b\, a \sinh(\alpha - \beta)$, then clearly:

$$A^2_{\triangle CAB} - A^2_{\triangle CA^*B} = \frac{1}{4}b^2 \, a^2 \tag{B.10}$$

Thus to find the area of $\triangle CAB$ in terms of its edge lengths, it suffices to find the area of $\triangle CA^*B$ and insert it in (B.10). Writing the area of $\triangle CA^*B$ in terms of its edge lengths, one has:

$$A^2_{\triangle CA^*B} = \frac{1}{16}\left((b^2 - a^2 - c^2)^2\right)$$

and using this in (B.10) yields:

$$A^2_{\triangle CAB} = \frac{1}{16}\left((a^2 + c^2 + b^2)^2 - 4c^2 b^2\right) \tag{B.11}$$

This can now be written as a Cayley-Menger determinant:

$$A^2_{\triangle CAB} = \frac{1}{16} \begin{vmatrix} 0 & 1 & 1 & 1 \\ 1 & 0 & b^2 & -a^2 \\ 1 & b^2 & 0 & c^2 \\ 1 & -a^2 & c^2 & 0 \end{vmatrix}.$$

B.0.3 Area of a NSS Triangle
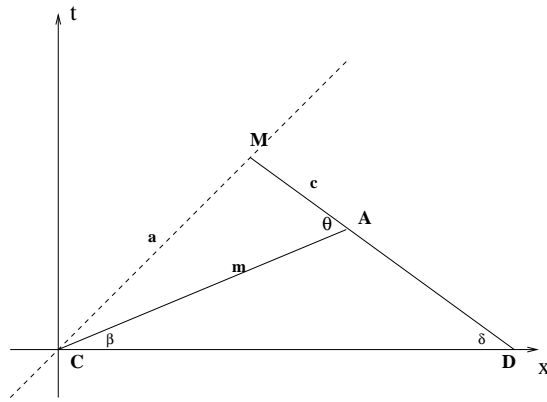
Figure B.3: $\triangle CAM$ is a NSS Triangle with $\overline{CM}$ being the null edge.

$\triangle CAM$ in figure (B.3) is a (NSS) triangle with sides $\overline{CA}$ and $\overline{AM}$ space-like and $\overline{CM}$ null. As was mentioned in chapter (3), drawing the null cone of a vertex in both a time-like and a space-like bone, produces this particular type of triangle. We choose to assign a real area to this type of triangle if it is part of a time-like bone and an imaginary area if it is part of a space-like bone. In the following discussion, we assume that $\triangle CAM$ is attributed a real area; were an imaginary area attributed to $\triangle CAM$, the modulus of this imaginary number would be the expression obtained in this section.

In triangle $\triangle CAM$, only one hyperbolic angle is defined and that is between vectors $\overline{AM}$ and $\overline{CA}$ as they are both space-like. Therefore, to calculate the area of $\triangle CAM$,

one wishes to find $|\overline{AM} \times \overline{CA}|$:

$$4A^2_{\triangle CAM} = |\overline{AM} \times \overline{CA}|^2 = (\overline{CA} \cdot \overline{AM})^2 - \overline{AM}^2 \overline{CA}^2$$

but [2]

$$\overline{CA} \cdot \overline{AM} = -m\,c\,\cosh\theta \tag{B.12}$$

and thus

$$A_{\triangle CAM} = \frac{1}{2}m\,c\,\sinh\theta \tag{B.13}$$

as expected. To see how this area can be expressed in terms of a Cayley-Menger determinant, it is enough to replace $\sinh\theta$ in equation (B.13) with its value in terms of the edge lengths. To do this, note that:

$$\overline{CA} + \overline{AM} = \overline{CM}$$
$$(\overline{CA} + \overline{AM}) \cdot (\overline{CA} + \overline{AM}) = \overline{CM} \cdot \overline{CM}$$
$$m^2 + c^2 = -2\overline{CA} \cdot \overline{AM}$$

but according to equation (B.12), we have

$$m^2 + c^2 = 2m\,c\,\cosh\theta$$

whence

$$\sinh^2\theta = \frac{(m^2 - c^2)^2}{4m^2c^2}$$

Therefore, one can rewrite the area of $\triangle CAM$ as:

$$A^2_{\triangle CAM} = \frac{1}{16}(m + c)^2(m - c)^2 \tag{B.14}$$

One can easily observe the resemblance of this formula with the Heron formula, keeping in mind that $\overline{CM}$ is missing simply because it is null and thus $|\overline{CM}|^2 = \overline{CM} \cdot \overline{CM} = 0$.

---

[2] The fact that this dot product has a negative sign comes from the nature of δ. The origin of this sign is more evident if one uses the expanded form of $\overline{CA} = |\overline{CA}|(\sinh\beta\hat{t} + \cosh\beta\hat{x})$ and $\overline{AM} = |\overline{AM}|(\sinh\delta\hat{t} - \cosh\delta\hat{x})$ to obtain the dot product, where $\hat{t}$ and $\hat{x}$ are the unit vectors in the t and x coordinate directions.

This, put into a Cayley-Menger determinant, looks as follows:

$$A^2_{\triangle CAM} = \frac{1}{16} \begin{vmatrix} 0 & 1 & 1 & 1 \\ 1 & 0 & m^2 & c^2 \\ 1 & m^2 & 0 & 0 \\ 1 & c^2 & 0 & 0 \end{vmatrix}$$

It is possible to write the surface area of a (NSS) triangle in another useful form that will be used in section (B.0.4). This expression will be given in terms of one of the space-like edges and the angle between the two space-like edges.

Start with

$$\overline{CA} + \overline{AM} = \overline{CM} \tag{B.15}$$

Taking the Dot product of both sides of (B.15) with $\overline{CM}$ and using the fact that $\overline{CM}$ is null one obtains:

$$\overline{CA} \cdot \overline{CM} = -\overline{AM} \cdot \overline{CM}$$

Since $\overline{CM}$ is a null vector in the first quadrant, it can always be written as:

$$\overline{CM} = a(\hat{t} + \hat{x})$$

where 'a' is a real and positive number. Then:

$$a\, m(\cosh \beta - \sinh \beta) = -a\, c(-\cosh \delta - \sinh \delta)$$
$$m(\cosh \beta - \sinh \beta) = c(\cosh \delta + \sinh \delta)$$

Solving for c, we have:

$$c = m\frac{(\cosh \beta - \sinh \beta)}{(\cosh \delta + \sinh \delta)}$$

which can be re-written as:

$$c = m(\cosh \beta - \sinh \beta)(\cosh \delta - \sinh \delta)$$
$$= m(\cosh (\delta + \beta) - \sinh (\delta + \beta))$$

In figure (B.3), $\delta + \beta = \theta$ [Birman & Nomizu 1984], and thus:

$$m = c(\cosh\theta + \sinh\theta)$$

Using this result in equation (B.13), one obtains:

$$A_{\triangle CAM} = \frac{1}{2}c^2(\cosh\theta + \sinh\theta)\sinh\theta \tag{B.16}$$

B.0.4   Area of a NST Triangle

Figure (B.4) shows $\triangle CAB$ along with the light cone of vertex B. Line segment BP is null
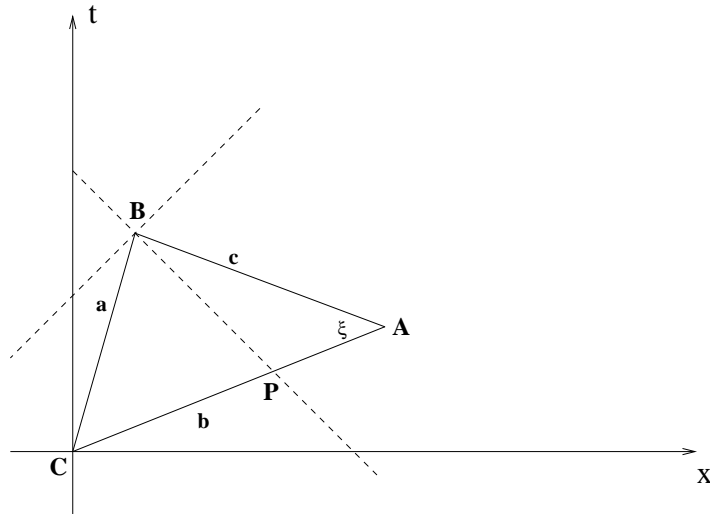
Figure B.4: The time-like bone $\triangle CAB$ is divided into a NST and a NSS triangle by the null line passing through B.

and thus divides $\triangle CAB$ into an (NSS) and an (NST) triangle. To calculate the area of $\triangle CBP$, it is easiest to subtract the area of $\triangle APB$ from that of $\triangle CAB$. Since $\triangle APB$ is a (NSS) triangle, its area can be obtained using an equation similar to (B.16):

$$A_{\triangle ABP} = \frac{1}{2}c^2(\cosh\xi - \sinh\xi)\sinh\xi \quad \text{where} \quad \cosh\xi = \frac{(b^2 + a^2 + c^2)}{2b\,c}$$

as shown in appendix (C). Thus the area of $\triangle ABP$, in terms of the edge lengths is given by:

$$A_{\triangle ABP} = \frac{A_{\triangle CAB}}{2b^2}\left((a^2 + b^2 + c^2) - 4A_{\triangle CAB}\right) \tag{B.17}$$

Since the area of $\triangle CBP$ is given by:

$$A_{\triangle CBP} = A_{\triangle CAB} - A_{\triangle APB}$$

One can use equation (B.17) to obtain the area of $\triangle CBP$ as

$$A_{\triangle CBP} = A_{\triangle CAB} - \frac{A_{\triangle CAB}}{2b^2}(a^2 + b^2 + c^2) + \frac{4A_{\triangle CAB}^2}{2b^2} \qquad \text{(B.18)}$$

The particular form of this equation facilitates the calculations of chapter (3).

Appendix C

Calculation of Hyperbolic Functions for angle ξ

In figure (B.4), it is clear that:

$$A_{\triangle CAB} = \frac{1}{2} b\, c \sinh \xi$$

from which:

$$\sinh^2 \xi = \frac{4A_{\triangle CAB}^2}{b^2 c^2}$$

and using the identity $\cosh^2 \xi - \sinh^2 \xi = 1$, one obtains:

$$\cosh^2 \xi = \frac{(b^2 + a^2 + c^2)^2}{4c^2 b^2}$$

The hyperbolic cotangent of ξ is then given by:

$$\coth \xi = \frac{(b^2 + a^2 + c^2)}{4A_{\triangle CAB}}$$

Appendix D

Flowchart of the Numerical Example

Start with a Pentatope with known edge lengths as a triangulation of a 3-sphere.(A.0.0)

Label the vertices [1] to [5]

Choose vertex [6] as the evolved counter-part of vertex [1].(A.0.1)

Connect vertex [6] to [1] with a time-like edge of norm "v" and with space-like edges of equal lengths to [2],[3],[4] and [5]. Take the norm of space-like edge to be "d". Produce the connection matrix. (A.0.1)

Calculate all the angles facing [16] in the triangles having [16] as an edge. (A.4)

Calculate the deficiencies on the triangular hinges having [16] as an edge. (A.1-A.3.4)

Choose "v" freely and solve equation (4.18) for "d". Call the obtained root d_0. (Block B)

Choose vertex [7] as the evolved counter-part of vertex [2].(C.0)

Connect vertex [7] to [2] with a time-like edge of norm "v" and with space-like edges of norm d_0 to vertices [1], [3], [4], [5] and [6]. Produce the connection matrix. (C.0)

Calculate all the angles facing [27] in the triangles having [27] as an edge. (C.4)

Calculate the deficiencies on the triangular hinges having [27] as an edge. (C.1-C.3.4)

Solve equation (4.18) for the norm of [67]. Call the obtained root l_0. This is the edge length of the next hypersurface. (Block D)

Figure D.1: The flowchart associated with one step of the evolution of the FRW lattice universe as described in section (4.5). The labels inside parentheses correspond to the blocks of code, as given in appendix (E), performing the tasks described.

Appendix E

Mathematica Code of the Numerical Example

This appendix contains the Mathematica code that was used in the reconstruction of the pentatope FLRW universe. The tasks performed by individual blocks and sub-blocks of the code are described in the flowchart of appendix (D) as well as the code itself.

```
(*Variable, Function and Module Defenitions*)
(*----------------------------------------------------*)
Clear[a]; Clear[v]; Clear[d]; Clear[el]; Clear[x];


(* The following module takes in a vertex and its evolved counter-
 part and returns all the triangular bones hanging at this
  edge. The output is a list called t. For example when this
  module is called with {1,6}, the following list is produced:
   t={{1,2,6},{1,3,6},{1,4,6},{1,5,6}} *)

Bones[vertices_] := (Module[{x, i, j}, g[x_] := 0; t = Array[g, vertices[[2]] - 2]; j = 1;
   For[i = 1, i ≤ vertices[[2]] - 1, ++i,
    If[MemberQ[vertices, i], ++i]; t[[j]] = Sort[Insert[vertices, i, 1]]; ++j]])


(* The following module takes in a list of triangular bones,
in particular the list produced by BONES and returns a list with
 the same number of components. For example, the first component of TE,
TE[[1]], is the list of all tetrahdra having [126] as a face. Thus,
TE[[1]]={{1,2,3,6},{1,2,4,6},{1,2,5,6}}. ''Count'' is the step of calculation we
  are at. Its value is either 1 or 2 because in the particular approach used,
after 2 steps (corresponding to the evolution of two vertices) the problem
 becomes identical to what we had two steps before, i.e. we have a hypersurface
 two vertices of which must be evolved to produce the next hypersurface. *)

TE[t_, count_] := (Module[{i, j, k, x, y}, f[x_, y_] := 0;
   te = Array[f, {Length[t], count + 2}];
    For[i = 1, i ≤ Length[t], ++i, j = 1; For[k = 1, k ≤ count + 2, ++k,
     While[MemberQ[t[[i]], j], ++j]; te[[i, k]] = Sort[Insert[t[[i]], j, 1]]; ++j]]])


(*The following module is called with the output of the previous module,
takes each component of TE,
and returns all the substets of that component with two members. For example L[[1]]=
 {{{1,2,3,6},{1,2,4,6}},{{1,2,3,6},{1,2,5,6}}, {{1,2,4,6},{1,2,5,6}}}. This output is
  essential in calculating the Dihedral angle between any two tetrahedral faces.*)

Lte[w_] := (Module[{i, r}, g[r_] = 0; L = Array[g, Length[w]];
   For[i = 1, i ≤ Length[w], ++i, L[[i]] = Subsets[w[[i]], {2}]]])


(*The following module returns the normal to each tetrahedral face,
the dihedral angle between which is sought. It then
 produces their dot product. More Description in Hartle's Paper.*)

DotOmega[t_, L_, el_, count_] :=
 (Module[{ii, jj, k, l, i, j, s, m, x, y}, g[x_] := 0; f[x_, y_] := 0;
    Dotomega = Array[f, {3, 3}];
    dotomega = Array[f, {Length[t], Length[L[[1]]]}];
    e[k_, l_] := (1 / 2) (el[[count, k]] + el[[count, l]] - el[[k, l]]);
    For[s = 1, s ≤ Length[t], ++s, For[ii = 1, ii ≤ Length[L[[s]]], ++ii, LL = L[[s, ii]];
     w1 = Complement[LL[[1]], {count}];
     w2 = Complement[LL[[2]], {count}];
     mm = Intersection[w1, w2];
     w1 = Append[mm, Complement[w1, mm][[1]]];
     w2 = Append[mm, Complement[w2, mm][[1]]];
     For[j = 1, j ≤ Length[w1], ++j,
      For[k = 1, k ≤ Length[w2], ++k, Dotomega[[j, k]] = e[w1[[j]], w2[[k]]]]];
     dotomega[[s, ii]] = (1 / ((3 !)^2)) Det[Dotomega]]]];)
```

```
(*The following module produces the volumes of the two terahedra the
 dihedral angle between which is sought. It then produces their product*)

Volume[t_, L_, el_, count_] := (Module[{ii, jj, k, l, i, j, s, m, x, y}, g[x_] := 0; f[x_, y_] := 0;
    volumematrix1 = Array[f, {3, 3}];
    volumematrix2 = Array[f, {3, 3}];
    volume = Array[f, {Length[t], Length[L[[1]]]}];
    e[k_, l_] := (1 / 2) (el[[count, k]] + el[[count, l]] - el[[k, l]]);
    For[s = 1, s ≤ Length[t], ++s, For[ii = 1, ii ≤ Length[L[[s]]], ++ii, LL = L[[s, ii]];
      w1 = Complement[LL[[1]], {count}];
      w2 = Complement[LL[[2]], {count}];
      For[j = 1, j ≤ Length[w1], ++j,
       For[k = 1, k ≤ Length[w2], ++k, volumematrix1[[j, k]] = e[w1[[j]], w1[[k]]];
        volumematrix2[[j, k]] = e[w2[[j]], w2[[k]]]]];
      volume[[s, ii]] =
       (1 / ((3 !) ^2)) Sqrt[Det[volumematrix1]] * Sqrt[Det[volumematrix2]]]]];)


(*The following module performs two jobs. It first produces the
 angle facing the edge with respect to which the action is varied. It then
 produces the coefficient of the deficit angle in Regge's Equation, namely,
the expression for the variation of the area of the bone with respect to the edge.*)

SSTAngle[edgelength_, t_, DE_, count_] := (Module[{i, j, x, y}, g[x_] := 0; f[x_, y_] := 0;
    SSTAngles = Array[g, Length[t]];
    ReggetermT = Array[g, Length[DE]];
    it = Intersection[t[[1]], t[[2]]];
    For[i = 1, i ≤ Length[t], ++i, m = Complement[t[[i]], {count, count + 5}][[1]];
     SSTAngles[[i]] = ArcCosh[
       (edgelength[[count, m]] + edgelength[[count, count + 5]] + edgelength[[m, count + 5]]) /
        (2 * Sqrt[edgelength[[count, m]] * Sqrt[edgelength[[m, count + 5]]]])]];
    For[i = 1, i ≤ Length[DE], ++i, ReggetermT[[i]] = (DE[[i]]) (Coth[SSTAngles[[i]]] -
        4 * (Sqrt[((edgelength[[count + 5, m]]) / (edgelength[[count, m]]))])
         (1 / Sinh[SSTAngles[[i]]]) (Exp[-2 * SSTAngles[[i]]]));
     ReggeEquation1 = Sum[0.5 * v * ReggetermT[[i]], {i, 1, Length[DE]}]
    ]])


(*This module produces the Deficit angle on
 each of the triangular bones produced by Module BONE*)

Deficit[DI_] := (Module[{i, j, x}, g[x_] := 0;
    DE = Array[g, Length[DI]];
    For[i = 1, i ≤ Length[DE], ++i, DE[[i]] = 2 * Pi - Sum[DI[[i, j]], {j, 1, Length[DI[[i]]]}]];
   ])


(*The following are two conversion functions to convert
 the triangulation edge length to FLRW radius and vice versa*)

ll[a_] := ((12 * (Pi^2) * (Sqrt[2]) / 5) * (a^3)) ^ (1 / 3);
aa[l_] := ((5 * (l^3)) / (12 * (Pi^2) * Sqrt[2])) ^ (1 / 3);


(*This line returns the maximum triangulation
 edge length once the maximum is radius is entered*)
ll[4.24413]
```

13.6814

(*Block A*)

```
(*A.0.0*)a = 13.6814; v = 0.01;
(* ''a'' is the length of triangulation and v is the lapse function*)
(*The following command will produce the matrix of edge lengths for the
 first step when vertex [1] is evolved to vertex [6] in the pentatope model*)
(*A.0.1*)el = {{0, a^2, a^2, a^2, a^2, -v^2}, {a^2, 0, a^2, a^2, a^2, d^2},
    {a^2, a^2, 0, a^2, a^2, d^2}, {a^2, a^2, a^2, 0, a^2, d^2},
    {a^2, a^2, a^2, a^2, 0, d^2}, {-v^2, d^2, d^2, d^2, d^2, 0}};
Module[{ii, jj, i, j, y, x}, g[y_] := 0; f[x_, y_] = 0; count = 1;
 (*A.1*)vertices = {count, count + 5};
 (*A.2.1*)Bones[vertices];
 (*A.2.2*)TE[t, count];
 (*A.2.3*)Lte[w = te];
 (*A.3.1*)DotOmega[t, L, el, 1];
 (*A.3.2*)Volume[t, L, el, 1];
 (*The cosine of the dihedral angle between
  any two tetrahedra is found by dividing dotomega by volume*)
 (*A.3.3*)DI = ArcCos[dotomega / volume];
(*A.3.4*)Deficit[DI];
 (*A.4*)SSTAngle[el, t, DE, 1];
]
```

(* Block B *)

```
(*B.1*)Plot[ReggeEquation1 + 70.87807553505367,
 {d, 5, 15}, AxesOrigin → {0, 0}, PlotRange → All]
```
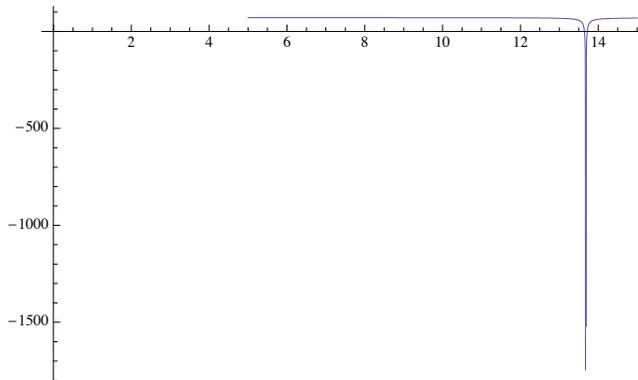


```
(*B.2*)
FindRoot[ReggeEquation1 + 70.87807553505367, {d, a - 0.0105}]

{d → 13.644412588636186`}
(*B.3*)
d = 13.644412588636186`;
```

```
(* Block C *)
(*The following is the edge length matrix after evolving vertex 2 to 7*)
(*C.0*)el = {{0, a^2, a^2, a^2, a^2, -v^2, d^2},
   {a^2, 0, a^2, a^2, a^2, d^2, -v^2}, {a^2, a^2, 0, a^2, a^2, d^2, d^2},
   {a^2, a^2, a^2, 0, a^2, d^2, d^2}, {a^2, a^2, a^2, a^2, 0, d^2, d^2},
   {-v^2, d^2, d^2, d^2, d^2, 0, x^2}, {d^2, -v^2, d^2, d^2, d^2, x^2, 0}};
Module[{ii, jj, i, j, y, x}, g[y_] := 0; f[x_, y_] = 0; count = 2;
 (*c.1*)vertices = {count, count + 5};
 (*c.2.1*)Bones[vertices];
 (*c.2.2*)TE[t, count];
 (*c.2.3*)Lte[w = te];
 (*c.3.1*)DotOmega[t, L, el, 2];
 (*c.3.2*)Volume[t, L, el, 2];
 (*c.3.3*)DI = ArcCos[dotomega / volume];
 (*c.3.4*)Deficit[DI];
 (*c.4*)SSTAngle[el, t, DE, 2];]
```

```
(* Block D *)
(*D.1*)Plot[ReggeEquation1 + 70.87807553505367, {x, 12, 15}, AxesOrigin → {0, 0}]
```
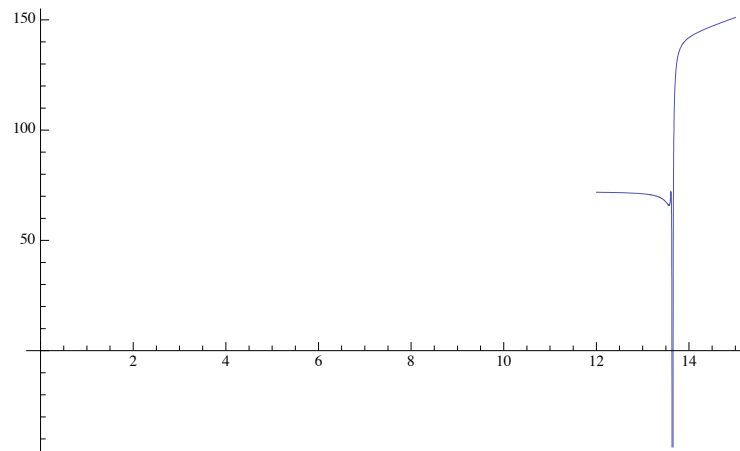


```
(*D.2*)FindRoot[ReggeEquation1 + 70.87807553505367, {x, a - 0.00002}, MaxIterations → 900]
(*x is indeed the length of the triangular edge on the next
 hypersurface. As we take the triangulation edges to be all equal,
finding x means finding the length of all the triangulation edges of the next hypersurface*)
```

$\{x \to 13.657 + 0. \, \mathbb{i}\}$

```
(*D.3*)
ReggeEquation1 + 70.87807553505367 /. x -> 13.656982593699464`
```

$6.71319 \times 10^{-8} + 0. \, \mathbb{i}$

Bibliography

[Abbott et al. 2004] LIGO Scientific Collaboration: B. Abbott et al., Nucl. Instrum. Meth. A517 154-179 (2004).

[Arnold 1997] V.I. Arnold, "Mathematical Methods of Classical Mechanics", Springer, 2nd edition (1997).

[Barrett et al. 1997] J.W. Barrett, M. Galassi, W.A. Miller, R.D. Sorkin, P. Tuckey, R.M Williams, Int. Journal of Theoretical Physics, Vol. 36, No. 4 (1997).

[Birman & Nomizu 1984] G.S. Birman, K. Nomizu, The American Mathematical Monthly, 91, 9 (1984).

[Brewin 1987] L. Brewin, Class. and Quantum Grav., 4 (1987).

[Chakrabarti et al. 1999] S. Chakrabarti, A.P. Gentle, A. Kheyfets, W.A. Miller Class. Quantum Grav., 16 (1999).

[Collins & Williams 1973] P.A. Collins, R.M. Williams, Phys. Rev. D 7 4 (1973).

[Collins & Williams 1974] P.A. Collins, R.M. Williams, Phys. Rev. D 10 10 (1974).

[Carroll 2004] S.M. Carroll, "SpaceTime and Geometry", Addison-Wesley (2004).

[Coxeter 1973] H.S.M Coxeter, "Regular Polytopes", Dover Publications (1973).

[De Felice & Fabri 2000] A. De Felice, E. Fabri, arXive:gr-qc/0009093 (2000).

[Dray 2004] T. Dray, "The Geometry of Special Relativity", Physics Teacher (India), 46 (2004).

[Ellis 2007] G.F.R. Ellis, Pramana 69 1 15 (2007).

[Font 2000] J.A. Font, "Numerical Hydrodynamics in General Relativity", Living Rev. Relativity, 3 (2000), 2. [Online Article]:cited on <1/May/2008>, http://www.livingreviews.org/Article/Volume3/2000-2Font.

[Hahn & Lindquist 1964] S. Hahn, R. Lindquist, Ann. Phys. 29, 304 (1964).

[Hamber 2007] H.W. Hamber, arXiv:hep-th/0704.2895 (2007).

[Hartle 1984] J.B. Hartle, Journal of Mathematical Physics, 26 (1985).

[Hartle 1984] J.B. Hartle, Journal of Mathematical Physics, 27 (1985).

[Heath 1921] T.L. Heath, "A History of Greek Mathematics", Volume II, Oxford University Press, (1921).

[Islam 1992] J.N Islam, "An Introduction to Mathematical Cosmology", Cambridge University Press (1992).

[Kar & SenCupta 2007] S. Kar, S. SenCupta, Pramana 69 1 49 (2007).

[Kobayashi & Nomizu 1963] S. Kobayashi, K. Nomizu, "Foundations of Differential Geometry", Vol I, Intersc. Publ. New-York London (1963).

[Lewis 1982] S.M. Lewis, Phys. Rev. D 25, 2 (1982).

[Miller 1995] M.A. Miller, Class. Quantum Grav. 12 (1995).

[Misner, Thorne & Wheeler (1972)] C.W. Misner, K.S. Thorne, J.A. Wheeler, "Gravitation", San Francisco, Freeman (1973).

[Regge 1961] T. Regge, Nuovo Cimento, 19, 558 (1961).

[Schutz 1999] B.F. Schutz, Class. Quantum Grav., 16 A131-A156 (1999).

[Sommerville 1958] D.M.Y. Sommerville, "An introduction to the geometry of n dimensions", Dover Publications (1958).

[Sorkin 1975] R.D. Sorkin, Phys. Rev. D 12, 2 (1975).

[Sorkin 1994] R.D. Sorkin, Int. Journal of Theoretical Physics, Vol. 33, No. 3 (1994).

[Stephani 2008] H. Stephani, "Relativity: An Introduction to Special and General Relativity", Cambridge University Press, 3rd edition (2008).

[Tuckey 1993] P.A. Tuckey, Class. and Quantum Grav., 10 L109-113 (1993).

[Wheeler 1964] J.A., Wheeler, "Geometrodynamics and the issue of the final state in Relativity", Groups and Topology, C. DeWitt and B. DeWitt , eds., p. 316. Gordon and Breach (1964).

[Wong 1971] C.Y. Wong, J. Math. Phys. 12, 70 (1971).

[Yaglom 1979] I.M. Yaglom, "A Simple Non-Euclidean Geometry and its Physical Basis", Springer (1979).